The Enhanced Diffusion of a Transversely Uniform Passive Scalar Quantity in Taylor Pipe Flow

Thomas Michael Nelson

A thesis submitted to the faculty of the University of North Carolina at Chapel Hill in partial fulfillment of the requirements for the degree of Master's of Science in the Department of Mathematics.

Chapel Hill
2013

Approved by

Richard McLaughlin

Roberto Camassa

David Adalsteinsson

ABSTRACT

THOMAS NELSON: The Enhanced Diffusion of a Transversely Uniform Passive Scalar
Quantity in Taylor Pipe Flow
(Under the direction of Professor Richard McLaughlin)

The term Taylor dispersion describes the work and a series of papers written by Geoffrey
Taylor in 1953 and 1954. These papers describe how a soluble substance spreads out when
introduced to a fluid flowing slowly through a pipe. [18][19][20] This fluid spreads out under
the combined action of molecular diffusion and a shear flow. In 2009, Camassa, Lin, and
McLaughlin considered the same problem as a pair of stochastic differential equations:

$$dx = Pe\left(\frac{1}{2} - r^2\right)dt + \sqrt{2}dW_1,$$

$$dr = \sqrt{2}dW_2$$

where W_1 is unbounded Brownian motion and W_2 is bounded Brownian motion. [6]
They derived an analytical solution, which provides an exact approach to the scalar variance evolution valid for all times. It is effective for channel and pipe flow for the case of
vanishing Neumann boundary conditions. The aim of this project is to use Monte-Carlo
simulations and experimental data to verify the analytic solution to the enhanced diffusion
of a transversely uniform, passive scalar quantity in a pipe due to an underlying flow.

ACKNOWLEDGEMENTS

CONTENTS

FIGURES

NOTATION

a - Radius of the tube (cm)

C - Concentration $(\frac{g}{cm^2})$

D - Natural diffusivity coefficient $(\frac{cm^2}{sec})$

D_{eff} - Effective diffusivity coefficient (or Taylor Diffusion Coefficient) when a solute is subjected to a parabolic flow $(\frac{cm^2}{sec})$

D^* - Non-dimensional diffusivity coefficient

d - Diameter of the pipe (cm)

dt - Change in time

dx - Change in longitudinal direction of the pipe

dr - Change in the radial direction

i - Index used to indicate moment being calculate

K - A constant that is the sum of $D + D_{eff}$ $(\frac{cm^2}{sec})$

L - Length of the pipe in the longitudinal direction (cm)

$M_i(\tau)$ - The ith moment of the Taylor-Aris pipe flow theory

$M_1(\tau)$ - The first moment of the Taylor-Aris pipe flow theory

$M_2(\tau)$ - The second moment of the Taylor-Aris pipe flow theory

μ_n - The nth zero of the Bessel Function

n - Index of the zero of the Bessel Function

PDE - Partial Differential Equation

Pe - The Peclet Number (non-dimensional)

pxpcm - Pixels per centimeter

r - Radial distance from the axis of the tube (cm)

r_{jump} - Variable representingrandom diffusion in the r-direction during the MC simulation

R - Random value generated from $\sqrt{-2\ln U_1}$ in Monte Carlo simulation

SDE - Stochastic Differential Equation

σ - The standard deviation of the plug of solute

$\sigma(\tau)$ - The standard deviation of the plug of solute as a function of non-dimensional time

t - Dimensional time (sec)

t_1 - One Taylor Time scale τ - Non-dimensional time

θ - Angle of a partical of concentration referenced on the cross section of the pipe

u - Velocity of the flow $\left(\frac{cm}{sec}\right)$

u_0 - Velocity of the flow at the axis $\left(\frac{cm}{sec}\right)$

U - Mean velocity flow $\left(\frac{cm}{sec}\right)$

U_1 - Independent random variable that is uniformly distributed on interval (0,1]

U_2 -Independent random variable that is uniformly distributed on interval (0,1]

UV - Ultra Violet (Light)

$V(\tau)$ - Variance of the flow as a function of non-dimensional time

ϕ - Random value generate from $2\pi U_2$ in the Monte Carlo simulation

W_1 - Unbounded Brownian Motion

W_2 - Bounded Brownian Motion

W_3 - Bounded Brownian Motion

x - The axial coordinate for the pipe in the longitudinal direction

x_{jump} - Variable representing random diffusion in the x-direction during the MC simulation

y - The distance from center of the pipe in the y-direction when using a 3D Cartesian coordinate system

y_{jump} - Variable representing random diffusion in the y-direction during the MC simulation

z - The distance from center of the pipe in the z-direction when using a 3D Cartesian coordinate system

z_{jump} - Variable representing random diffusion in the z-direction during the MC simulation

Introduction

1   Introduction

The term Taylor dispersion describes the work and a series of papers written by Geoffrey Taylor in 1953 and 1954. [18][19][20] These papers describe how a soluble substance spreads out when introduced to a fluid flowing slowly through a pipe. Taylor solved the problem by considering the flow as a Partial Differential Equations (PDE). Employing Taylor's assumption that the concentration is symmetrical about the central line of the pipe, C is only a function of r, x, and t. Thus the equation for diffusion is

$$D\left(\frac{\partial^2 C}{\partial r^2} + \frac{1}{r}\frac{\partial C}{\partial r} + \frac{\partial^2 C}{\partial x^2}\right) = \frac{\partial C}{\partial t} + u_0\left(1 - \frac{r^2}{a^2}\right)\frac{\partial C}{\partial x} \tag{1}$$

Here C is the concentration, x is the distance along the tube, r is the radial distance from the axis to the tube, t is time, u_0 is the velocity at the center of the tube, a is the radius of the tube, and D is the molecular diffusion coefficient. Additionally, it is assumed that D is independent of C.

$$\frac{\partial^2 C}{\partial x^2} << \frac{\partial^2 C}{\partial r^2} + \frac{1}{r}\frac{\partial C}{\partial r} \tag{2}$$

So that the equation (1) now becomes

$$D\left(\frac{\partial^2 C}{\partial r^2} + \frac{1}{r}\frac{\partial C}{\partial r}\right) = \frac{\partial C}{\partial t} + u_0\left(1 - \frac{r^2}{a^2}\right)\frac{\partial C}{\partial x} \tag{3}$$

Using this PDE, Taylor considered two special cases:

1) C at very, very short times and

2) C at very long times.

At very short times, the advection from the underlying flow dominates diffusion and the plug develops a parabolic profile. The flow is parabolic in nature because, in a pipe, the liquid moves faster at the center and is hindered by friction at the boundary.

But after a time t_1, diffusion causes the plug to regain its transversely uniform profile. The plug becomes a longer, transversely uniform quantity moving through the pipe at a constant velocity at all points in the pipe.

This is referred to as one Taylor time scale and Taylor showed that

$$t_1 = \frac{a^2}{(3.8)^2 D} \tag{4}$$

where a is the pipe radius and D is the natural diffusion of the dye. Taylor used Potassium Permanganate ($KMnO_4$) in his experiments with a diffusivity of $D = .7 \times 10^{-5} \frac{cm^2}{s}$. The current experiments use fluorescein dye with a diffusivity of $D = 4.9 \times 10^{-6} \frac{cm^2}{s}$. For a pipe of .5 cm diameter with fluorescein dye this is approximately 15 minutes.

In 1956, Aris continued Taylor's work developing method of moments for pipe flow, comparing the effective or enhanced diffusion coefficient with the natural diffusion coefficient. [2] Aris then developed a procedure for calculating the moments from the concentration curves produced in Taylor's experiments. For his moment equations Aris used a non-dimensional time τ which is calculated by

$$\tau = \frac{Dt}{a^2} \tag{5}$$

where D is the natural diffusivity, a is the radius of the pipe, and t is dimensional time measured in seconds.

In general the ith moment is given by

$$M_i(\tau) = \int x^i \frac{I(x,\tau)}{N} dx \tag{6}$$

where $I(x,\tau)$ is an intensity curve as a function of length and non-dimensional time and N is the integral of the intensity curve. Once the moments were calculated, Aris then defined V as the variance of the distribution of solute about the moving origin. This then led to the variance being calculated as

$$V(\tau) = \frac{M_2 - M_1^2}{2\tau} \tag{7}$$

where M_1 is the first moment and M_2 is the second moment.

In 2009, Camassa, Lin, and McLaughlin considered the same problem as a pair of stochastic differential equations (SDE):

$$dx = Pe\left(\frac{1}{2} - r^2\right) dt + \sqrt{2}dW_1, \tag{8}$$

$$dr = \sqrt{2}dW_2 \tag{9}$$

where W_1 is unbounded Brownian motion and W_2 is bounded Brownian motion. [6] In their solution, which holds for all times, they showed that the variance of the concentration was given by

$$V(\tau) = \frac{D_{eff}}{D} = \frac{(M_2(\tau)) - (M_1(\tau))^2}{2\tau} = 1 - \frac{\sigma^2}{2\tau} + \frac{Pe^2}{192}\left(1 - \frac{1}{15\tau}\left(1 - 46080\sum_0^\infty \frac{e^{-\mu_n^2\tau}}{\mu_n^8}\right)\right) \tag{10}$$

where D_{eff} is the enhanced diffusivity, D is the natural diffusivity, σ is the standard deviation of the plug, Pe is the Peclet number, τ is non-dimensional time, μ_n is the nth zero of the Bessel function, $M_2(\tau)$ is the second moment of the concentration curve, and $M_1(\tau)$ is the first moment. Here, Pe is a Peclet number, the ratio of the rate of advection of the plug from the flow and the natural rate of diffusion of the dye and is defined to be

$$Pe = \frac{au_0}{D} \tag{11}$$

where a is the pipe radius, u_0 is the flow velocity, and D is the natural diffusivity of the dye.

In the 2009 paper the group then conducted a multi-scale analysis and derived the asymptotic solution to the PDE. In this analysis they applied the Fredholm Alternative and produced the homogenized/effective diffusion equation. They then determined that the diffusion enhancement scales quadratically with the Peclet number with a constant at large times. This agreed with the classical result for Taylor dispersion. They showed that for pipe geometry the variance scaled by time converges to an asymptote line at

$$y = \frac{Pe^2}{192} \tag{12}$$

The goal of this project is to verify this formula against Monte Carlo simulations of the SDEs. The next step in the research process will be to compare the analytical and numerical results to experiment results.

2 Mathematical Background

2.1 1911: A. Griffiths

Taylor's first paper referenced the 1911 work of A. Griffiths. Griffiths did not attempt the full mathematical treatment of a passive scalar in pipe flow. Rather he began what he called an elementary consideration that would later be used in Taylor's experiments. He stated that the intensity of the passive scalar solute was not constant over the cross-section of a tube unless the capillary tube was of infinitely small bore. He then introduced the idea that the movement at the center of the column must measure the mean speed of the flow. Taylor would comment in his first paper Griffiths had formed a good qualitative picture of the solution. However, Taylor then stated that the statements of Griffiths two experimenta results seemed remarkable though Griffiths does not comment on them in this sense. This led Taylor to further pursue the diffusion of a passive scalar quantity in pipe flow. [13]

2.2 1953-1954: G.I. Taylor

G.I. Taylor is credited with conducting the original experiments concerning the evolution of passive scalar particles in pipe flow. Many subsequent works have theoretically addressed the anomalous regime before Taylor's asymptotic theory becomes valid. However, fairly limited experimental works have been performed to confirm these results. Taylor's initial thoughts for application of the study would be for physiologists who may wish to know how a soluble salt is dispersed in blood streams. Taylor's analytic solution began by looking at dispersion by advection alone. He started

by showing that in a circular pipe of radius a, the velocity u at a distance r from the central line is

$$u = u_0\left(1 - \frac{r^2}{a^2}\right)$$

where u_0 is the maximum velocity at the axis. Thus the velocity profile or shear flow is shown below

The solute at time $t = 0$ is distributed symmetrically so that the concentration C is

$$C = f(x, r),$$

after time t the concentration will be

$$C = f(x - ut, r).$$

In Taylor's experiments he used the mean value, C_m, of the concentration over the cross-section of the tube measured. He defined C_m as

$$C_m = \frac{2}{a^2} \int_0^a C_r dr.$$

Taylor then looked at the molecular diffusion. He assumed that the concentration is symmetrical about the central line of the pipe so that C is a function of r, x, and t only (i.e. there is no need to consider the θ term). The equation for diffusion is

$$D\left(\frac{\partial^2 C}{\partial r^2} + \frac{1}{r}\frac{\partial C}{\partial r} + \frac{\partial^2 C}{\partial x^2}\right) = \frac{\partial C}{\partial t} + u_0\left(1 - \frac{r^2}{a^2}\right)\frac{\partial C}{\partial x}$$

With the following initial conditions:

$$\frac{\partial^2 C}{\partial \theta^2} \approx 0, \quad \frac{\partial^2 C}{\partial x^2} << \frac{\partial^2 C}{\partial r^2} + \frac{1}{r}\frac{\partial^2 C}{\partial \theta^2}, \quad \left.\frac{\partial C}{\partial r}\right|_{r=1} = 0$$

and the equation reduces to

$$D\left(\frac{\partial^2 C}{\partial r^2} + \frac{1}{r}\frac{\partial C}{\partial r}\right) = \frac{\partial C}{\partial t} + u_0\left(1 - \frac{r^2}{a^2}\right)\frac{\partial C}{\partial x}$$

Additionally, using the Bessel function of order zero, Taylor was able to derive the time necessary for the radial variation of C to die down to $1/e$ of its initial value was

$$t_1 = \frac{a^2}{(3.8)^2 D}$$

This led to the condition that

$$\frac{L}{u_0} >> \frac{a^2}{(3.8)^2 D}$$

where L is the length of the tube. This shows that any time the dispersing material is spread over the length of the tube that the time necessary for advection to make an appreciable change in C is of order L/u_0. This t_1 is often referred to as a Taylor time scale.

Taylor tested his analytical theory by measuring the dispersion of potassium permanganate in water. He used 1 percent by weight of potassium permanganate ($KMnO_4$) and 99 percent of slightly acidulated water. In a pipe of .05 cm radius the solution was a transparent dark purple. He was then able to verify his analytic solutions at short and long times. At short times he was able to verify his solutions when the effect of molecular diffusion is negligible. At long times he was able to verify his solutions when molecular diffusion is significant. He was then able to verify his measured diffusion cofficients for $KMnO_4$ against Landolt and Bornsteins tables in Furth and Ullmann (1927). His experimental results were remarkably close to that of these tables. [18]

In 1954, Taylor would continue his work and explored the analogous problem of dispersion in turbulent flow. He again was able to verify his theoretical predictions. He did this turbulent flow verification with both smooth and very rough pipes. He also found that a small amount of curvature increased the dispersion greatly. At the time, the practical application of this was a method used by engineers for measuring the flow in large water mains. They would inject a packet of salt into the main at one point and to measure the electrical conductivity of the water at another point

downstream from the point of injection. [19]

Also in 1954, Taylor's third paper on pipe flow covered the conditions under which dispersion of a solute in a stream of solvent can be used to measure molecular diffusion. In this paper Taylor proves an assumption used in his 1953 paper through analysis. His conclusion of this paper showed that the combined effect of longitudinal advection and radial molecular diffusion gave rise to a separate diffusion coefficient.

$$D_{eff} = \frac{a^2 U^2}{48D}$$

Where D is the molecular diffusion coefficient, a is the radius of the tube, and U is the mean velocity of the flow. This would later be referred to as the Taylor Diffusion coefficient.

Taylor pioneered the study of diffusion in pipe flows. He wrote much of the theory that is still used today and did some of the subjects first experiments. One of his final conclusions is that the distribution of concentration C is eventually a Gaussian function of distance along the pipe axis. However, it is important to note that Taylor was only able to model the systems diffusion for only short and very long times. [20]

2.3   1956: Aris

Rutherford Aris, while working for Imperial Chemical industries, built upon Taylors previous work. While corresponding with Taylor he applied the method of moments to Taylors approach and published on the dispersion of a solute in a fluid flowing through a tube in 1956. Aris provided a new basis for the Taylor Analysis which removed the restrictions imposed on some of the parameters and described the distribution of the solute in terms of its moments in the direction of flow. He showed that the rate of growth of the variance is proportional to the sum of the molecular diffusion coefficient, D, and the Taylor diffusion coefficient. He state that if V is the variance of the distribution of solute about the moving origin the it is

$$V = \frac{1}{s} \int \int_S dy dz \int_{-\infty}^{+\infty} (x - Ut)^2 C(x, y, z, t) dx$$

then

$$\lim_{t \to \infty} \frac{1}{2} \frac{dV}{dt} = D + \frac{a^2 U^2}{48D} = K$$

Here again, U is the mean velocity and a radius of the tube. However, Aris maps his concentration in terms of x, y, and z instead of x, and r. Here K is the sum of the moleculare diffusion coefficient, D, and the effective diffusion coefficient D_{eff}. He gave an expression for K in the most general case and showed that a finite distribution of solute tends to become normally distributed. [2]

2.4   1966: Lighthill

Lighthill was one of the first authors to publish a study the concentration evolution in the period between Taylor's case one and case two. He commented that for larger pipes the flow times were too small Taylor's theory to apply. Lighthill assumed a radially uniform initial distribution of the tracer and that it was localized longitudinally as a *delta*-function. Lighthill determined an exact solution for the concentration with respect to transverse diffusion while negating the lonitudinal diffusion and interactions with the pipe's boundary. He did this in terms of a Fourier series analysis. His solution was valid for times before the tracer interact strongly with the tube wall. This was before the Taylor regime. [15]

2.5   1970: Chatwin

Chatwin expands on the previous work by Taylor and Aris in pipe flow. He derives an asymptotic series for the distribution of concentration based on the assumption that the diffusion of solute obeys Ficks law. The first term is the Gaussian function, and the succeeding terms describe the asymmetries and other deviations from normality observed in practice. He applies the theory to Poiseuille flow in a pipe of radius a and he concludes that three terms of the series describe C satisfactorily if $Dt/a^2 > 0.2$. He also showed that the initial distribution of C has little effect on the approach to normality in most cases of practical importance.

Chatwin then showed that through expansion methods one could see that the initial transient evolution would be initial condition dependent. However, this should die off within the first diffusive

timescale, making it less interesting from the point of view of his work. [7][8][9]

2.6 1975, 1982: Barton

N.G. Barton of the University of Queensland, Australia continued Chatwins work on the asymptotic series of concentration distributions. His 1975 paper was written in reference to when there is a small density difference between the solvent and the dissolved solute. Barton derived the asymptotic series for the induced density currents and for the distribution of solute in the case when the molecular diffusivity is constant throughout the pipes cross-section. These series led to the asymptotic forms of the moments of the distribution. His theory predicts that the additional dispersion due to buoyancy effects is proportional to the square of the Rayleigh number and depends on the Peclet number of the flow. Barton was able to achieve agreement with his results and those of Chatwins theory.

In Barton's 1982 paper he reworks the Aris moment equations by solving them via the separation of variables method. Through this analysis, Barton is able to obtain equations for the second and the third moments. These moment equations are valid for all times and are of particular importance for when the moments are required at short or moderate times. They are also useful if information is required about the distribution of contaminant across the cross-section. This theory is capable of generalization to handle dispersion under different boundary conditions and in two-phase flows. [4]

2.7 2001: Latini and Bernoff

In 2001, Latini and Bernoff continued Lighthill's analysis of Taylor's tracer dispersion in laminar pipe Poiseuille flow. They divided the tracer dispersion into three regimes. Using the small non-dimensional diffusion, D^*, the first regime for small times is $t << D^{*-1/3}$. In this Diffusive regime, diffusion dominates advection yielding a spherically symmetric Gaussian dispersion cloud. The third regime is the classical Taylor regime which measure the dispersion at long times. Represented at $t >> D^{*-1}$, the tracer is homogenized transversely across the pipe and diffuses with a Gaussian distribution longitudinally. They then defined the intermediate regime to be $D^{*-1/3} << t <<$

D^{*-1}. In this Anomalous regime the longitudinal diffusion is anomalous with a width proportional to D^*t^2 and a distinctly asymmetric longitudinal distribution. Here they said that the tracer diffusiving transversley and being sheared longitudinally dominates over the longitudinal diffusion. This is because during this regime, a majority of the tracer has not yet interacted with the pipe's boundary. Here the distribution is distinctly asymmetric and is advected with the pipe's centerline velocity.
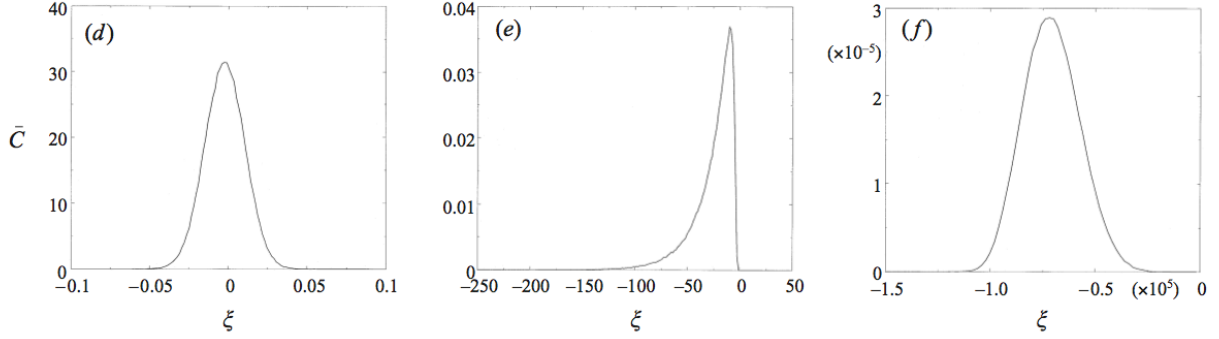
Figure 2.1: This figure from Latini and Bernoff's 2001 paper shows the concentration distributions along the three regimes described above. $\bar{C}$ represents the concentration on the y-axis and ξ represents the axial position on the x-axis. (d) is a numerical simulation of the diffusive regime, (e) is of the anomolous regime at t=1250, and (f) is of the Taylor regime. This shows the asymmetric and peaked distribution of the concentration during the anomalous regime.

Latini and Bernoff proposed a new solution valid in this regime and verified their results numerically. They concluded that these results suggest that anomalous diffusion is a hallmark of the shear dispersion of point discharges at times earlier than the Taylor regime. [14]

2.8   2009: Camassa, Lin, McLaughlin

In their 2009 paper, Camassa et. al. then showed a stochastic approach to the problem could provide an analytic formula for the variance of concentration for uniform transverse initial data which is valid at all times with boundary conditions enforced. The initial work done was for a initial condition uniform in the transverse direction and delta function in the flow direction. It can be shown that the introduction of a length scale in the initial condition simply shifts their original result by a constant value. They obtained statistical moments by using the known Greens function for the heat equation subject to vanishing Neumann Boundary conditions. With this they were

able to explicitly calculate the moments needed to compute the scalar variance. They started by reviewing the long time limits via multi-scale asymptotic for pipe and channel flow to compute the effective diffusivities. Then, using the stochastic differential equation for pipe flow, they computed the complete variance valid for all times. They showed that the long time limit of the variance agreed precisely with the multi-scale asymptotic calculations in all cases. With this conclusion they showed that the variance predicted by Latini and Bernoff, using free space methods, arises directly from the stochastic differential equation approach. They did this by replacing the bounded Brownian motion with free space Brownian motion. [6]

CHAPTER 3

Practical Applications

3 Practical Applications

Taylor dispersion is the enhanced diffusion of a passive scalar due to underlying molecular motion in flow. This has broad implication in general transport theories ranging from physical chemistry and hydrodynamics to industrial engineering applications.

3.1 Numerical Simulation of Contaminant Dispersion in Estuary Flows

In 1982 C.M. Allen wrote a paper on the numerical simulation of contaminant dispersion in estuary flows. Her reason for researching this topic was that if a contaminant is released into an estuary, it would be important to be able to predict the dispersion of the material and to know the maximum amounts of concentration at a particular time and place. To do this she modeled a channel flow problem using Taylor's transport diffusion theory for laminar and oscillatory turbulent flow. However, for an estuary, the special conditions assumed by Taylor do not always hold. She used the necessary conditions discussed in Chatwins 1980 paper that were when a sufficiently long time has elapsed since the release of the contaminant. Here the cross-sectional area is independent of longitudinal distance and time, the turbulence is statistically stationary in time, and the contaminant is passive.

To do this Allen used the random walk technique, in which a pollutant source is represented by a large number of particles whose path is tracked, by using a computer, as they move through the fluid. In her calculations she used up to 20,000 particles. This method models the physical system much more accurately than a finite difference model. The technique also easily adapts for changes in variables such as topography, velocity profile and source geometry. The random walk

technique generally uses less computer time and storage than finite difference methods for 2D and 3D models. Also, the accuracy of the method is dependent on the resolution required and the size of contaminant patch in comparison with the total size of the model. In her paper, Allen used this method to simulate the detailed space and time variation of materials dispersing from a pollutant source. [1]

3.2 Mixing Thermocapillary Flows

In 2004 a group of researchers from the departments of chemical and electrical engineering at Princeton University wrote an article on the study of mixing in thermocapillary flows on micropatterned surfaces. Their goal was to numerically determine efficient mixing configurations for microfluidic transport subject to free surface flows. Their work investigated the characteristics of advective and diffusive mixing in continuous-mode streaming of thermocapillary microflows on chemically micropatterned surfaces. They wanted to optimize mixing time and mixing length for various geometries and parameter ranges. They provided full numerical solutions to extract these optimal operating conditions.

The numerical solutions were obtained by finite element method calculations of the advection diffusion equation in three-dimensional space. They used triangular elements with linear or quadratic basis functions. They conducted this analysis across three distinct mixing regimes. The group refers to thise regimes as 1) analogues of purely diffusive dynamics, 2) Rhine-Young shear-augmented diffusion, and 3) Taylor-Aris dispersion. The Peclet numbers and coefficient of diffusivity D tend to agree with the three regimes discussed by Latini and Bernoff in 2001. The group then was able to verify their numerical analysis experimentally using confocal fluorescence microscopy measurements of the interfacial diffusive broadening in adjacent flowing streams. [11]

3.3 Transport of Nutrients in Bones

Another work, published in 2005 by G.H. Goldsztein, discussed the transport of nutrients in bones. In this article the author notes that bones are porous media with complex microgemetries. He specifically addresses some of the longer bones in the human extremities, osteons, such as the

femur. He states that there are a system of pores in bones that are interconnected by thin channels called canaliculi embedded in the bone. These channels and pores form a connected system known as the lacunar-canalicular system which is filled with fluid and responsible for the transport of nutrients and waste products within the bone.

To study this phenomenon, the author set up a one-dimensional model of the lacunar-canalicular system. He states that the nutrients are transported along the length of canal by advection and Taylor dispersion similar to that of a pipe or capillary. He assumes that the lacunar-canalicular system is filled with fluid and does not contain any nutrients initially. Nutrients are then introduced into the system and transported by diffusion and a laminar flow. He shows that the system exhibits a diffusion-like macroscopic behavior and derives an effective diffusion coefficient given explicitly in terms of the geometry of the system and the applied velocity field. He concludes by saying although he has provided the simplest model possible that keeps the relevant physics, there is much more experimental and theoretical studies are required for a better and more clear understanding of the processes responsible for the transport of nutrients in bones. [12]

Experimental Methods

4 Experimental Methods

A series of experiments have been performed using two pipe diameters (1mm and 5mm) and two dyes (KMnO4 with diffusivity of 0.7×10^{-5} cm^2/sec and fluorescein with diffusivity of 4.9×10^{-6} cm^2/sec). The focus of these experiments wer in the laminar regime where the underlying flow could be assumed parabolic.

4.1 Experimental Setup

The apparatus consists of a glass pipe, about 25 cm in length. The pipe is mounted to a clear PVC reservoir which is set up on a C-track running the length of the table. The reservoir has a drain hose leading from the bottom and is closable by a brass ball valve. The other end of the pipe is mounted in a three point retaining ring which is also height adjustable. The end of the pipe is attached to a 60 mL syringe by a short length of flexible tubing. The syringe is mounted to a mechanical syringe pump. The Harvard Apparatus syringe pump is managed by a touch-screen control box. The pump can run forward and backward at different speeds and is programmable.
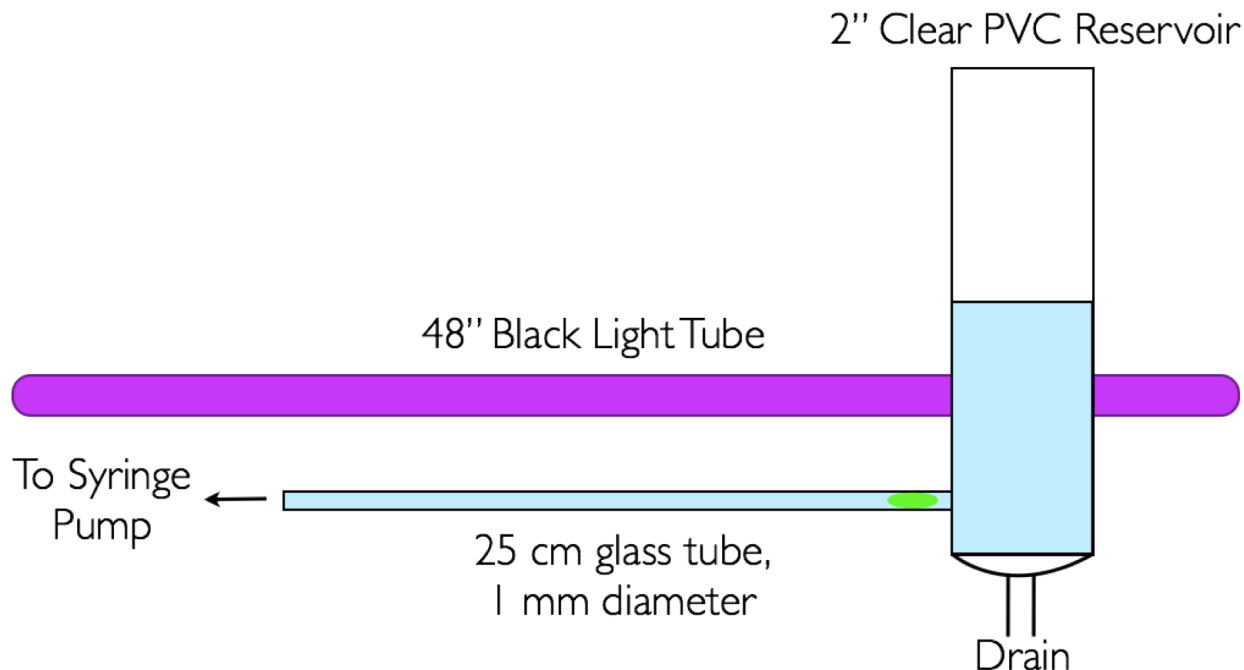
Figure 4.1: This figure is a representation of the experimental apparatus (not to scale).

To facilitate interchangeability of the glass tubes, the pipe-reservoir interface has been fit with a small piece of vinyl of which a hole, slightly smaller than the pipe diameter, is drilled. The pipe is inserted snuggly into the vinyl piece and the vinyl piece is held tightly to the reservoir by a hose clamp. When tightened, this provides a water-tight seal between the vinyl piece and the reservoir without the need for wet agents.

4.2 Preparing the Experiment

For each dye a uniform diffused lighting was provided. In the case of $KMnO_4$, the diffused light source was a fluorescent tube and diffuser plate placed directly behind the glass tube. When processing the data an empty tube image is subtracted from each image to recover pure dye signal. For the fluorescein, several ultra violet (UV) black lights were placed above and below the glass tube. The advantage of the fluorescein is that only the dye signal is measured by the camera initially. This reduced any noise associated with tube boundaries and background lighting.

4.2.1 Fluorescein Water

In the most recent versions of the experiment, the passive scalar quantity is a plug of fluorescein dye. The dye emits light when under UV light which is very easy for the camera to pick up. The optimal concentration used for the dye is 0.4 grams per liter of water. The reason for this is that the theory deals with concentration while using a digital camera only intensity is measured. The chart below shows that within a certain concentration regime (from about 0.30 to 0.60 g/L), there is a linear relationship between concentration and intensity.
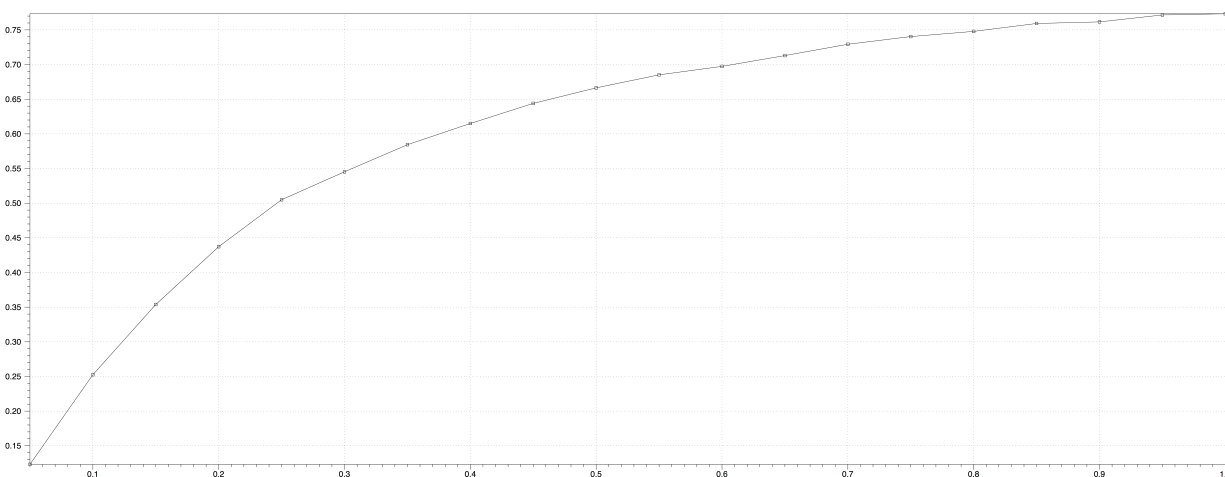
Figure 4.2: In the chart above the x-axis is concentration from 0.00 g/L to 1.00 g/L measured in increments of 0.05 g/L. The y-axis is intensity from 0 to 0.75. A 0.4 g/L solution is used is that after preparing the plug the dye has become slightly diluted, putting it safely within this linear region.

4.2.2 Measuring Pixels per Centimeter

An important parameter for data analysis is pixels per centimeter (pxpcm). Initially the experiment was set up limiting the viewing window to about 15 cm. This produced an image resolution of about 120 pxpcm. The project then integrated a shopbot XYZ stage to enchance the camera view clarity. The digital camera is mounted to the XYZ stage and can receive manual or program movements to travel in the x-direction paralleling the passive scalar plug of dye. With the integration of the XYZ stage, the field of view is now approximately 4 cm and the pxpcm resolution achieved is in

the range of 350-400 pxpcm. To measure the pxpcm of a specific run, a picture is taken at the magnification used for the run with a gridded ruler mounted just in front of the tube. This picture can then be analyzed in a DataTank script that produces the pixel per cm used in the experiment.

4.2.3 Eliminating Tube Bowing

Another important procedure to do before running the experiment is to ensure that the tube is straight and there is no bowing. In the cases of using a very small tube (1 mm inside diameter) tube bowing is a common problem. As discussed in Chapter 2, Taylor time of the experiment (the t_1 calculated by Taylor) increases quadratically with pipe radius. For a 0.1 cm diameter pipe, this time is only about 1 minute. For a larger tube, say a tube with a 0.5 cm diameter, the time is 15 minutes. Therefore the smaller tube diameter has the advantage of requiring less time for each experiment.

However, analysis of the experimental data showed that an irreconcilable error is being introduced by undulations in the bore of the .1 cm diameter tube (which is only guaranteed accurate within 10 percent). Therefore, the experment switched to a larger tube with a inner diameter of .5 cm. There is much less tube bowing, however, the time of each experimental run has greatly increased. However, if small tubes are used again, it is essential for data analysis that the tubes be straight. An example for how to eliminate tube bowing is contained in the experimental procedures guide.

4.2.4 Pulling the Plug

This next section discusses the methods used to introduce the passive scalar quantity into the tube for the experiment. When using the small tubes, it is important that those running the experiment be extremely careful not to disturb the tube after the bowing has been eliminated.

Establishing a Closed System. The first step is to turn on the UV black light. Then remove the syringe from the pump and carefully remove the vinyl tubing. Fill a clean beaker with water and draw water into the syringe. There will be some air bubbles in the syringe. Over a trash can or a sink, tap the syringe while pushing the plunger to get ride of these bubbles. Now the syringe

should be completely filled with water. Attach the vinyl tube to the syringe. Ensuring the ball valve is closed, fill the PVC reservoir with distilled water until the water is a few centimeters above the pipe. If using a small pipe, make sure the end of the vinyl tube is in a small beaker and if using a larger pipe, make sure a larger beaker is sitting under the tube to prevent spills. When the water has flowed through the tube and taken with it any excess air bubbles, attach the syringe and the glass tube via the vinyl tube. During this process it is important to eliminate all air bubbles in the connection. Now the experimental apparatus is a totally closed system: water in the reservoir, water in the tube, water in the syringe, with no air bubbles. Carefully mount the syringe in the syringe pump with the plunger back in its clamp. Then tighten the large black knobs to hold the syringe in place and the small black knobs to hold the syringe plunger.

Pulling the Plug. Now, release the ball valve to drain the reservoir. Carefully pour in the fluorescein water until it is about a centimeter above the pipe. Wait a few minutes for the water-fluorescein interface to calm down from the turbulence. On the syringe pump control screen select the program Plug Small or Plug Large, depending on the tube size. Both of these programs withdraw the syringes at a very slow constant rate for 5 minutes. It will then pause for 5 minutes and repeat for 10 cycles. The reason for pulling the plug this slow at 5 minute intervals is that it is imperative to have as close to a transversely uniform plug as possible. Experimental runs have shown that even pulling at these slow speeds introduces a slight parabolic profile into the plug. While the program runs (for approximately 100 minutes), it is important to watch the plug and stop the program when about 1 to 2 centimeters of fluorescein has entered the tube. This usually takes about 40 minutes. After stopping the program, wait a few minutes for the water in the pipe to become still. Drain the fluorescein and discard. Using a 1 gallon jug, carefully pour water down the sides of the reservoir, avoiding the end of the pipe, to clear away any excess fluorescein. Close the ball valve and fill the reservoir until the water is about 2 cm above the pipe. Wait a few minutes for the fluorescein-water interface to settle and restart the Plug Small or Plug Large program. After another 40 minutes, a fluorescein plug about 3 cm in length surrounded by water on both sides by should be near the reservoir. It is important that the back of the plug be completely visible. It may be helpful to view the pipe through the camera to make certain. Finally, wait about 15 minutes for the plug to settle and diffuse.

4.3 Running the Experiment

To run the experiment select the default program called Withdrawal. While the data analysis is in terms of velocity (cm/sec), the syringe pump uses enter a flux measurement mL/hour. In the DataTank analysis script, the parameters collapser has an input field called Desired Velocity (cm/sec). This script then converts the Desired Velocity to mL/hr. Then use the syringe pump to enter the desired velocity. For typical small tube runs a standard velocity is 0.0147 cm/sec (0.4156 mL/hr). For typical large tube runs a standard velocity is 0.03675 cm/sec (1.039 ml/hr).

During the experiment images are then captured at an interval ranging from 5 frames per second to 1 frame every 6 seconds depending on the size of the pipe and the flow rate. Pictures are taken using a Nikon D-300 camera with a 24x120 mm lense. Unlike the work of Taylor, the majority of the data collected was during the first "Taylor-timescale" ($\frac{a^2}{3.8^2 D}$) rather than much after it. Intensity information is then used to study the concentration evolution.

To setup the camera, navigate the menu to the Interval Time Shooter option. Set the number of pictures to 999. For the small pipe, set time time between shots to 1 sec. For the larger pipe, set the time to 6 seconds between shots. Then close the blackout curtains so there is no external light shining on the apparatus. The only light shining directly or indirectly on the pipe should be the UV black light. Once the the system is set and ready, simultaneously press the Start Program button on the syringe pump and the Ok button on the camera. The experiment is now started and can take anywhere between five minutes and an hour and a half, depending on your tube size and flow velocity. Refrain from touching the table while the experiment is active and minimize movement in and out of the curtained area to prevent invasive light from being captured by the camera.

When the experiment is complete, turn off the camera, syringe pump, and black light. The system can then be reset for the next iteration of the experiment. The pictures can then be downloaded from the digital camera memory card to the computer that will be used for the data analysis.

The Reynolds number for these experiments ranged between 10 and 500 depending on the flow rate and pipe diameter used. Flow rates were typically between 0.012 and 0.5 cm/sec. In each case the density of the dyed solution and of the clear solution were measured and kept within 0.0005 g/mL. Note that the $KMnO_4$ at the concentration prescribed by Taylor, 1 percent by

weight density difference (0.03 g/mL) between solution and dyed solution was significant. This was enough difference to cause the breaking of top/bottom symmetry of the passive scalar concentration in the evolving flow. This was especially noticeable in the larger tube. Hence, when conducting the $KMnO_4$ experiments the density mismatch was corrected by using trace amounts of $NaCl$ to increase the solute density to match that of the dyed solution. Cross diffusion between $NaCl$ and $KMnO_4$ was assumed negligible.

4.4   Analyzing the Data with DataTank

Once the images have been downloaded to the computer the post processing can begin. The intensity of the light that is captured by each digital image can be used to measure the concentration of the liquid in two dimensional space. It is important to note that the radial geometry of the pipe will partailly skew the data. So much of the data used will be taken from a horizontal slice that runs along the center of the pipe. This data taken from this slice will have the least amount of skewing. The concentration data can then be used to draw the intensity plots, calculate the moments and variance, and draw the variance scaled by time or the variance not scaled by time plots. These variance plots can then be compared to the analytic solutions to determine the accuracy of the experimental methods. The analytic solution will also be used to test the accuracy of the Monte Carlo simulation. Additionally, slice lines are taken at the lower center and the lower boundary of the image.

4.4.1   Cropping and Rotating the Images

Each digital image records a field of view of about 4 in. horizontally and 2.7 in. vertically. Since the only part of the image needed for analysis is the length of the pipe, much of the access of the image can be cropped. This is an important step and must be done with care. Cropping the images properly will greatly decrease the amount of time needed for analyzing the data. To do this the images are imported into the DataTank script. The images can then be cropped and rotated as an entire package. The image being presented in the output monitor can be changed using a time slider in DataTank. The rotating is necessary to ensure that the center of all images are lined up

with the center line slice in the bitmap. Once the proper cropping and rotation has been achieved, the images can then be processed into an external package file. This external package file will contain all the images, cropped and rotated, and can be imported back into DataTank for analysis. This process allows the user to easily change between datasets without having to crop and rotate the images each time. Additionally, the images can be made into a QuickTime movie set to any desired play length.

4.4.2 Intensity Plots

Most of the analysis is now handled by the DataTank script. The first meaningful plot that is drawn is the intensity plot. These plots measure the intensity (or concentration) of the fluid along the horizontal slice lines.
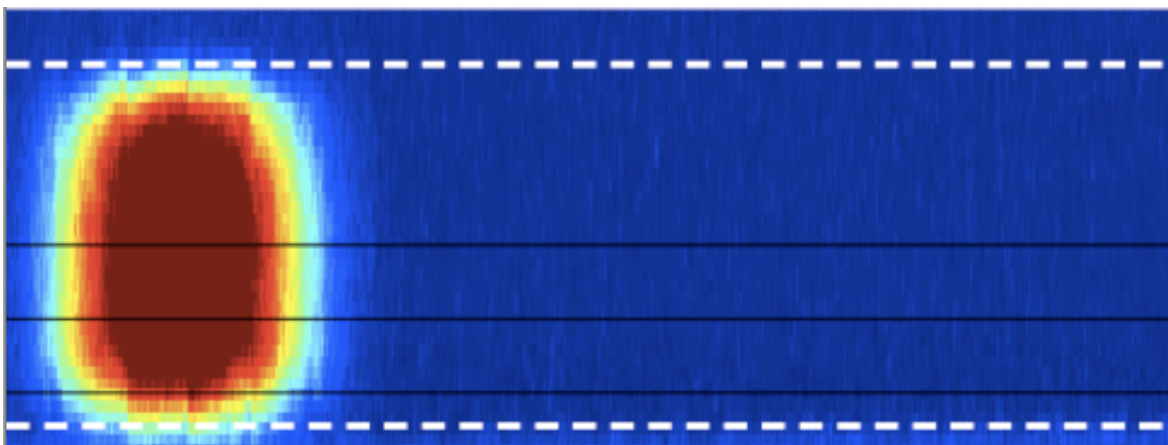
Figure 4.3: The figure above shows a plug of fluorescein dye prior to an experimental run. The three black horizontal lines represent the slice lines for which the intensity curves are drawn. The top black line is the Partial Planar Slice (Center), the second black line is the Partial Planar Slice (Middle) and the bottom black line is the Partial Planar Slice (Boundary).

The script plots the intensity (nondimension varying from 0 to 1) of the bitmap along the slice lines on the y-axis and the horizontal distance measured in pixel on the x-axis. This plot can then be redrawn over all times. This means that each digital image has its unique intensity plot. The plots produced show the standard Gaussian curves of varying maximum intensity depending on the vertical location of the slice as shown in Figure 4.3
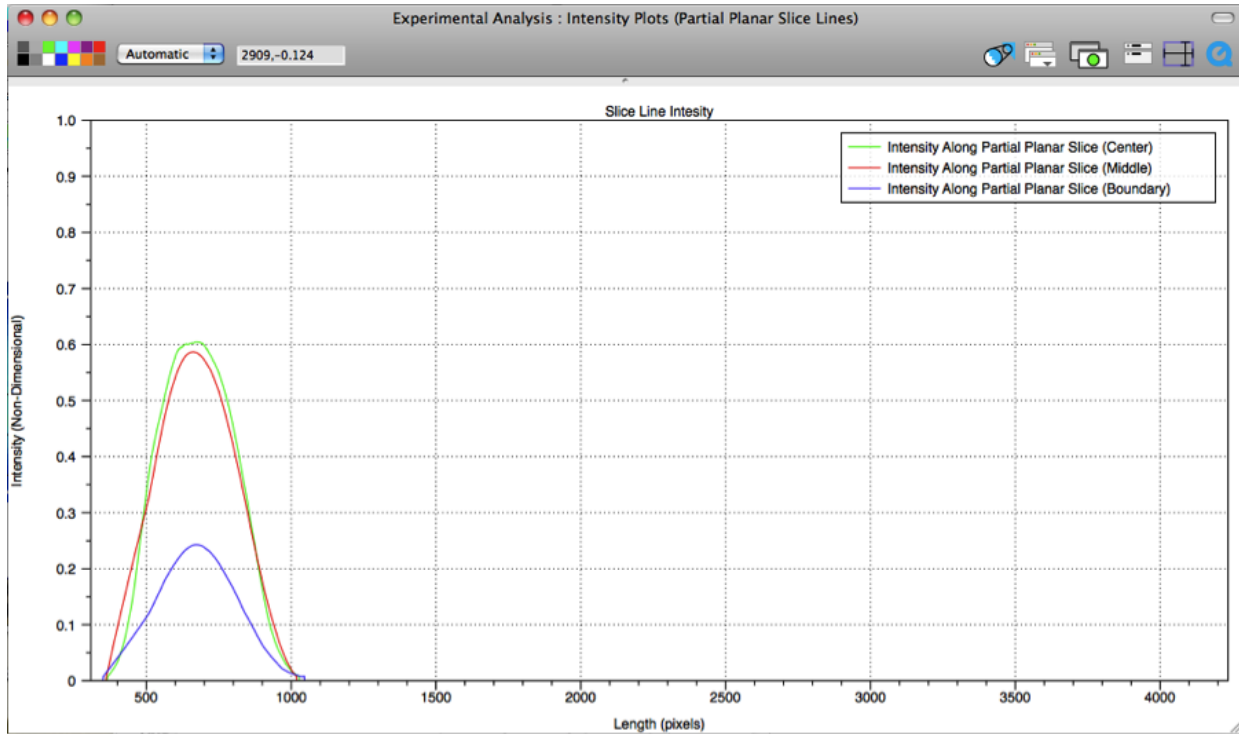
Figure 4.4: In the above chart, image intensity (non-dimensional from 0 to 1) is shown on the y-axis over the horizontal distance measured in pixels on the x-axis. The intensity is graphed over 3 separate partial planar slices of the pipe.

An alternate method of plotting the intensity is to show a y-Averaging of the intensities of the bitmap. If the bitmap or image is a M x N array of numbers, each number, then each number represents some intensity from 0 to 1. The -Averaging means tha the script takes the average of each column and returns a 1 x N matrix of numbers which is then sampled over time. This produces the y-Average intensity curve.
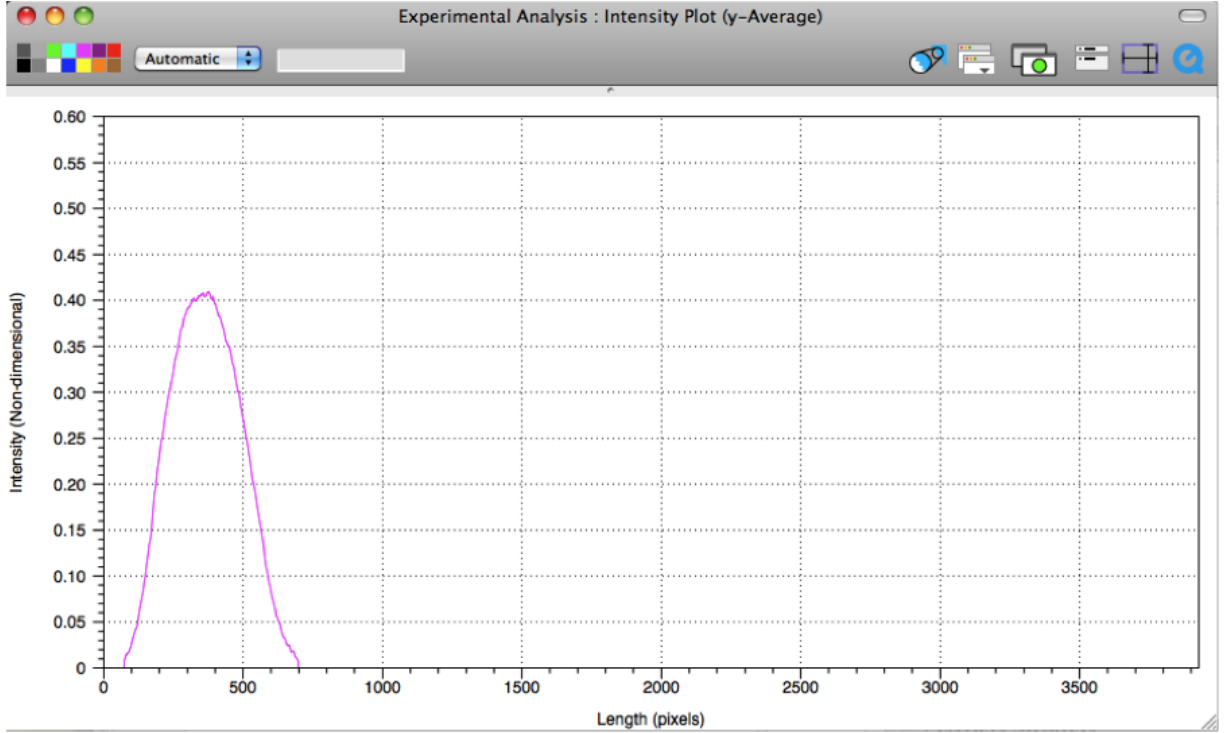
Figure 4.5: In the above chart, image intensity (non-dimensional from 0 to 1) is shown on the y-axis over the horizontal distance measured in pixels on the x-axis. The average intensities of the three partial planar slices of the pipe are graphed here.

4.4.3 Calculating the Moments and Variance

These intensity curves are then integrated via an external C++ code written with Xcode. This essentially gives the "area under the curve", which can then be used to calculate the moments. In the expermental data the Gaussain intensity curves do not actually fall completely to zero. There are some very small residual intensities to the left and right of the curve that must be comensated for. Therefore an external C++ program call "cut noise" eliminates these values to the left and right of the gaussian curve once they fall below a particular error threshold. This allows the integral of the curve to produce an finite value that is used to calculate the moments. This threshold is typically 0.0075 (non-dimensional intensity value) that can be adjusted in the parameters section of the script.

The procedure for calculating the moments follows the Taylor-Aris theory. In general the ith

moment is given by

$$M_i(\tau) = \int x^i \frac{I(x,\tau)}{N} dx$$

where $I(x,\tau)$ is an intensity curve as a function of length and non-dimensional time and N is the integral of the intensity curve. Once the moments have been calculated, the variance is easily deduced by algebraically combining the moments. By the Camassa, Lin, and McLaughlin equation already discuss the variance is given by the following equation

$$V(\tau) = \frac{M_2 - M_1^2}{2\tau}$$

where M_1 is the first moment and M_2 is the second moment.

4.4.4 Variance - Scaled by Time vs. Not Scaled by Time

In Camassa, Lin, and McLaughlin's theory both the time (τ) and variance, $V(\tau)$, are non-dimensional. The non-dimensional variance can then be plotted as a function of the non-dimensional time. To visually analyze the intensity curves, there are two choices. The first is to view variance scaled by time, for which the variance is divided by the non-dimensional time in equation (10). The second is variance not scaled by time. This is represented by the follwoing formula

$$V(\tau) = \tau \left(1 + \frac{Pe^2}{192} \left(1 - \frac{1}{15\tau} \left(1 - 46080 \sum_0^\infty \frac{e^{-\mu_n^2 \tau}}{\mu_n^8} \right) \right) \right)$$

Both are equally valid and useful. With the variance scaled by time, the variance approaches a horizontal asymptote line calculated by the analytical solution. Whereas the variance not scaled by time asymptotically approaches a slope. Visually, this slope can be harder to compare the experimental results to the analytic solution.

However, the variance not scaled by time ends up being much more helpful when compared to experimental results to plots of analytic solutions. This is because of the effects the plug length has on the variance. Ideally, the experimental procedures are able to control plug length so finely that variance is only a function of position and time. Unfortunately, plug length is one of the harder

parameters to control and small changes in plug length can have big effects on variance. However, if variance not scaled by time is considered, the effect of plug length can be negated by shifting down the y-axis by the value of the variance at t = 0. Therefore, the variance of multiple runs can be compared without having to take plug length into account.
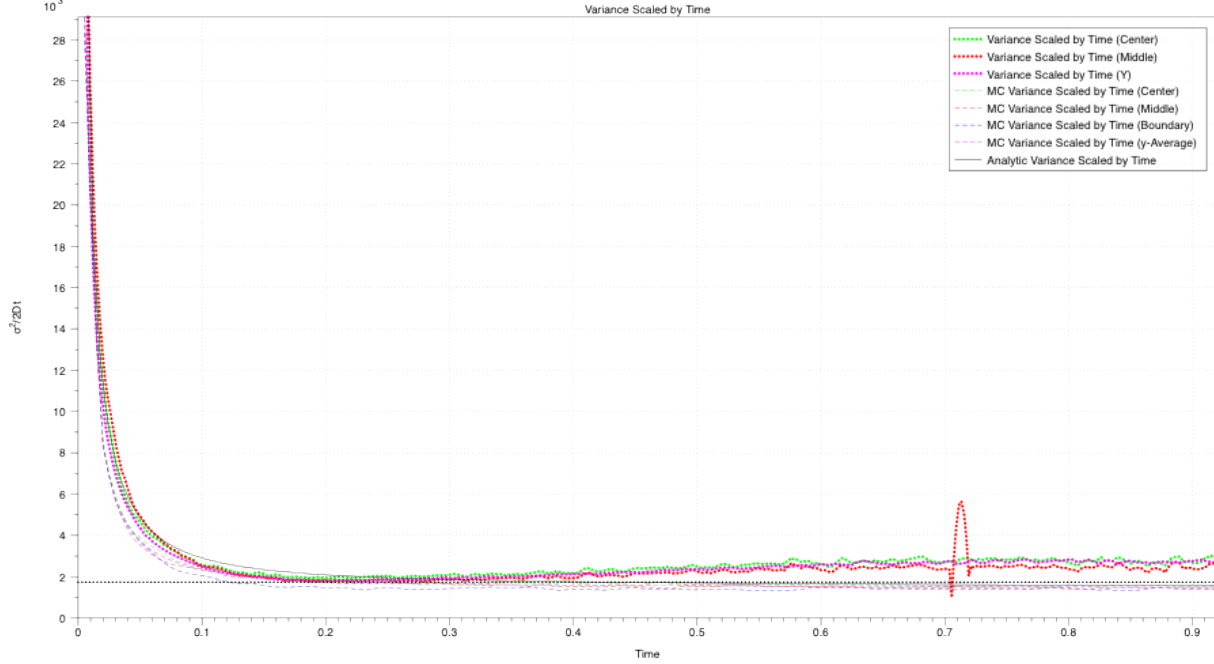
Figure 4.6: In the above chart, the x values, non-dimensional time are represented by $\tau = \frac{tD}{a^2}$ which has units $(sec) * ((pixels^2/sec)/pixels^2) = 1$. And the y values, nondimensional variance are represented by $variance/D$ which has units $(cm^2/sec)/(cm^2/sec) = 1$. The green, red, and purple dotted lines are the variance calculated from experimental data (taken 12 April 2012) across the center line, middle line, and y-Average, respectively. The colored dashed lines represent the Monte-Carlo simulation variances scaled by time. Finally, the solid black line represents the analytic solution of the variance scaled by time.

4.4.5   Calculating the Analytical Solution

As shown in the figure 4.6, it is necessary to have an analytic solution to the problem to compare the experimental data against. The experimental analysis script is an external C++ script that calculates and renders a plot of the analytic solution to the experimental run that is being analyzed.

The script takes the parameters from the parameters collapser of the DataTank script as inputs and plots the analytic solution on the same variance plots as the experimentally calculated variances. The script essentially solves the problem analytically for each unique experiment based on its physical parameters.

```cpp
double Computation(DTDoubleArray zeroes,double NMax,double Pe,double SD,
                   double ts)
{
    // Calculate Variance SCALED BY TIME with fixed Peclet

    double SSM = 0;
    // Calculate summation
    for( double k = 1; k < NMax; k++ ) {
        double mu2 = pow( zeroes(k), 2 );
        double mu8 = pow( zeroes(k), 8 );

        SSM += exp( -mu2 * ts )/mu8;
    }

    double Var = 1 + pow(SD,2)/(2*ts) + pow(Pe,2)/192 * ( 1 - 1/(15*ts) * (1-46080*SSM) );

    double toReturn = (Var);

    return toReturn;
}
```

Figure 4.7: The above code written in C++ calculates the Variance Scaled by Time. It uses the following inputs: Zeros of the Bessel Function as mu, NMax is the upper limit of the summation, Pe is the Peclet number, SD is the standard deviation of the plug of dye, and ts is the non-dimensional timestep. It then returns the Variance Scaled by Time for all discrete time values.

```
double Computation(DTDoubleArray zeros,double NMax,double Pe,double ts)
{
    // Calculate Variance NOT SCALED BY TIME with fixed Peclet

    double SSM = 0;
    // Calculate summation
    for( double k = 1; k < NMax; k++ ) {
        double mu2 = pow( zeros(k), 2 );
        double mu8 = pow( zeros(k), 8 );

        SSM += exp( -mu2 * ts )/mu8;
    }

    double Var = ts * ( 1 + pow(Pe,2)/192 * (1 - 1/(15*ts)*(1-46080*SSM)));

    double toReturn = (Var);

    return toReturn;
}
```

Figure 4.8: The above code written in C++ calculates the Variance Not Scaled by Time. It uses the following inputs: Zeros of the Bessel Function as mu, NMax is the upper limit of the summation, Pe is the Peclet number, and ts is the non-dimensional timestep. It then returns the Variance Not Scaled by Time for all discrete time values.

As mentioned in the previous section, the plug length is irrelevant for calculating the variance not scaled by time. However, for the variance scaled by time, the code needs to know the standard deviation of the plug, σ in equation (10).

This is calculated in the collapser Parameters Standard Deviation of the DataTank script. However, the theory calls for a transversely uniform plug. This is virtually impossible to achieve with the current apparatus.

Numerical Scheme: Monte Carlo Method

5 Numerical Scheme: Monte Carlo Method

In the cases of many real world physical problems, the systems of equations to model them can become quite large. In many instances, even with the best methods and algorithms available, the computation times can be too great. The Monte Carlo method is a technique in which a large quantity of randomly generated numbers are used to simulate a physical syste to find an approximate solution. The computational time for this method can often be much less than normal numerical methods. The larger the number of random samples used in the simulation, the more accurate the solution will be. The information from this numerical simulation can then be used to compare to analytical solutions and experimental data. The Monte Carlo Method will be used to simulate the pair of stochastic differential equaitons:

$$dx = Pe\left(\frac{1}{2} - r^2\right)dt + \sqrt{2}dW_1, \tag{13}$$

$$dr = \sqrt{2}dW_2 \tag{14}$$

In this problem advection and diffusion effect the concentration at two very disparate time scales. The large scale time measures the Advection part of the equation. The change in concentration here is due to the flow in the pipe. This portion is solved deterministically based on radial parabolic pipe flow. The smaller time scale represents the change in concentration due to the molecular diffusion. This is where the Monte Carlo simulation's random data is used to model the change in concentration. The Monte Carlo code then uses continuously sampled random variables to simulate a change in concentration in x and r directions.

This could also be modeled in 3D where the parabolic flow is described as:

$$u(y, z) = 1 - (y^2 + z^2) - \frac{1}{2} = \frac{1}{2} - y^2 - z^2 \qquad (15)$$

Then the SDEs are:

$$dx = Pe\left(\frac{1}{2} - y^2 - z^2\right) dt + \sqrt{2}dW_1, \qquad (16)$$

$$dy = \sqrt{2}dW_2 \qquad (17)$$

$$dz = \sqrt{2}dW_3 \qquad (18)$$

This method would require the sampling of three random variables to determine the diffusion in the x,y, and z directions. This is consistent with the 2D model because $y^2 + z^2 = r^2$.

5.1 Monte Carlo Algorithm

1) Input the physical parameters for the simulation (pipe diameter, meand flow speed, and diffusivity coefficient).

2) Determine number of random walks, the time step, and initial condition desired.

3) Model the flow deterministically while using random walk technique to model the diffusion.

4) Process the data in the form of Histogram and Moment calculations

5) Compare simulation data to numerical solutions to determine maximum error in simulation.

6) Repeat from step 2 until error threshold is met.
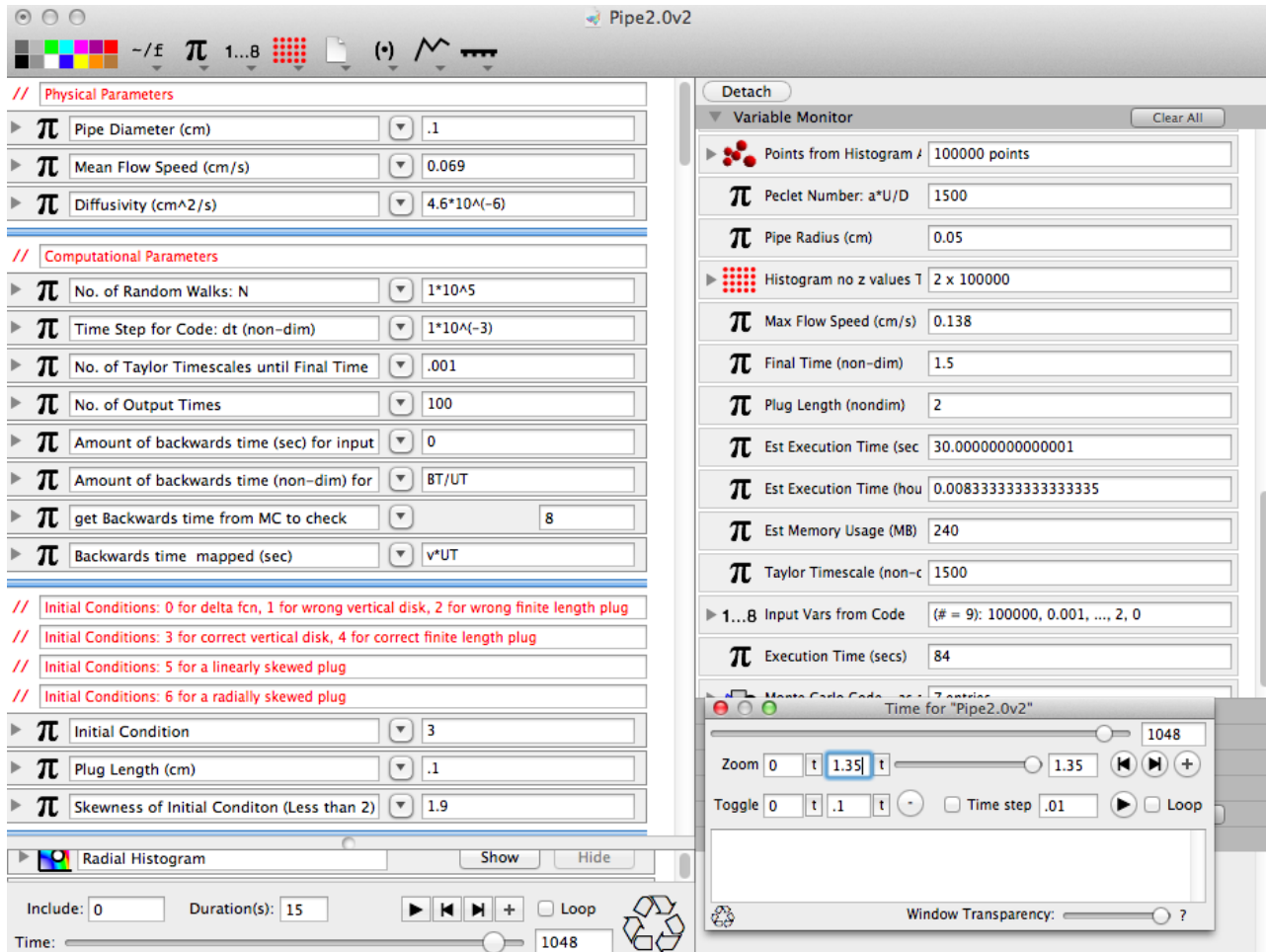
Figure 5.1: This figure shows the DataTank graphical user interface that runs the Monte Carlo simulation code. Under Physical parameters the pipe diameter, mean flow speed and diffusivity is inputted (this will determine Pe as well). Then the computational parameters are chosen along with the initial condition. Once this is inputted, then the simulation can run and the data can be analyzed.

5.2 Monte Carlo C++ Code

To run the Monte Carlo code, determine the desired number of particles and advect them with the given flow deterministically plus random noise representing the diffusion. Each particle is treated independently. The evolution of the particles collective behavior can then be studied. For this reason the the more particles used the more accurate the data is. However, a balance must be

achieved between the desired number of particles and the computation time available. After some studies, on optimal solution was determined to be 100,000 particles with a time step of 10^{-3}. A run of this size carries about an 84 second execution time to complete.

```cpp
/////////////////////////////////////////////////////////////////////////////
//    Main routine
/////////////////////////////////////////////////////////////////////////////

void Computation(double N,double dt,double Peclet,double t_final,double NoOuts,
                 double UnitTime,double InitCond,double plugL,double ICskew,
                 double Backward_Time_Fraction,double Seed,
                 DTSeriesGroup<DT_RetGroup> &computed);

int main(int argc,const char *argv[])
{
    DTSetArguments(argc,argv);

    DTDataFile inputFile("Input.dtbin",DTFile::ReadOnly);
    DTDataFile outputFile("Output.dtbin",DTFile::NewReadWrite);
    outputFile.SaveIndex();

    // Input variables.
    double N = inputFile.ReadNumber("N");
    double dt = inputFile.ReadNumber("dt");
    double Peclet = inputFile.ReadNumber("Peclet");
    double t_final = inputFile.ReadNumber("t_final");
    double NoOuts = inputFile.ReadNumber("NoOuts");
    double UnitTime = inputFile.ReadNumber("UnitTime");
    double InitCond = inputFile.ReadNumber("InitCond");
    double plugL = inputFile.ReadNumber("plugL");
    double ICskew = inputFile.ReadNumber("ICskew");
    double Backward_Time_Fraction = inputFile.ReadNumber("Backward_Time_Fraction");
    double Seed = inputFile.ReadNumber("Seed");

    // Output series.
    DTSeriesGroup<DT_RetGroup> computed(outputFile,"Var");

    // The computation.
    clock_t t_before = clock();
    Computation(N,dt,Peclet,t_final,NoOuts,UnitTime,InitCond,plugL,ICskew,Backward_Time_Fraction,Seed,computed);
    clock_t t_after = clock();
    double exec_time = double(t_after-t_before)/double(CLOCKS_PER_SEC);

    // The execution time.
    outputFile.Save(exec_time,"ExecutionTime");
    outputFile.Save("Real Number","Seq_ExecutionTime");

    // The errors.
    DTSaveError(outputFile,"ExecutionErrors");
    outputFile.Save("StringList","Seq_ExecutionErrors");

    return 0;
}
```

The Main Routine handles the inputs of the code and creates the computation. It takes the inputs from an input file. They are N is the number of particles, dt is the time step, $Peclet$ is the Peclet number (determined by the physical parameters), t_final is the stopping time based on one Taylor Time Scale, $NoOuts$ is data outputs; $UnitTime$ is the dimensional time, BCs represent the boundary conditions being used, and $plugL$ is the plug length for the simulation. All of these inputs can be manually determined and inputted into the DataTank Script. The code also initiates two counting mechanisms to determine the computational time of the simulation.

```
/* velocity profile */
// mean zero to do the case with walls
// radial parabolic flow with mean 1/2 (double checked)
// 1 - (y^2+z^2) - 1/2
double u_fcn(double y, double z)  {
    double u = (0.5 - pow(y,2.) - pow(z,2.));
    return u;
}

#include "DTRandom.h"

/* The Monte Carlo Simulation */

void Computation(double N,double dt,double Peclet,double t_final,double NoOuts,
                 double UnitTime,double InitCond,double plugL,double ICskew,
                 double Backward_Time_Fraction,double Seed,
                 DTSeriesGroup<DT_RetGroup> &computed)
{

    DTProgress progress;
    DT_RetGroup returnStructure; // Fill this at each time value.

    double x, y, z, x_jump, y_jump, z_jump, rad, theta, rSkew, maxSkew;
    int k, k1, k2, count1, count2, i, j;
```

The above section of the code sets the 2D and 3D parabolic shear flow and begins the Monte Carlo simulation. The shear flow is calculate as a function of distance from the radial axis as described above. The next section establishes the computation that takes the inputs and establishes all needed doubles and integers for running the simulation.

```
// Variables used for Box Muller Random Number Generator
// double u1,u2;
/* vertical line initial condition; in reality a disk */
else if(ICint==3) {
    x = 0;
    // rad = gsl_rng_uniform(r);
    rad = r.UniformOpen();
    rad = sqrt(rad);
    //theta = 2. * PI * gsl_rng_uniform(r);
    theta = 2. * PI * r.UniformOpen();
    y = rad*cos(theta);
    z = rad*sin(theta);
}
/* finite length plug initial condition */
else if(ICint==4) {
    //x = gsl_rng_uniform(r);
    x = r.UniformOpen();
    x = (x-0.5)*plugL;
    //rad = gsl_rng_uniform(r);
    rad = r.UniformOpen();
    rad = sqrt(rad);
    // theta = 2. * PI * gsl_rng_uniform(r);
    theta = 2. * PI * r.UniformOpen();
    y = rad*cos(theta);
    z = rad*sin(theta);
}
```

The next section of code defines the initial conditions of the problem. The initial conditions are selected by the input variable BCs. If $BCs = 3$ the computation uses the vertical line initial condition or a disk. If $BCs = 4$ the computation uses the finite length plug initial conditon.

Figure 5.2: This figure shows the (x,y) Histogram representation of the intial conditions. The picture on the left represents initial conditon 3 which is the vertical disk of dye solute. The picture on the right represents a plug of finite lenth for the initial condition of the dye solute.

```
// Use Box Muller transform
u1 = rand_step*sqrt(fabs(2*r.UniformOpen()));
u2 = 2*M_PI*r.UniformOpen();
x_jump = u1*cos(u2);
//y_jump = u1*sin(u2);
r_jump = u1*sin(u2);
//u1 = rand_step*sqrt(fabs(2*r.UniformOpen()));
//u2 = 2*M_PI*r.UniformOpen();
//z_jump = u1*cos(u2);


if(count2<Backward_Time_Fraction){
    flow_direction=-1;
}
else{
    flow_direction=1;
}
/* dX = u(y,z) + sigma dW1 */
x = x + flow_direction*u_fcn(y,z)*dt + x_jump;
/* dY = sigma dW2 */
//y = y + y_jump;
/* dZ = sigma dW3 */
//z = z + z_jump;
//theta = 2. * PI * gsl_rng_uniform(r);
theta = 2. * PI * r.UniformOpen();
y = r_jump*cos(theta);
z = r_jump*sin(theta);

/* reflecting boundary conditions for walls */
// I am almost certain that this is the wrong BC
// because I need to reflect off of the wall at the same angle that I hit the wall
// which this does not do, but its a sensible start
if(pow(y,2.)+pow(z,2.) > 1.)  {
    rad = sqrt( pow(y,2.)+pow(z,2.) );
    y = (2. - rad)/rad * y;
    z = (2. - rad)/rad * z;
} // out of boundary conditions //

} // out of time-loop //
```

The next section of code calculates the solution to the SDEs using the Box Muller Transform random numbers. Box Muller transform is a pseudo-random number sampling method for generating pairs of independent, normally-distributed random numbers. The inputs must be a uniformly distributed

random numbers. Here the diffusion in the x and r directions are represented by x_{jump} and r_{jump}, respectively. These variables are defined as

$$x_{jump} = R \cos \phi = \sqrt{-2 \ln U_1} \cos (2\pi U_2)$$

$$r_{jump} = R \sin \phi = \sqrt{-2 \ln U_1} \sin (2\pi U_2)$$

Where U_1 and U_2 are independent random variable that are uniformly distributed in the interval (0,1]. Then x_{jump} and r_{jump} are independent random variable with a standard normal distribution. In the 3D version the Box Muller method is repeated to determine y_{jump} and z_{jump} the same way. The code then updates the x and r values for the 2D method and the x, y, and z values for the 3D method using the reflecting boundary conditions. During the loop it outputs a percentage complete update by outpuint the iterations complete over the total iterations.

```
/* return the Input to the Output file for convenience */
DTMutableDoubleArray InputList(9);
InputList(0) = N;
InputList(1) = dt;
InputList(2) = Peclet;
InputList(3) = t_final;
InputList(4) = NoOuts;
InputList(5) = UnitTime;
InputList(6) = InitCond;
InputList(7) = plugL;
InputList(8) = Backward_Time_Fraction;
InputList(9) = Seed;
returnStructure.InputVars = InputList;

/* output the moments to DataTank */
double tND = 0.0;              // Non-Dim Time //
double tDim = 0.0;      // Dimensional Time (seconds) //

for(k1 = 0; k1 < NoOuts1; k1++) {

    /* output moments */
    returnStructure.M1 = M1[k1];
    returnStructure.M2 = M2[k1];
    returnStructure.M3 = M3[k1];
    returnStructure.M4 = M4[k1];

    /*output the Hist array */
    for(count1 = 0; count1 < Nint; count1++) {
        HistOut(count1,0) = HistArray[count1][k1][0];
        HistOut(count1,1) = HistArray[count1][k1][1];
        HistOut(count1,2) = HistArray[count1][k1][2];
    }
    returnStructure.Hist = HistOut;

    /* ouput time dependent values to output file */
    computed.Add(returnStructure,tDim);
    tND = tND+dt1;
    tDim = tND * UnitTime;
}  // out of time dt1 loop //

/* end the computation */
```

This final section of code produces the two time outputs to show the computation time of the simulation. It then returns all the input values as outputs to the graphical user interface for conveniece purposes. Finally, it outputs the moments and the histogram arrays to DataTank for analysis. Now the Monte Carlo Simulation moments and variance plots can be drawn and analyzed via the DataTank scripts.

6 Numerical Results

The results of the Monte Carlo simulations tend to agree with the analytical theory presented by Camassa, Lin, and McLaughlin. As discussed, the data can be viewed in a number of ways. This can be done through the moment Histogram array, the variance scaled by time and the variance not scaled by time. Once the standard number of particles and time steps were adopted, then studies could be developed to test different physical parameters. Some of the parameters studied were changing the flow rate (and thus the Peclet number), looking at different initial conditions, and varying the size of the plug length. The purpose of these studies are to have multiple varying data sets that can be compared to experimental data.

6.1 Moment Histograms

The moment histogram are capable of producing 2D images and 3D renderings of what the plug evolution looks like during the advection-diffusion process. These are useful for creating videos of the plug evolution and other visualization purposes. Additionally, the histograms are used for creating the moment data that is used for the variance plots. This is done similar to the analysis of the experimental data by creating partial planar slice lines. These lines are drawn at the center of the tube, on the boundary, and halfway between the boundary and the center. A sample of pictures of the visualizations are contained below.
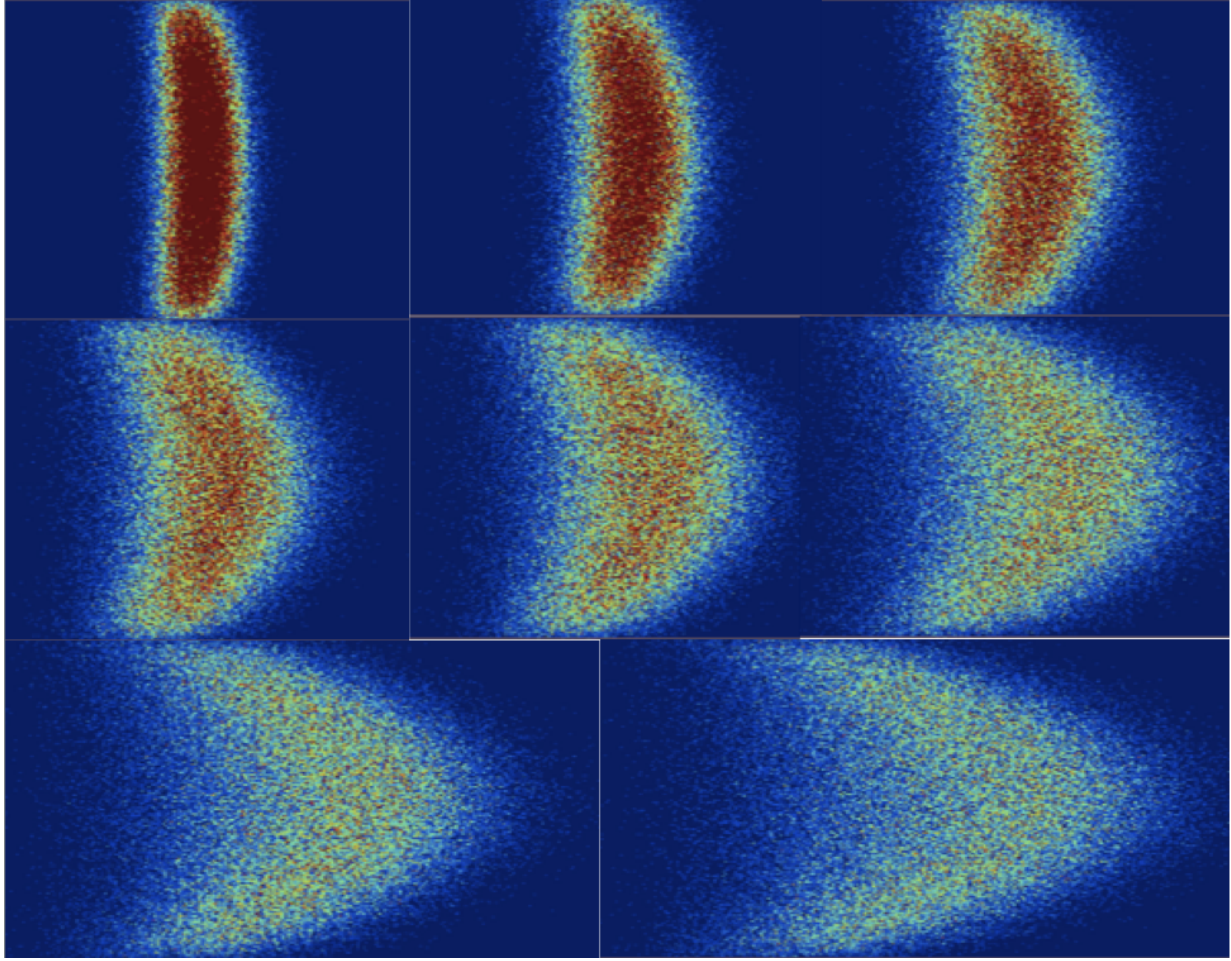
Figure 6.1: The figure above shows pictures of the (x,y) Histogram of the plug evolution for initial condition 3 (Disk). From left to right, top to bottom the eight pictures show the plug evolution at timesteps 2, 4, 6, 8, 12, 16, 20 and 24.
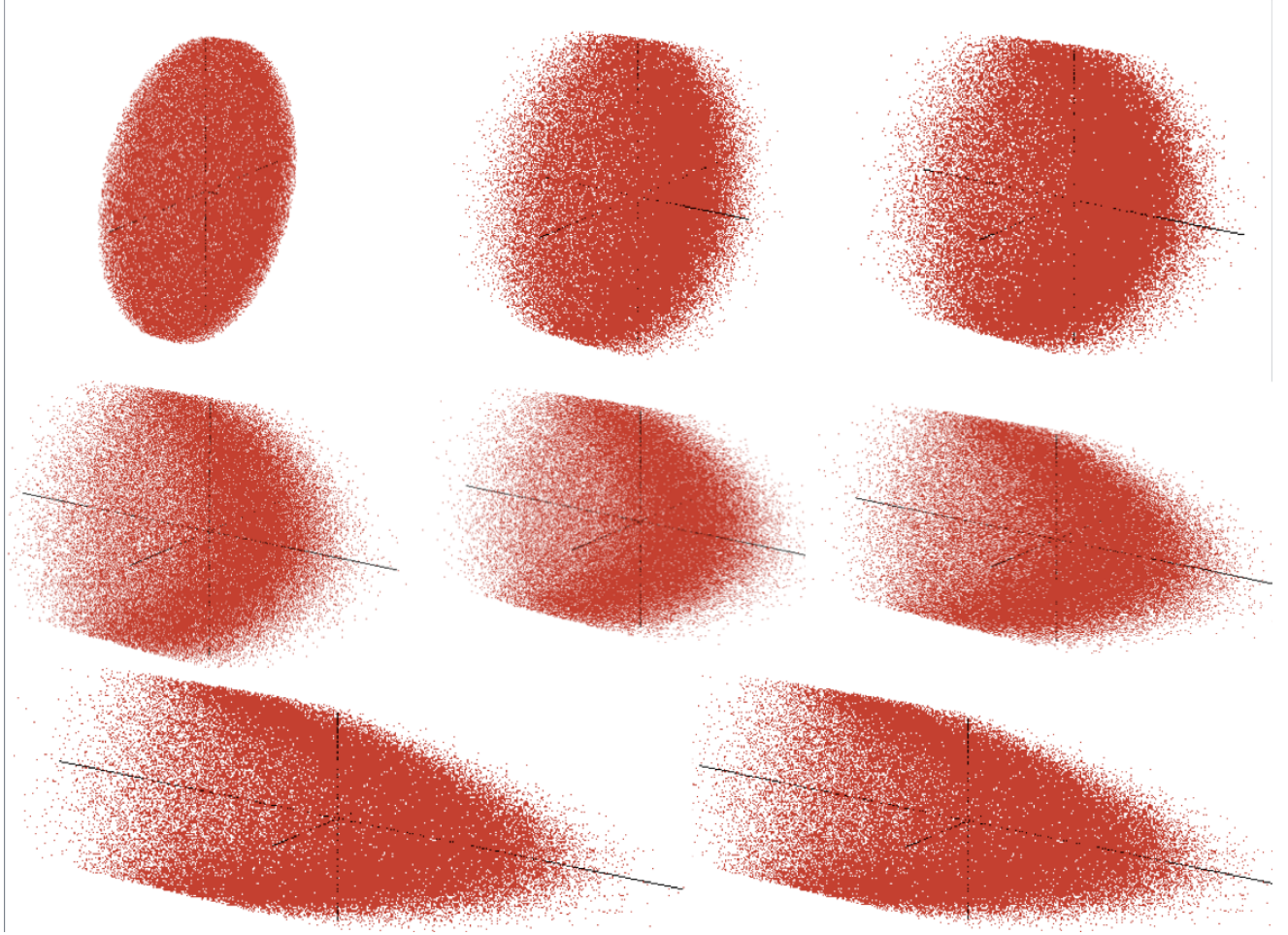
Figure 6.2: The figure above shows pictures of a 3D rendering of the Histogram array of the plug evolution for initial condition 4 (Plug of Finite Length). From left to right, top to bottom the eight pictures show the plug evolution at timesteps 1, 5, 9, 13, 21, 29, 45 and 61.

6.2 Variance Scaled by Time

The variance scaled by time studies were run for both the disk initial condition and the plug of finite length initial condition. The first study was for the disk initial condition. Here the Peclet was varied from 150-2500. This was done with a constant pipe diameter of .1 cm and constant diffusivity coefficient of 4.9×10^{-6}. The only physical parameter changed was the mean flow speed. The lines drawn are representative of the y-average concentrations.
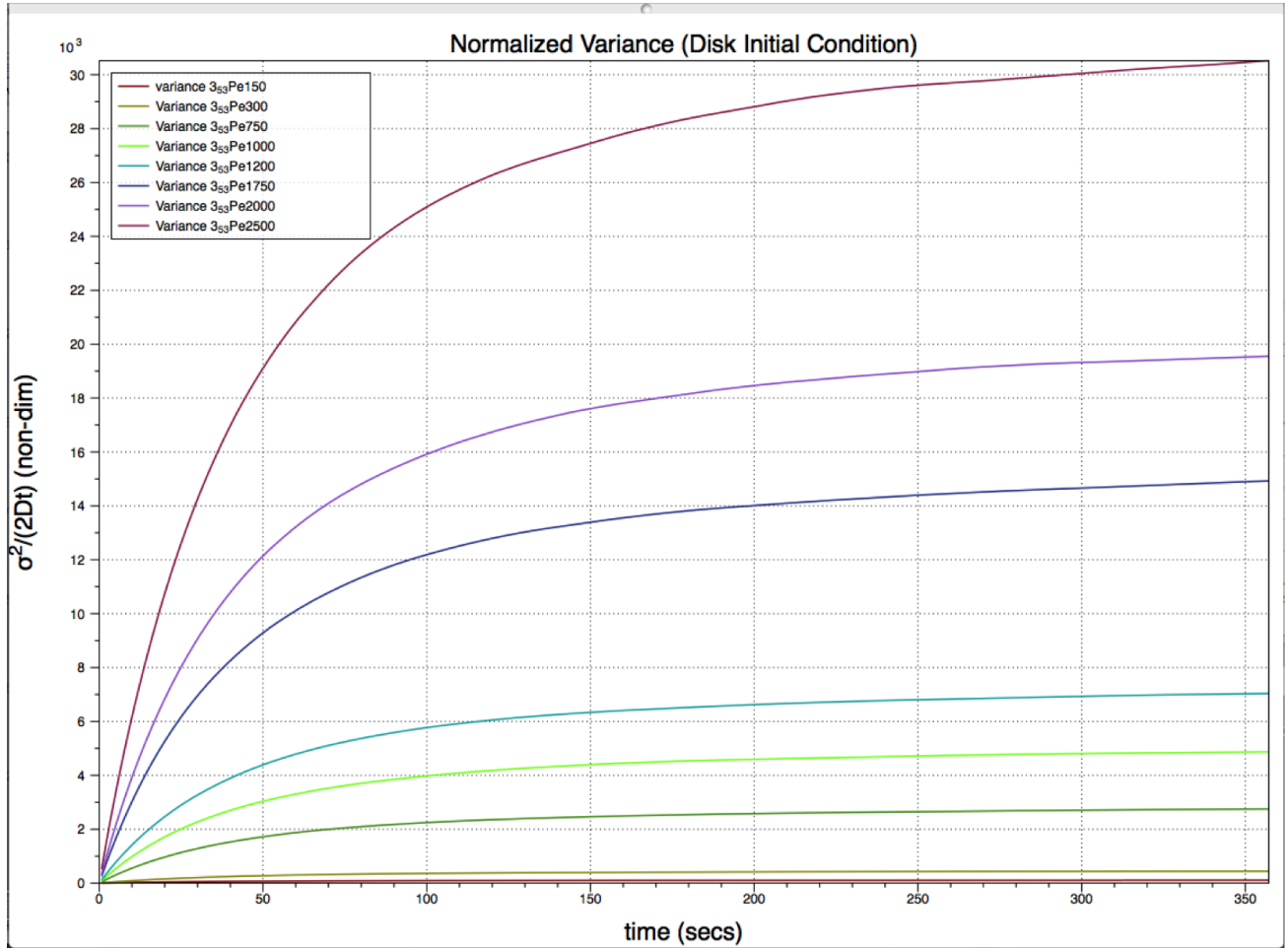

Figure 6.3: The figure above shows variance scaled by time using the disk initial condition. Holding all other variables constant, the Peclet number was varied from 150 to 2500. All of the data sets converge to the Asymptote line of $\frac{Pe^2}{192}$ which is consistent with the analytical theory. For example the blue line that represents the Peclet number of 1200 converges to 7500.

The next variance study conducted uses initial condition four, a plug of finite length. In the next nine figures the graphs represent the variance scaled by time. All were conducted with a pipe of .1 cm diameter and a diffusivity coefficient of 4.9×10^{-6}. Again the only physical parameter change was mean flow speed. Thus the Peclet number varies and data was created for Peclet numbers of 150, 300, 750, 1000, 1200, 1750, 2000, 2500, and 5000. All of the plots contain the Monte Carlo simulated variance scaled by time at the partial planar slices at the center, boundary, and middle. Additionally, the graphs contain the y-average solution and the analytical solution.
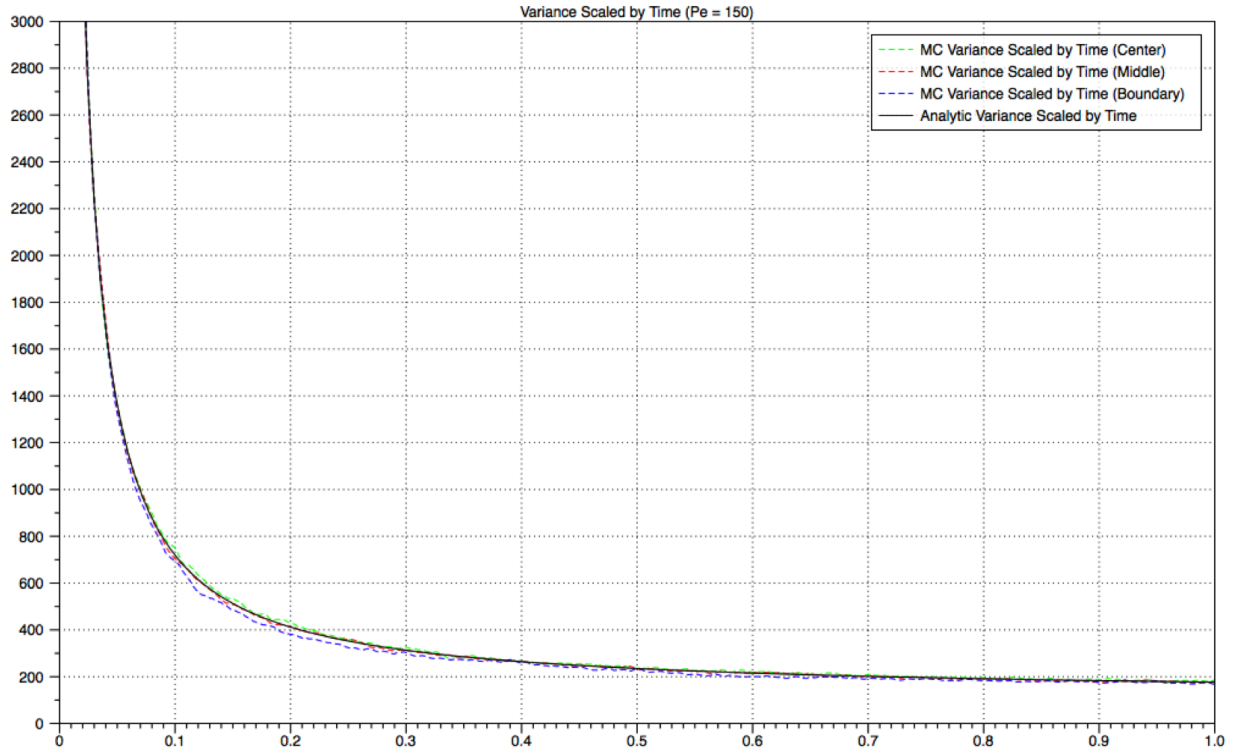

Figure 6.4: This figure shows variance scaled by time on the y-axis and time on the x-axis. This data represents a 150 Peclet number.

Figure 6.5: This figure shows variance scaled by time on the y-axis and time on the x-axis. This data represents a 300 Peclet number.

Figure 6.6: This figure shows variance scaled by time on the y-axis and time on the x-axis. This data represents a 750 Peclet number.
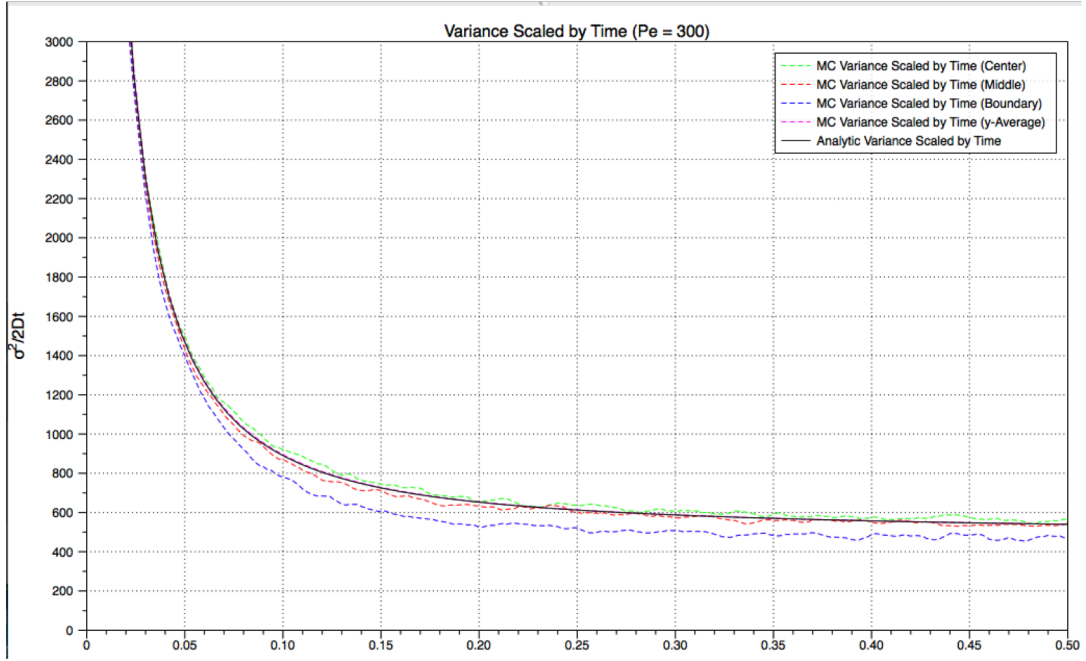
Figure 6.7: This figure shows variance scaled by time on the y-axis and time on the x-axis. This data represents a 1000 Peclet number.
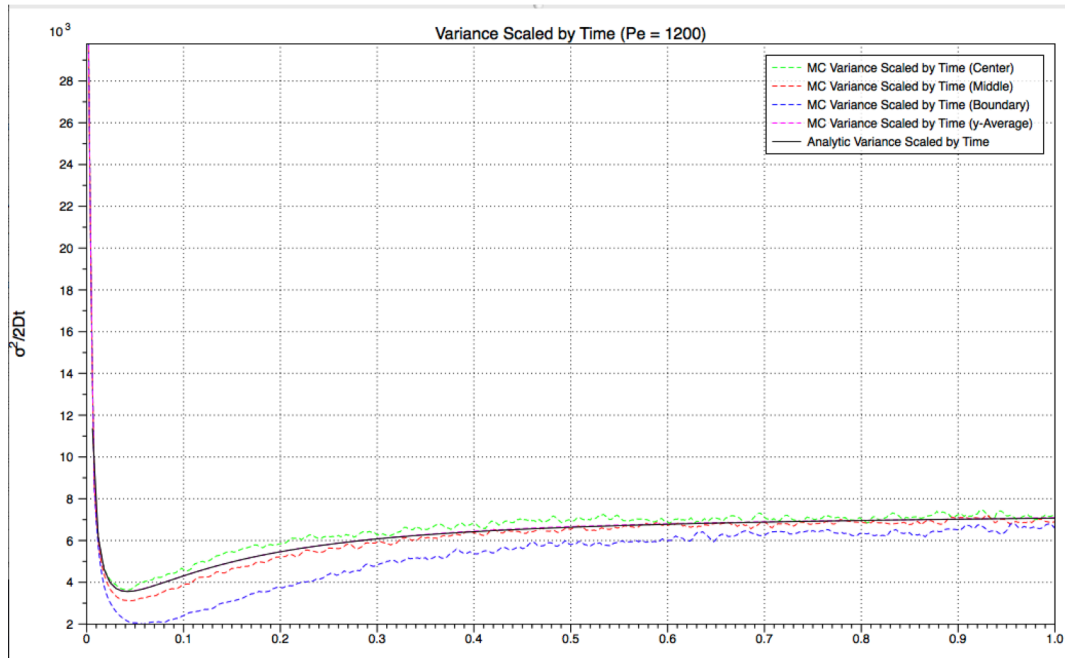
Figure 6.8: This figure shows variance scaled by time on the y-axis and time on the x-axis. This data represents a 1200 Peclet number.
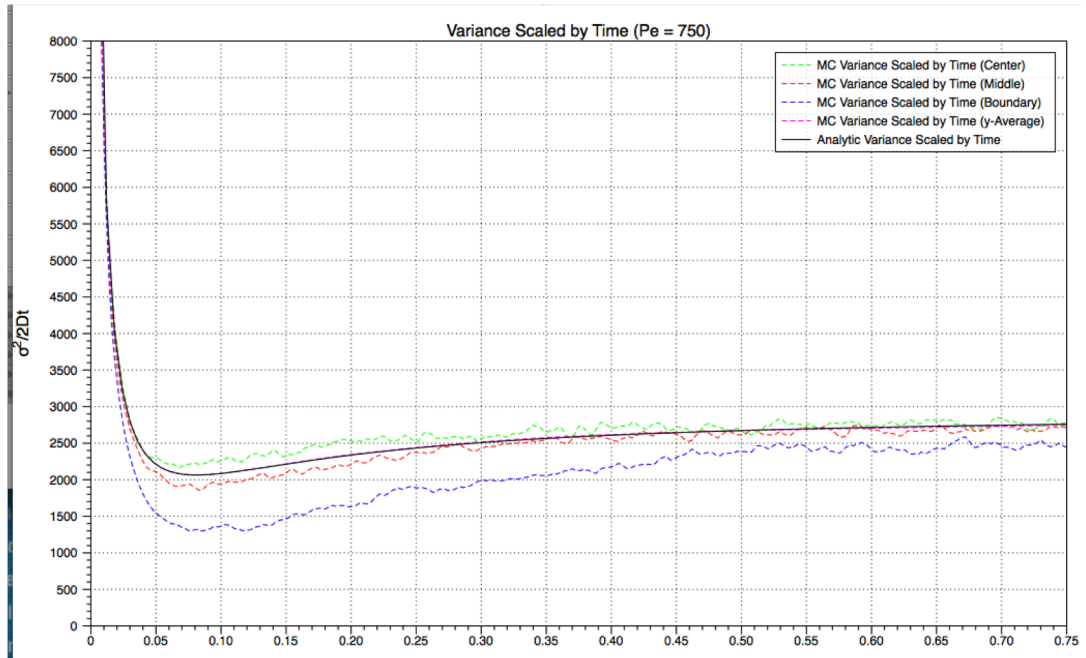
Figure 6.9: This figure shows variance scaled by time on the y-axis and time on the x-axis. This data represents a 1750 Peclet number.
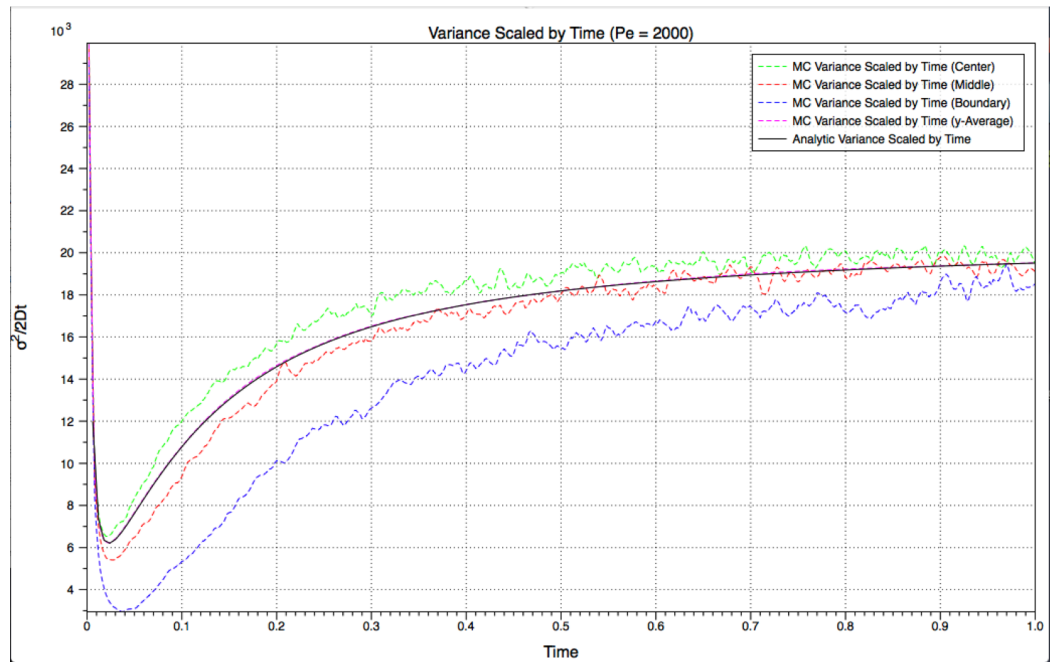
Figure 6.10: This figure shows variance scaled by time on the y-axis and time on the x-axis. This data represents a 2000 Peclet number.

Figure 6.11: This figure shows variance scaled by time on the y-axis and time on the x-axis. This data represents a 2500 Peclet number.
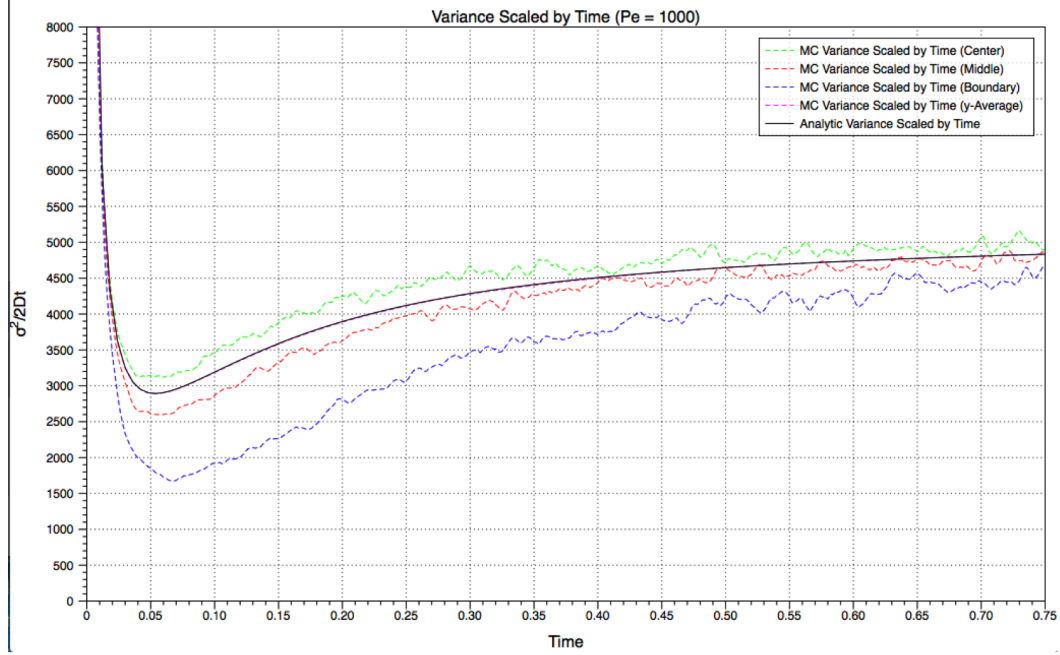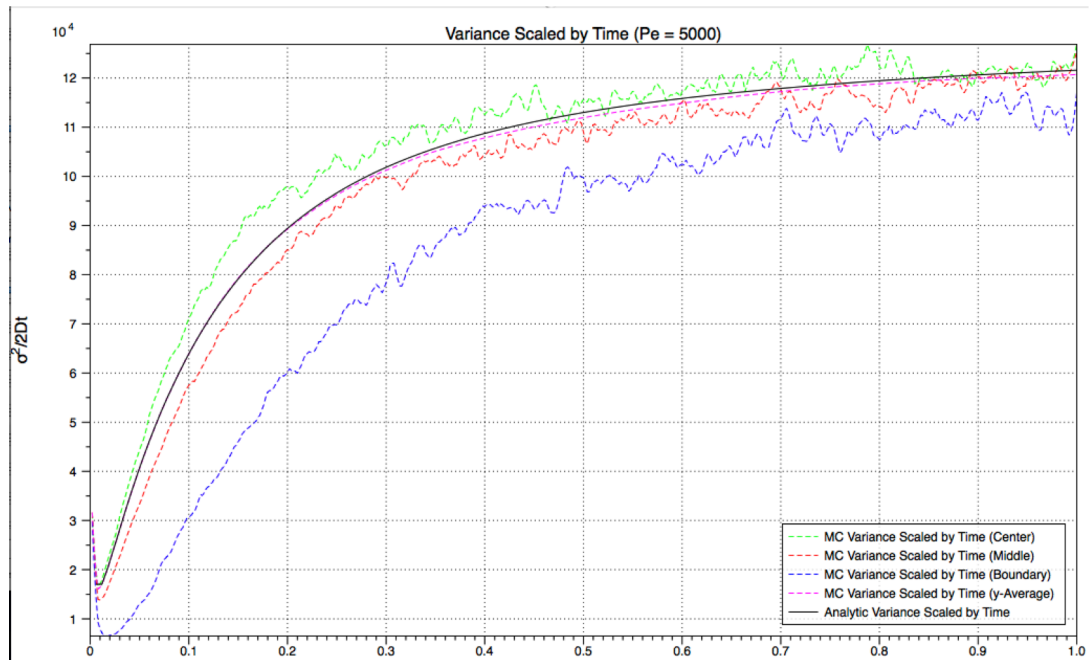

Figure 6.12: This figure shows variance scaled by time on the y-axis and time on the x-axis. This data represents a 5000 Peclet number.
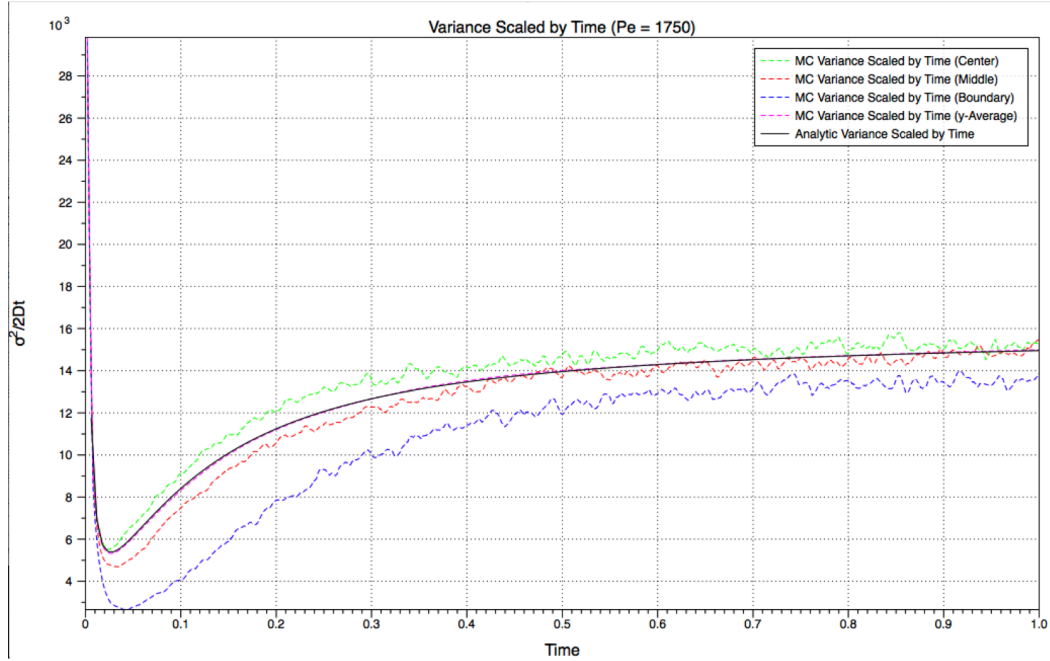
The final variance scaled by time chart shows the y-average values the previous 9 charts on one single chart. This gives a more complete picture of how a varying Peclet number can effect the Variance scaled by time.
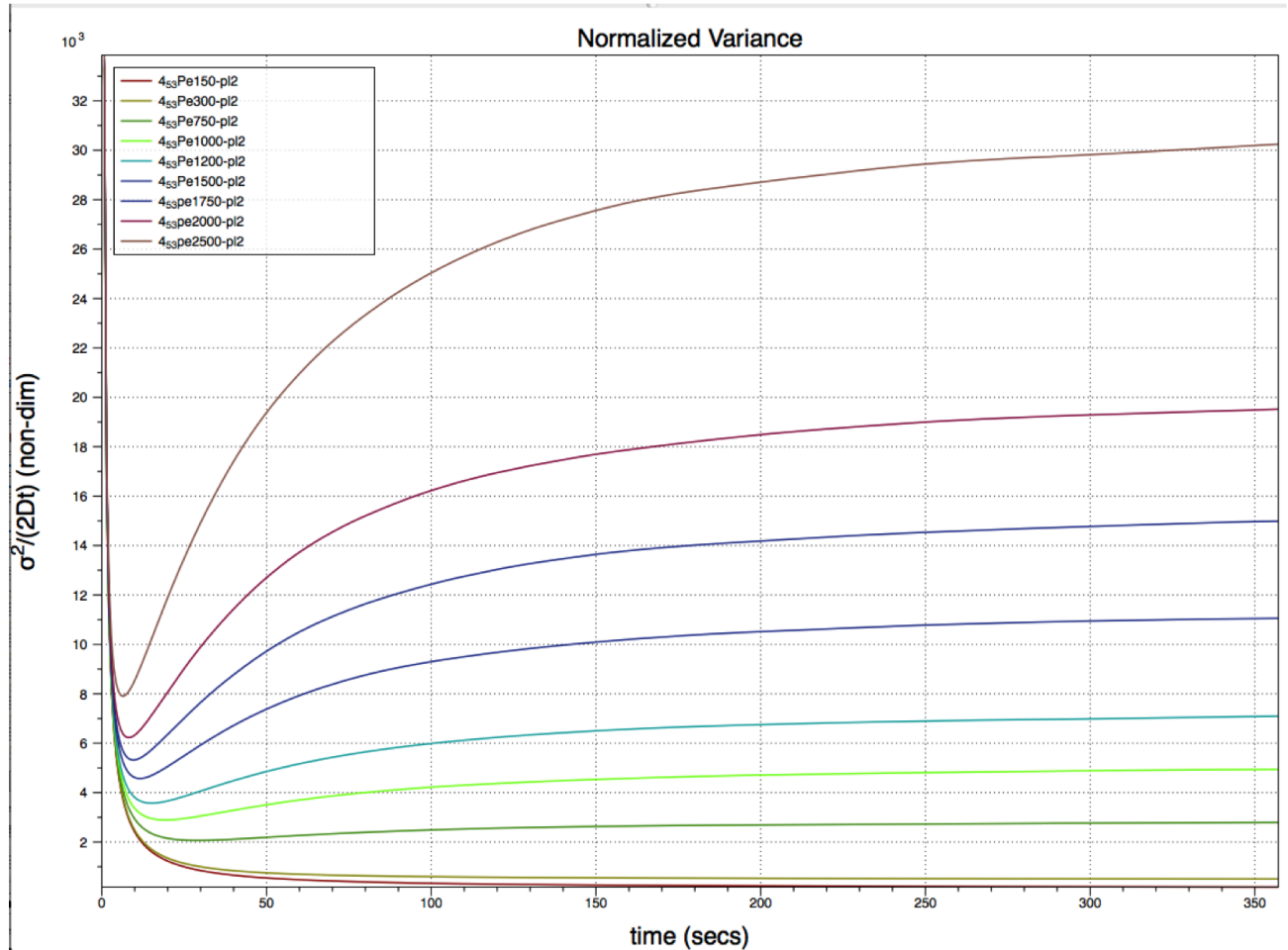
Figure 6.13: This figure shows the y-Average Variance Scaled by Time from figures 6.4 to 6.12

6.3   Variance Not Scaled by Time

The final variable analysis conducted was to vary plug length keeping all other conditions constant. The Monte Carlo simulations that were run kept a constant pipe diameter of .1 cm, a constant diffusivity coefficient of 4.9×10^{-6}, and a constant mean speed velocity of $0.0735 \frac{cm}{sec}$. This made all the runs have a Peclet number of 1500. Then the plug length was varied from 1 cm to 10 cm. The easiest way to show this data was graph it as Non-Normalized Variance or Variance not scaled by time.
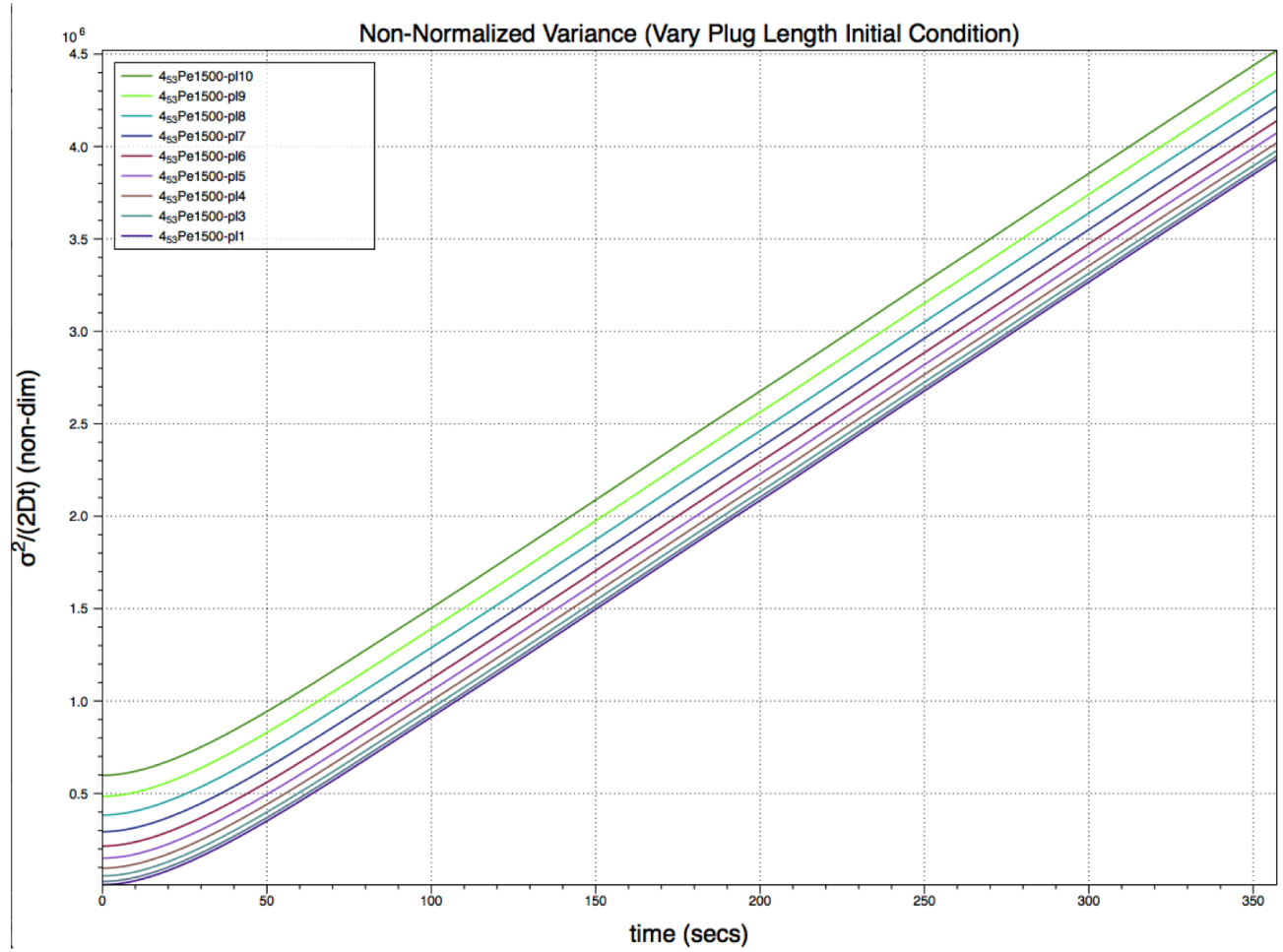
Figure 6.14: This figure shows the Non-Normalized Variance of 10 separate Monte Carlo simulation runs. All variables are held fixed except the plug length, which varies from 1 cm to 10 cm.

This data is consistent with the theory as the variance quickly becomes linear after one Taylor time scale:

$$t_1 = \frac{a^2}{(3.8)^2 D} = \frac{.05^2}{(3.8)^2 (4.9 \times 10^{-6})} = 35.33 \; sec$$

7 Experimental Results

The current results focus on the production of intensity curves and the normalized variance for each set of experimental data. The normalized variance is then compared to the analytic and numerical solutions produced in the previous sections. To this point, most of the experimental data does not consistently agree with the analytic and numerical solutions. For the two data sets taken on 6/11/12 and 9/17/12 the data was close enough to produce meaningful error plots for the normalized variance. For these two data sets, the errors are shown in two separate charts: Absolute Error and Relative Error. The following table shows the available data.

	Date	ID (cm)	Peclet	Velocity (cm/s)	Pixels per cm	Concentration of Fluorescein (g/L)	Liquid Used	Comments
M1	3/25/11	0.05	612	0.06000	110	0.25	Water	Data Conducted by Will Miliken
M2	3/28/11	0.05	612	0.06000	110	0.25	Water	Data Conducted by Will Miliken
M3	3/30/11	0.05	750	0.07350	115	0.25	Water	Data Conducted by Will Miliken
M4	4/4/11	0.05	750	0.07350	115	0.25	Water	Data Conducted by Will Miliken
M5	7/15/11	0.05	600	0.05880	112	0.30	Water	Data Conducted by Will Miliken
M6	8/1/11	0.05	600	0.05880	112	0.30	Water	Data Conducted by Will Miliken
M7	2/17/12	0.05	600	0.05880	130	0.40	Water	Data Analyzed, Does not Match
M8	3/20/12	0.05	175	0.01720	116	0.40	Water	Data Analyzed, Does not Match
M9	3/22/12	0.05	125	0.01225	116	0.40	Water	Data Analyzed, Does not Match
M10	3/23/12	0.05	150	0.01470	112	0.40	Water	Data Analyzed, Does not Match
M11	4/3/12	0.05	150	0.01470	112	0.40	Water	Data Analyzed, Does not Match
M12	4/12/12	0.05	150	0.01470	117	0.40	Water	Data Analyzed, Does not Match
N1	6/7/12	0.25	375	0.03675	120	0.60	Water	Plug too long, Asymmetrical
N2	6/11/12	0.25	375	0.03675	110	0.60	Water	Data Analyzed, Best Data Taken
N3	6/12/12	0.25	375	0.03675	192	0.60	Water	Plug too long, Asymmetrical
N4	7/25/12	0.25	375	0.03675	351	0.60	Water	Asymmetrical plug, reflection issues
N5	7/30/12	0.25	375	0.03675	355	0.60	Water	Asymmetrical plug
N6	9/10/12	0.25	375	0.03675	348	0.60	Water	Tube Reflection Issues, Asymmetrical
N7	9/17/12	0.25	375	0.03675	262	0.60	Water	Data Analyzed, Does not Match
N8	9/24/12	0.25	375	0.03675	265	0.60	Water	Asymmetrical plug, reflection issues
N9	10/1/12	0.25	375	0.03675	267	0.60	Salt Water	Data not Analyzed Yet
N10	10/8/12	0.25	375	0.03675	261	0.60	Salt Water	Turbulence when Dye Introduced
N11	10/22/12	0.25	375	0.03675	261	0.60	Salt Water	Data Analyzed, Does not Match
N12	10/29/12	0.25	375	0.03675	261	0.60	Karo	Data Analyzed, Does not Match
N13	11/5/12	0.25	375	0.03675	X	0.60	Karo	Data Not Found on Hard Drive
N14	11/12/12	0.25	375	0.03675	X	0.60	Water/Karo	Data Not Found on Hard Drive
N15	11/26/12	0.25	375	0.03675	X	0.60	Water/Karo	Data Not Found on Hard Drive
N16	12/3/12	0.25	375	0.03675	265	0.60	Water	Asymmetrical plug, reflection issues
N17	1/22/13	0.25	375	0.03675	260	0.60	Water	Tube Reflection Issues, Asymmetrical
N18	2/12/13	0.05	150	0.01470	260	0.30	Water	Bowing in Tube, Data Unusable
N19	2/18/13	0.05	150	0.01470	262	0.30	Water	Bowing in Tube, Data Unusable
N20	2/28/13	0.05	150	0.01470	262	0.30	Water	Plug Not Visible in Data
N21	3/4/13	0.05	300	0.02940	350	0.30	Water	Data not Analyzed Yet

Figure 7.1: The above table shows the experimental data taken from 3/25/11 to 3/4/13. The rows highlighted in yellow indicate experiments that have been analyzed and included in this section.

7.1 Experimental Results 3/22/12

The following is the experimental results for the data taken on 3/22/12. The inner diameter of the tube used was $0.10\ cm$. The Peclet Number was 125 with a velocity of $.01225\ \frac{cm}{s}$. The passive scalar used was $0.4\ \frac{g}{L}$ Fluorescein in Dionized Water and the fluid in the system was Dionized Water. The pixels per cm measured for this experiment was 116. The data was analyzed and intensity plots with bitmap images were produced at images 1, 250, and 447. The shooting interval was 1 frame per second with a total of 450 frames (7 minutes, 30 seconds elapsed time). The Normalized Variance plots were drawn comparing the center and middle partial planar slices and Y-Average to the analytic solution.
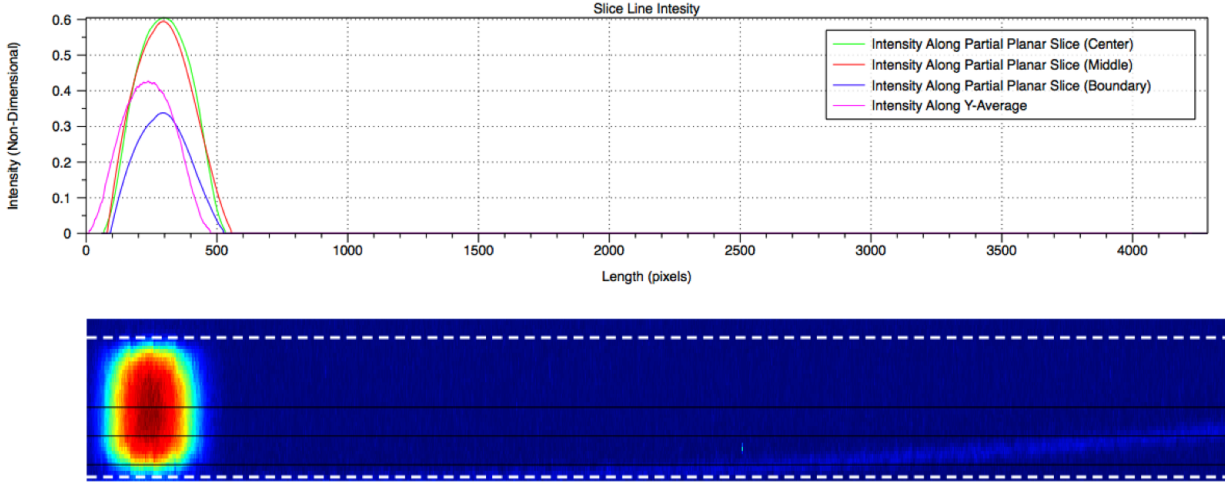
Figure 7.2: The chart above (upper) shows the Intensity (Non-Dimensional) vs. the Position in the Tube (measured in Pixels) of the bitmap image (lower). The intensity plots are shown for the Center, Middle, and Boundary Partial Planar Slices and the intensity along the Y-Average. This data represents Image 1 (1 second elapsed time) of the data set taken on 3/22/12.
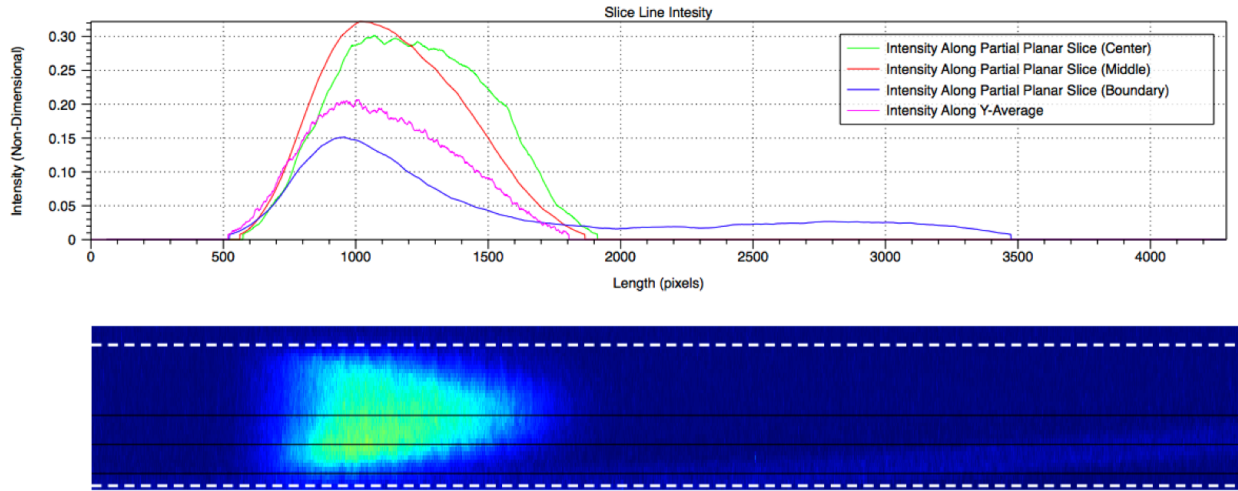

Figure 7.3: The chart above (upper) shows the Intensity (Non-Dimensional) vs. the Position in the Tube (measured in Pixels) of the bitmap image (lower). The intensity plots are shown for the Center, Middle, and Boundary Partial Planar Slices and the intensity along the Y-Average. This data represents Image 250 (4 minutes, 10 seconds elapsed time) of the data set taken on 3/22/12.
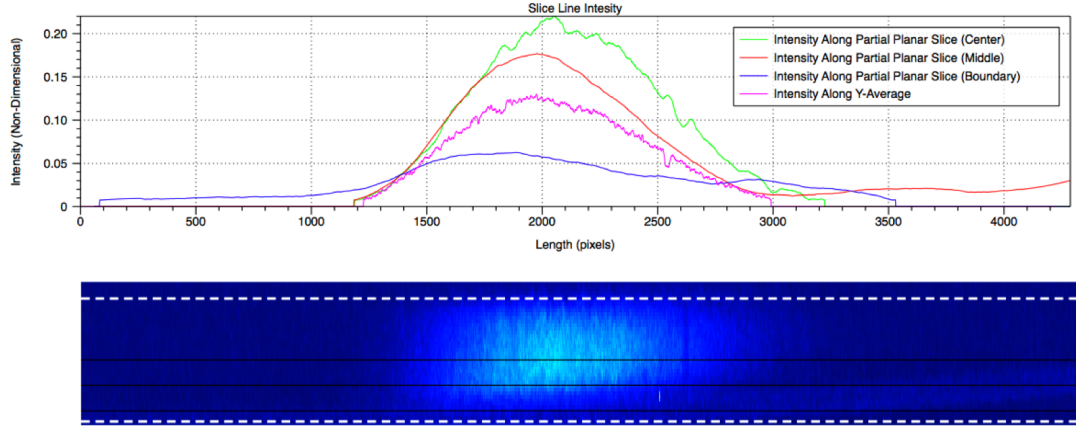
Figure 7.4: The chart above (upper) shows the Intensity (Non-Dimensional) vs. the Position in the Tube (measured in Pixels) of the bitmap image (lower). The intensity plots are shown for the Center, Middle, and Boundary Partial Planar Slices and the intensity along the Y-Average. This data represents Image 447 (7 minutes, 27 seconds elapsed time) of the data set taken on 3/22/12.
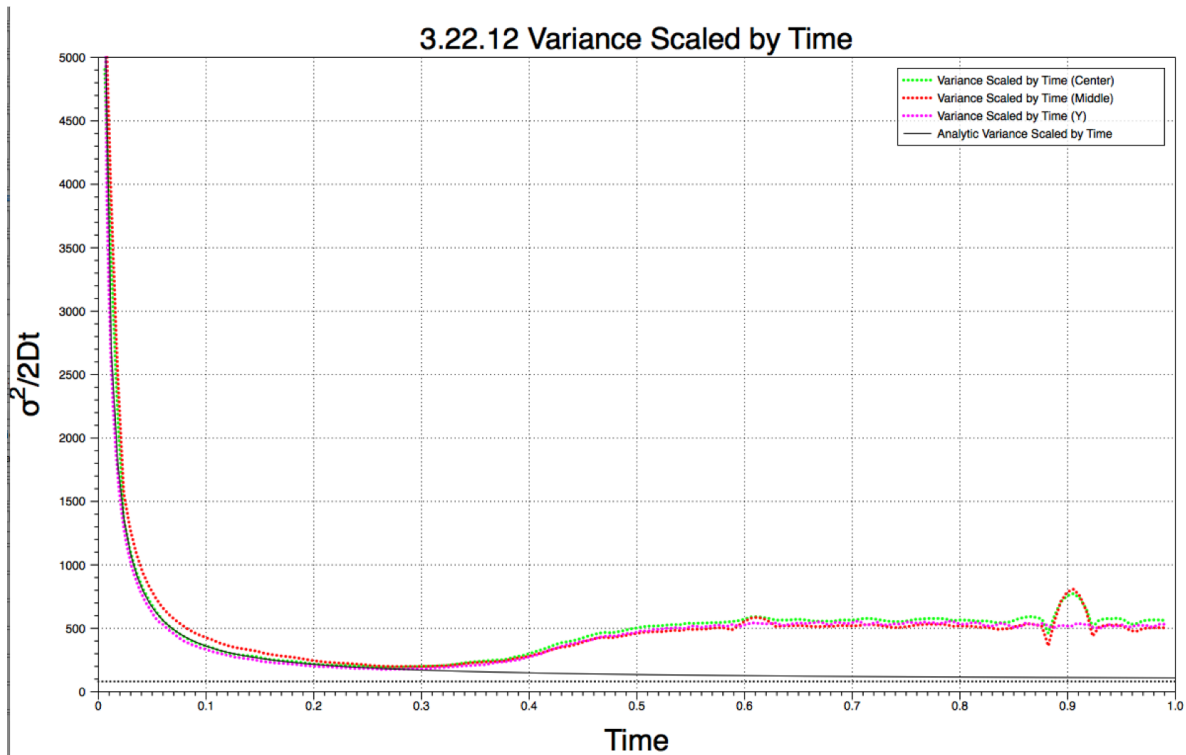
Figure 7.5: The chart above shows the Normalized Variance (Non-Dimensional) vs. Time (Non-Dimensional). The Normalized Variance plots are shown for the Center and Middle Partial Planar Slices, the Y-Average, and the Analytic Solution. This data represents all 450 images (7 minutes, 30 seconds elapsed time) of the data set taken on 3/22/12.

The initial condition of the plug shown in Figure 7.2 shows a nearly symmetrical plug with respect

to the longitudinal axis. The intensity plot is consistent with what is expected by the numerical simulations. However, in the bitmap of Figure 7.3, 4 minutes, 10 seconds into the experiment, shows a slight asymmetry in the longitudinal axis. Frame 250 occurs at apporimately 0.55 non-dimensional time in Figure 7.5. It is seen that the experimental normalized variance has risen well above the analytic solution by that point. Although the intensity plots seem to be reasonable, the significant difference in normalized variance is not. Due to the significant inaccuracies of the normalized variance shown Figure 7.5 an error study did not produce meaningful data. At this point, the source of this error is unknown. A further discussion of the possible errors will be considered in the following chapter.

7.2 Experimental Results 4/12/12

The following is the experimental results for the data taken on 4/12/12. The inner diameter of the tube used was 0.10 cm. The Peclet Number was 125 with a velocity of .01225 $\frac{cm}{s}$. The passive scalar used was 0.4 $\frac{g}{L}$ Fluorescein in Dionized Water and the fluid in the system was Dionized Water. The pixels per cm measured for this experiment was 117. The data was analyzed and intensity plots with bitmap images were produced at images 1, 65, 172, and 402. The shooting interval was 1 frame per second with a total of 450 frames (7 minutes, 30 seconds elapsed time). The Normalized Variance plots were drawn comparing the center and middle partial planar slices and Y-Average to the analytic solution.

Figure 7.6: The chart above (upper) shows the Intensity (Non-Dimensional) vs. the Position in the Tube (measured in Pixels) of the bitmap image (lower). The intensity plots are shown for the Center, Middle, and Boundary Partial Planar Slices and the intensity along the Y-Average. This data represents Image 1 (1 second elapsed time) of the data set taken on 4/12/12.
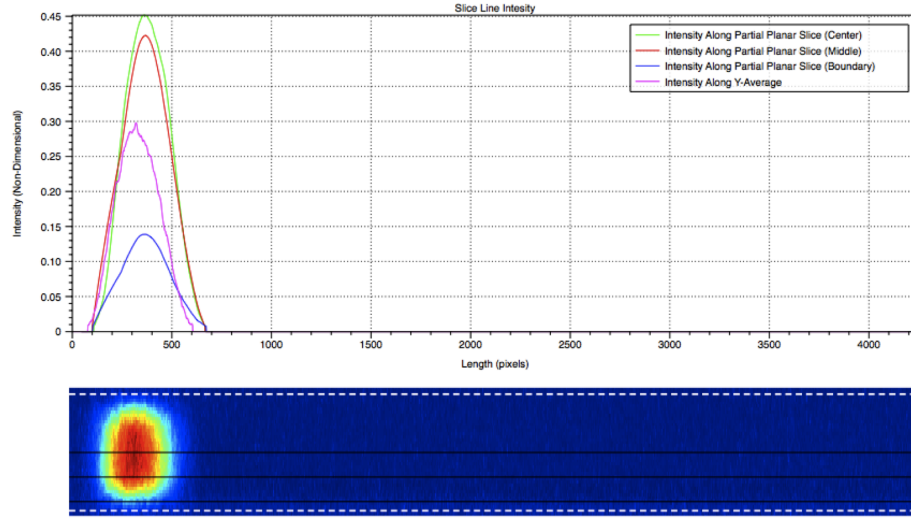

Figure 7.7: The chart above (upper) shows the Intensity (Non-Dimensional) vs. the Position in the Tube (measured in Pixels) of the bitmap image (lower). The intensity plots are shown for the Center, Middle, and Boundary Partial Planar Slices and the intensity along the Y-Average. This data represents Image 65 (1 minute, 5 seconds elapsed time) of the data set taken on 4/12/12.

Figure 7.8: The chart above (upper) shows the Intensity (Non-Dimensional) vs. the Position in the Tube (measured in Pixels) of the bitmap image (lower). The intensity plots are shown for the Center, Middle, and Boundary Partial Planar Slices and the intensity along the Y-Average. This data represents Image 172 (2 minutes, 52 seconds elapsed time) of the data set taken on 4/12/12.
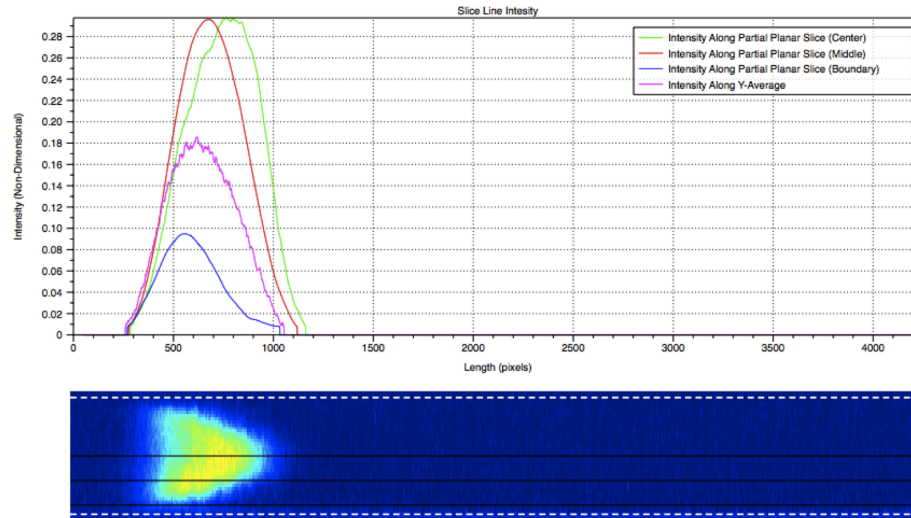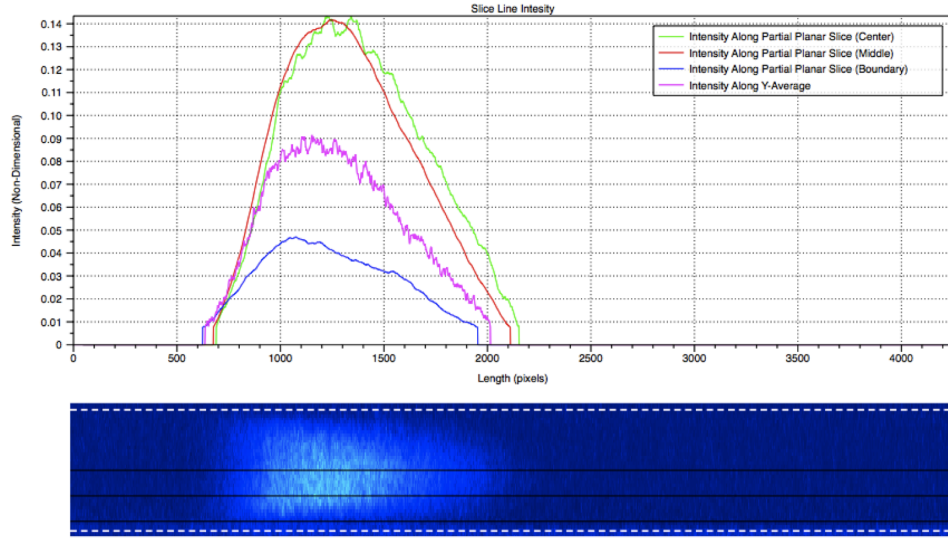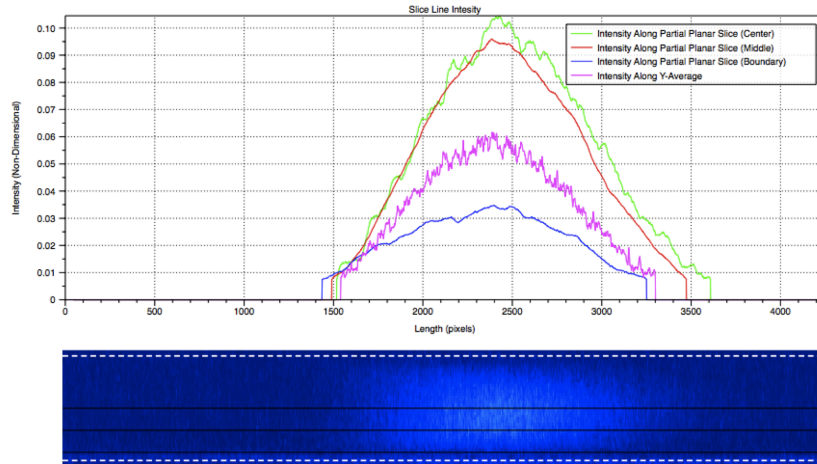

Figure 7.9: The chart above (upper) shows the Intensity (Non-Dimensional) vs. the Position in the Tube (measured in Pixels) of the bitmap image (lower). The intensity plots are shown for the Center, Middle, and Boundary Partial Planar Slices and the intensity along the Y-Average. This data represents Image 402 (6 minutes, 42 seconds elapsed time) of the data set taken on 4/12/12.

Figure 7.10: The chart above shows the Normalized Variance (Non-Dimensional) vs. Time (Non-Dimensional). The Normalized Variance plots are shown for the Center and Middle Partial Planar Slices, the Y-Average, and the Analytic Solution. This data represents all 450 images (7 minutes, 30 seconds elapsed time) of the data set taken on 4/12/12.

The initial condition of the plug shown in Figure 7.6 shows a nearly symmetrical plug with respect to the longitudinal axis. The intensity plot is consistent with what is expected by the numerical simulations. The bitmaps shown in Figures 7.7 through 7.9 show the symmetry of the plug holding, better than in the 3/22/12 experiment. However, the data shown for the normalized variance in Figure 7.10 strays from analytic solution much sooner than the 3/22/12 experiment. Due to the significant inaccuracies of the normalized variance shown Figure 7.10 an error study did not produce meaningful data. Again, the reason for this error is unknown and further discussion will be in the next chapter.

7.3   Experimental Results 6/11/12

The following is the experimental results for the data taken on 6/11/12. The inner diameter of the tube used was 0.50 cm. The Peclet Number was 375 with a velocity of .03675 $\frac{cm}{s}$. The passive scalar used was 0.6 $\frac{g}{L}$ Fluorescein in Dionized Water and the fluid in the system was Dionized Water. The

pixels per cm measured for this experiment was 110. The data was analyzed and intensity plots with bitmap images were produced at images 1, 250, and 447. The shooting interval was 1 frame every 6 seconds with a total of 999 frames (1 hour, 39 minutes, 54 seconds elapsed time). The Normalized Variance plots were drawn comparing the Y-Average to the analytic solution. Additionally shown is the error difference between the Y-Average and Analytic Solutions. This error was then graphed separately and was used to plot relative error of the Y-Average and the analytic solution.

Figure 7.11: The chart above (upper) shows the Intensity (Non-Dimensional) vs. the Position in the Tube (measured in Pixels) of the bitmap image (lower). The intensity plots are shown for the Center, Middle, and Boundary Partial Planar Slices and the intensity along the Y-Average. This data represents Image 98 (9 minutes, 48 seconds elapsed time) of the data set taken on 6/11/12.
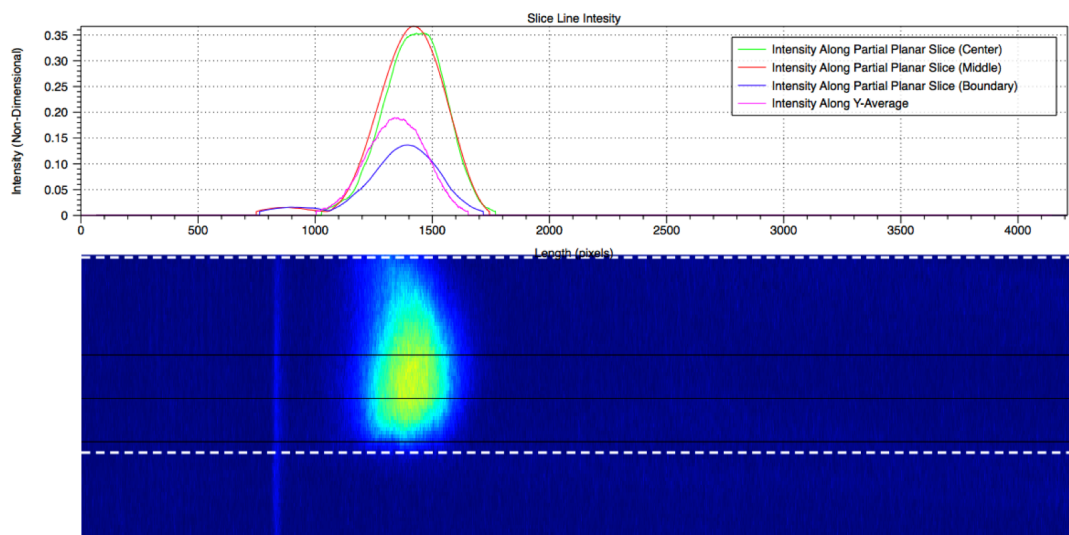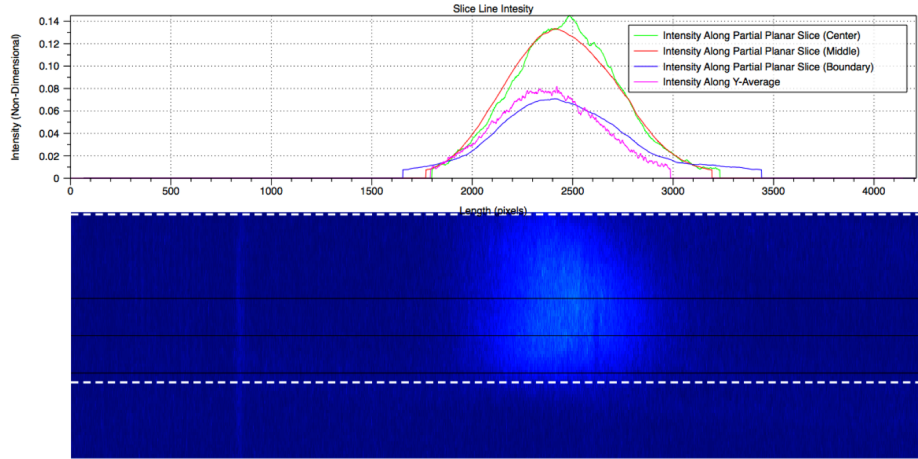
Figure 7.12: The chart above (upper) shows the Intensity (Non-Dimensional) vs. the Position in the Tube (measured in Pixels) of the bitmap image (lower). The intensity plots are shown for the Center, Middle, and Boundary Partial Planar Slices and the intensity along the Y-Average. This data represents Image 617 (1 hour, 1 minute, 42 seconds elapsed time) of the data set taken on 6/11/12.
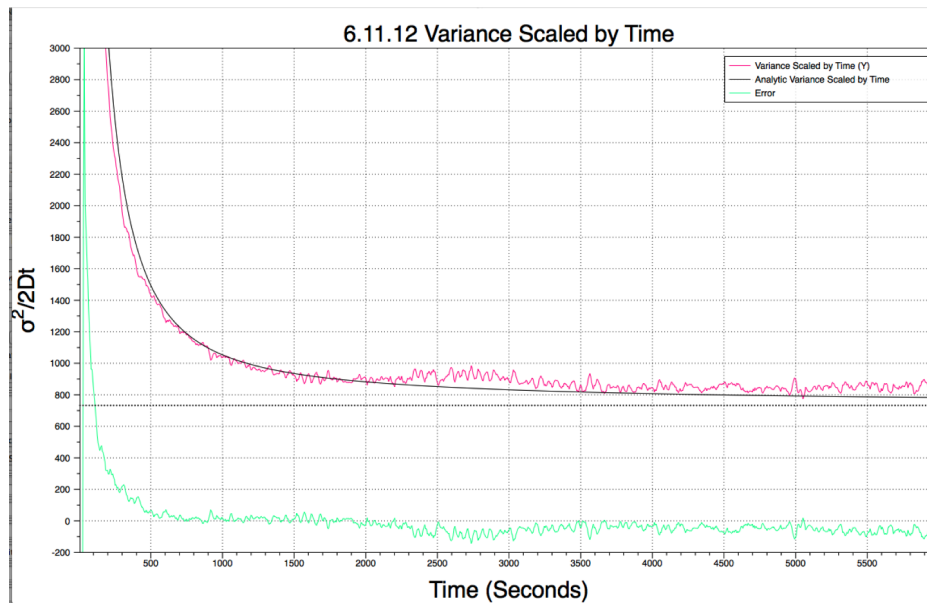

Figure 7.13: The chart above shows the Normalized Variance (Non-Dimensional) vs. Time (Seconds). The Normalized Variance plots are shown for the Y-Average and the Analytic Solution. Additionally shown is the error difference between the Y-Average and Analytic Solutions. This data represents all 999 images (1 hour, 39 minutes, 54 seconds elapsed time) of the data set taken on 6/11/12.

59
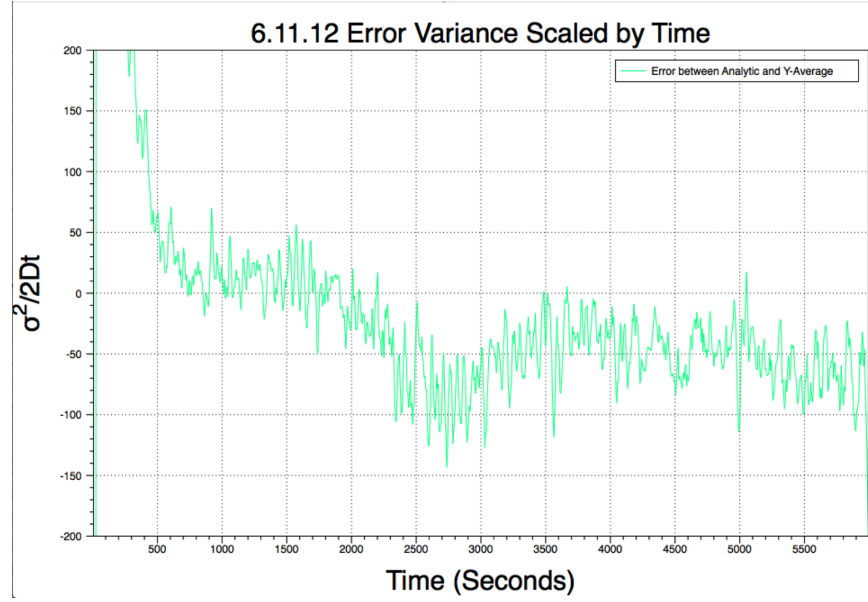
Figure 7.14: The chart above shows the Normalized Variance (Non-Dimensional) vs. Time (Seconds). The Normalized Variance plots is shown for the error or difference between the Y-Average and Analytic Solutions. This data represents all 999 images (1 hour, 39 minutes, 54 seconds elapsed time) of the data set taken on 6/11/12.

Figure 7.15: The chart above shows the Normalized Variance (Non-Dimensional) vs. Time (Seconds). The Normalized Variance plots is shown for the relative error between the Y-Average and Analytic Solutions. This data represents all 999 images (1 hour, 39 minutes, 54 seconds elapsed time) of the data set taken on 6/11/12.
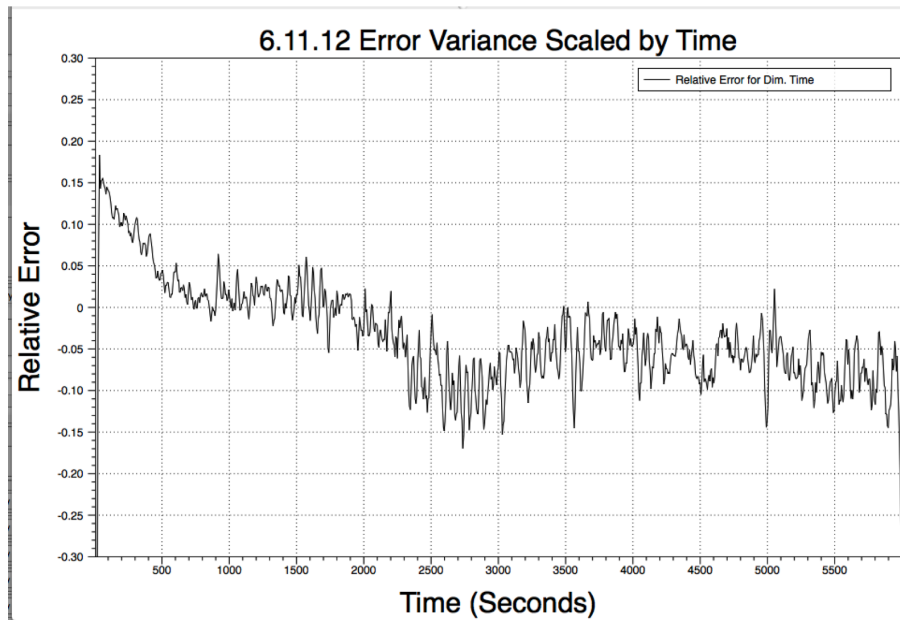
The data produced by this experiment is the most promising of all the data analyzed in the last

60

two years. The initial condition of the plug started out symmetrical and maintained its symmetry as seen in Figures 7.11 and 7.12. The intensity plots are consistent with the numerical simulations. Figure 7.13 shows the Y-Average normalized variance almost consistently matching the analytic solution. The figure also shows the error between the analytic solution and the Y-Average normalized variance. Figure 7.14 shows this error more precisely. The error seems large in this plot. However, Figure 7.15 shows that the relative error of the two normalized variances to vary between -20.0 % and +20.0 %. A relative error of +/- 20 % is the closest experimental data we have available to achieving the analytic solution. Unfortunately, this does not provide an accurate enough account to agree with the experimental and numerical data.

7.4 Experimental Results 9/17/12

The following is the experimental results for the data taken on 9/17/12. The inner diameter of the tube used was 0.50 cm. The Peclet Number was 375 with a velocity of .03675 $\frac{cm}{s}$. The passive scalar used was 0.6 $\frac{g}{L}$ Fluorescein in Dionized Water and the fluid in the system was Dionized Water. The pixels per cm measured for this experiment was 262. The data was analyzed and intensity plots with bitmap images were produced at images 160 and 435. The shooting interval was 1 frame every 6 seconds with a total of 999 frames (1 hour, 39 minutes, 54 seconds elapsed time). The Normalized Variance plots were drawn comparing the Y-Average to the analytic solution. Additionally shown is the error difference between the Y-Average and Analytic Solutions. This error was then graphed separately and was used to plot relative error of the Y-Average and the analytic solution.

Figure 7.16: The chart above (upper) shows the Intensity (Non-Dimensional) vs. the Position in the Tube (measured in Pixels) of the bitmap image (lower). The intensity plots are shown for the Center, Middle, and Boundary Partial Planar Slices and the intensity along the Y-Average. This data represents Image 160 (16 minutes elapsed time) of the data set taken on 9/17/12.
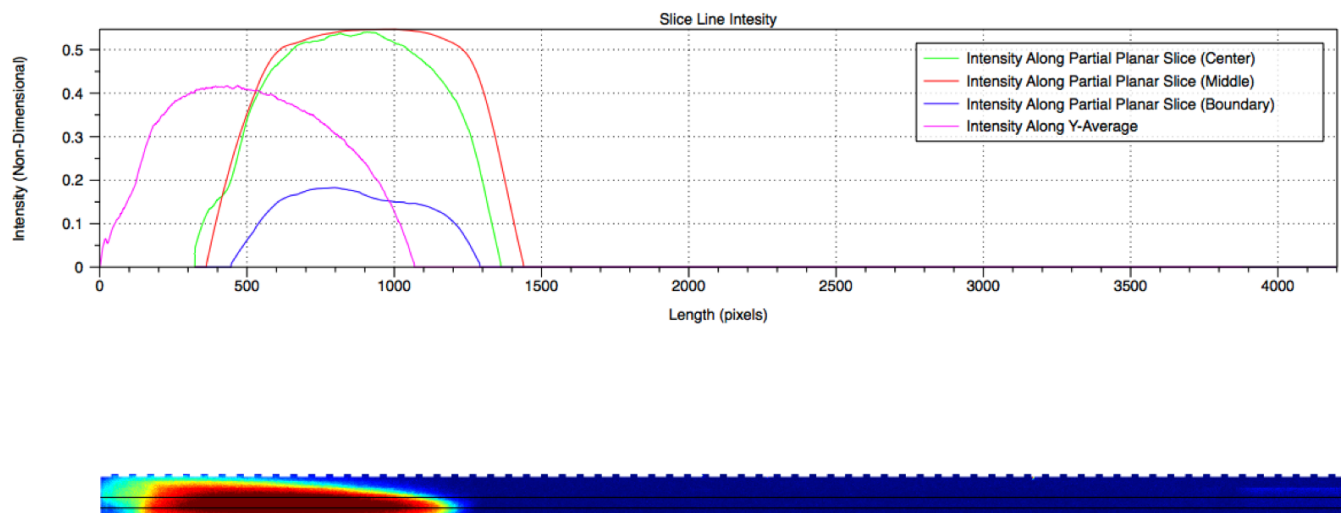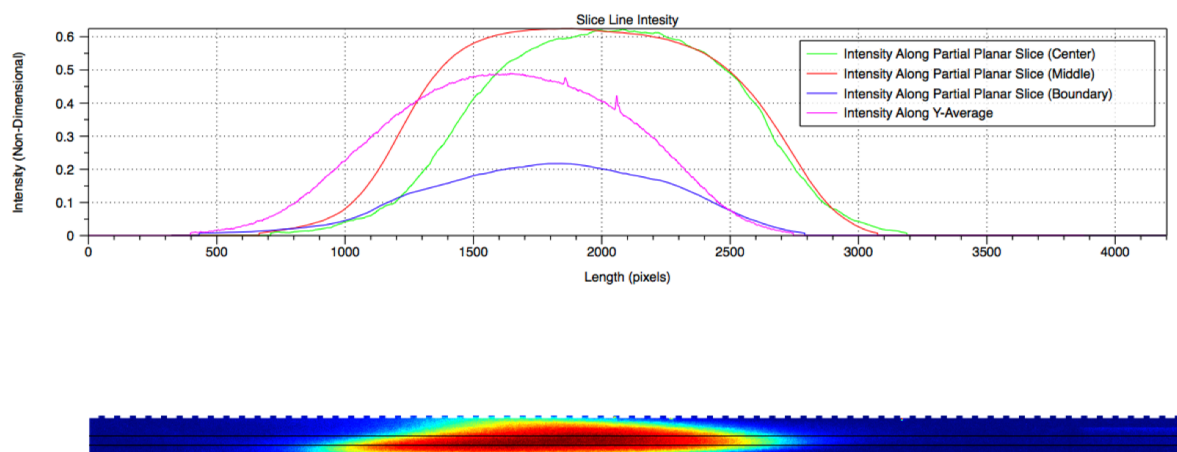

Figure 7.17: The chart above (upper) shows the Intensity (Non-Dimensional) vs. the Position in the Tube (measured in Pixels) of the bitmap image (lower). The intensity plots are shown for the Center, Middle, and Boundary Partial Planar Slices and the intensity along the Y-Average. This data represents Image 435 (43 minutes, 30 seconds elapsed time) of the data set taken on 9/17/12.

Figure 7.18: The chart above shows the Normalized Variance (Non-Dimensional) vs. Time (Seconds). The Normalized Variance plots are shown for the Y-Average and the Analytic Solution. Additionally shown is the error difference between the Y-Average and Analytic Solutions. This data represents all 999 images (1 hour, 39 minutes, 54 seconds elapsed time) of the data set taken on 9/17/12.
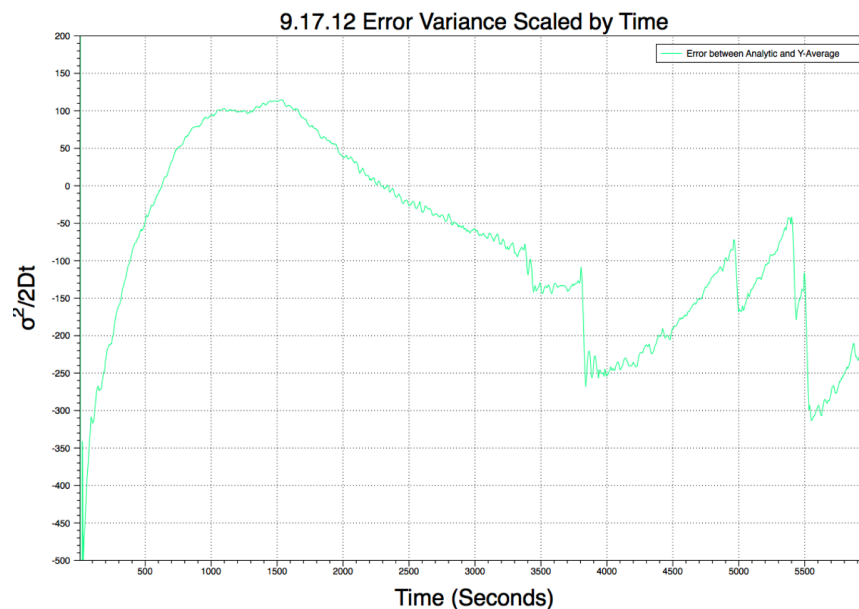
Figure 7.19: The chart above shows the Normalized Variance (Non-Dimensional) vs. Time (Seconds). The Normalized Variance plots is shown for the error or difference between the Y-Average and Analytic Solutions. This data represents all 999 images (1 hour, 39 minutes, 54 seconds elapsed time) of the data set taken on 9/17/12.
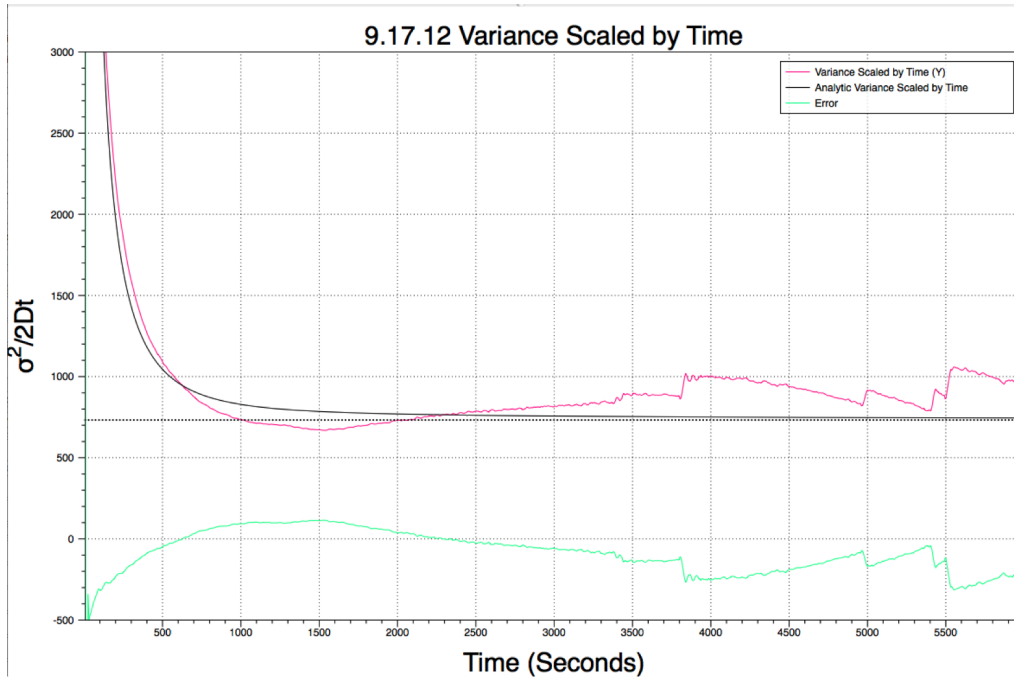

Figure 7.20: The chart above shows the Normalized Variance (Non-Dimensional) vs. Time (Seconds). The Normalized Variance plots is shown for the relative error between the Y-Average and Analytic Solutions. This data represents all 999 images (1 hour, 39 minutes, 54 seconds elapsed time) of the data set taken on 9/17/12.
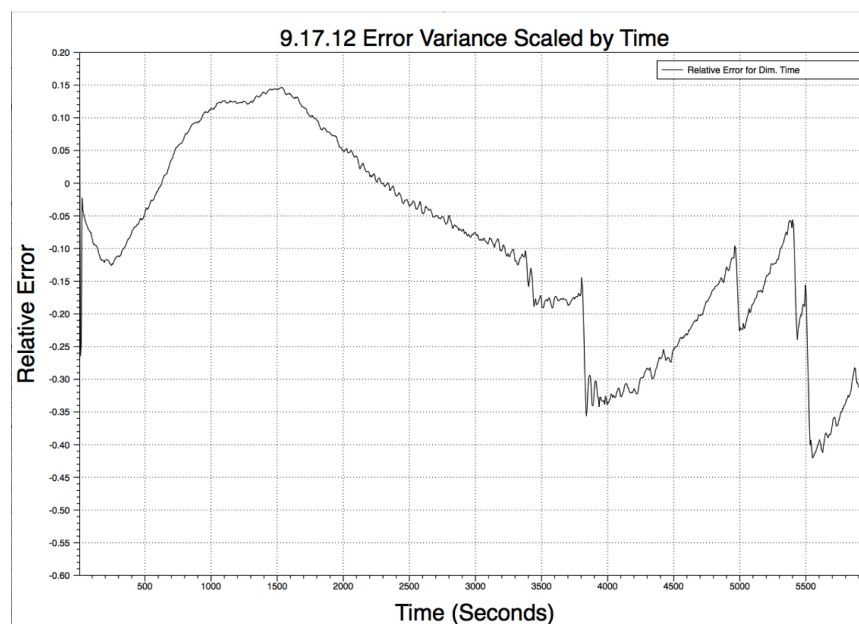
64

The initial condition of the plug did not start out symmetrical and maintained its asymmetry as seen in Figures 7.16 and 7.17. However, the intensity plots are reasonable when compared with the numerical simulations. Figure 7.18 shows the Y-Average normalized variance and the analytic solution. However, the data does not match the analytical solution as well as the 6/11/12 results. The figure also shows the error between the analytic solution and the Y-Average normalized variance. Figure 7.19 shows this error more precisely. Again, the error seems large in this plot. However, Figure 7.20 shows that the relative error of the two normalized variances to vary between -45.0 % and +15.0 %. This relative error is extremely large as well and suggest that the experimental data does not match the numerical and analytical solutions. However, it is the second best data analyzed to date.

7.5   Experimental Results 10/22/12

The following is the experimental results for the data taken on 10/22/12. The inner diameter of the tube used was 0.50 cm. The Peclet Number was 375 with a velocity of .03675 $\frac{cm}{s}$. The passive scalar used was 0.6 $\frac{g}{L}$ Fluorescein in dionized water and the fluid in the system was salt and dionized water. The pixels per cm measured for this experiment was 261. The data was analyzed and intensity plots with bitmap images were produced at images 164, 309, and 800. The shooting interval was 1 frame every 6 seconds with a total of 999 frames (1 hour, 39 minutes, 54 seconds elapsed time). The Normalized Variance plots were drawn comparing the center, middle, and boundary partial planar slices to the analytic solution.

Figure 7.21: The chart above (upper) shows the Intensity (Non-Dimensional) vs. the Position in the Tube (measured in Pixels) of the bitmap image (lower). The intensity plots are shown for the Center, Middle, and Boundary Partial Planar Slices. This data represents Image 164 (16 minutes, 24 seconds elapsed time) of the data set taken on 10/22/12.

Figure 7.22: The chart above (upper) shows the Intensity (Non-Dimensional) vs. the Position in the Tube (measured in Pixels) of the bitmap image (lower). The intensity plots are shown for the Center, Middle, and Boundary Partial Planar Slices. This data represents Image 309 (30 minutes, 54 seconds elapsed time) of the data set taken on 10/22/12.
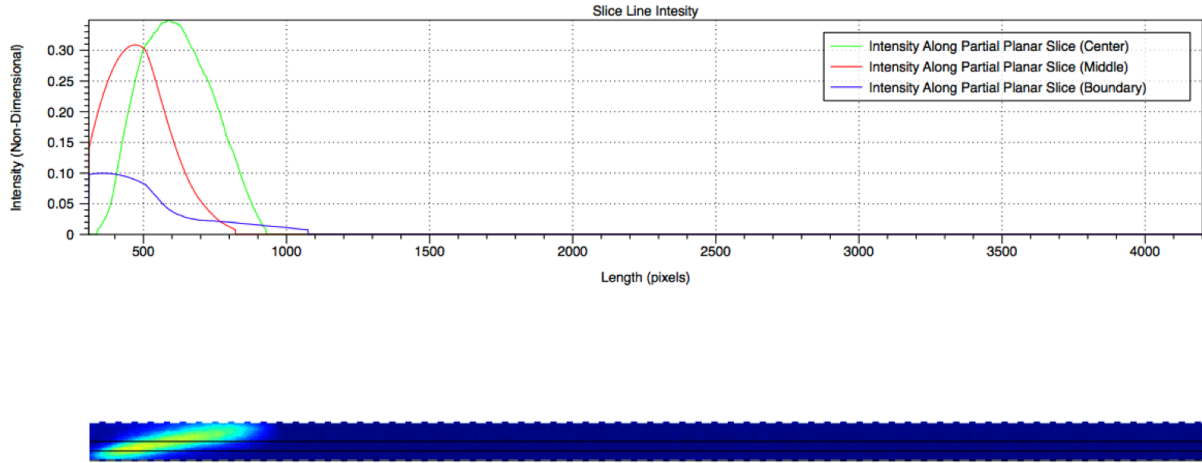
Figure 7.23: The chart above (upper) shows the Intensity (Non-Dimensional) vs. the Position in the Tube (measured in Pixels) of the bitmap image (lower). The intensity plots are shown for the Center, Middle, and Boundary Partial Planar Slices. This data represents Image 800 (1 hour, 20 minutes elapsed time) of the data set taken on 10/22/12.
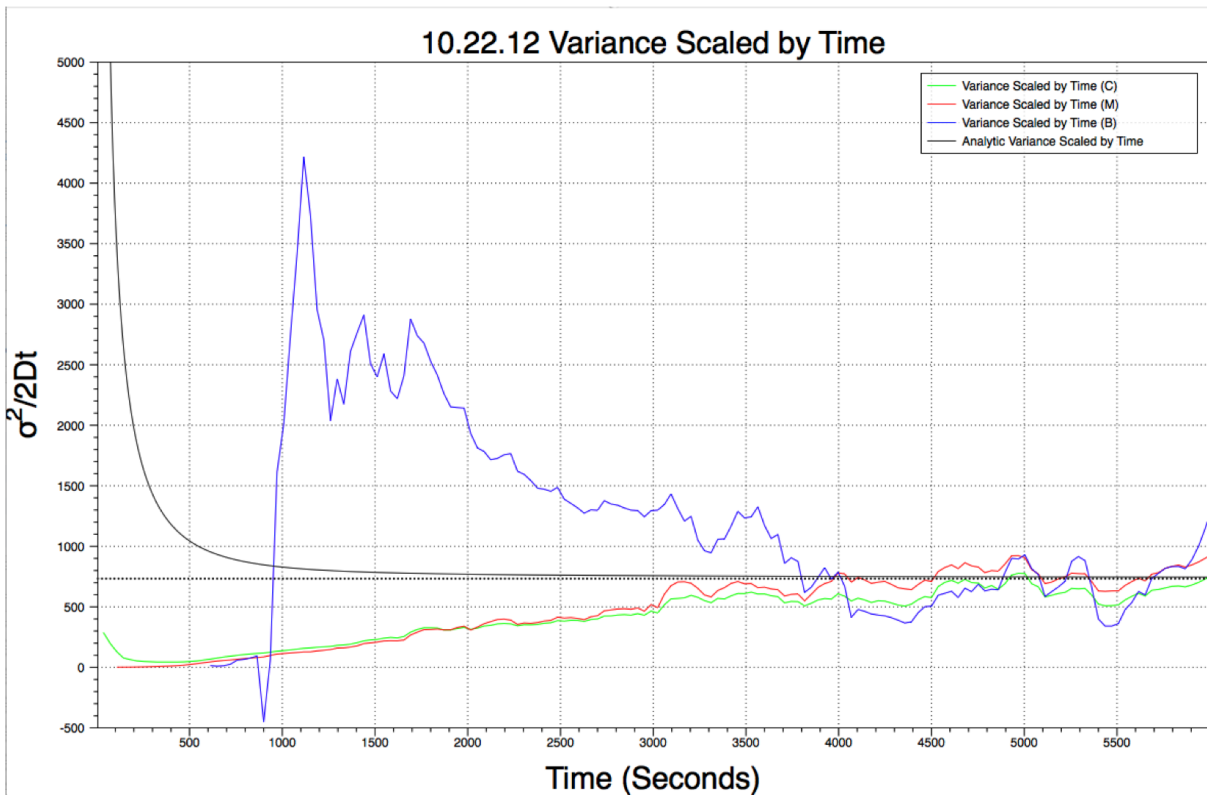
Figure 7.24: The chart above shows the Normalized Variance (Non-Dimensional) vs. Time (Seconds). The Normalized Variance plots are shown for the Center, Middle, and Boundary Partial Planar Slices and the Analytic Solution. This data represents all 999 images (1 hour, 39 minutes, 54 seconds elapsed time) of the data set taken on 10/22/12.

Upon further analysis of the experimental data, it is apparent that the salt water was more dense then the fluorescein water. That is why Figures 7.21 through 7.23 we see an asymmetrical plug where the passive scalar remains mostly at the top of the tube. Due to the asymmetry of the plug, the Y-Average data for the intensity and normalized variance could not be produced. Therefore, the data is only shown for the partial planar slices. Due to the significant inaccuracies of the normalized variance shown Figure 7.24 an error study did not produce meaningful data.

7.6 Experimental Results 10/29/12

The following is the experimental results for the data taken on 10/29/12. The inner diameter of the tube used was 0.50 cm. The Peclet Number was 375 with a velocity of .03675 $\frac{cm}{s}$. The passive scalar used was 0.6 $\frac{g}{L}$ Fluorescein in Karo Syrup and the fluid in the system was Pure Karo Syrup. The pixels per cm measured for this experiment was 261. The data was analyzed and intensity plots with bitmap images were produced at images 50, 205, and 535. The shooting interval was 1 frame every 6 seconds with a total of 999 frames (1 hour, 39 minutes, 54 seconds elapsed time). The Normalized Variance plots were drawn comparing the center, middle, and boundary partial planar slices to the analytic solution.
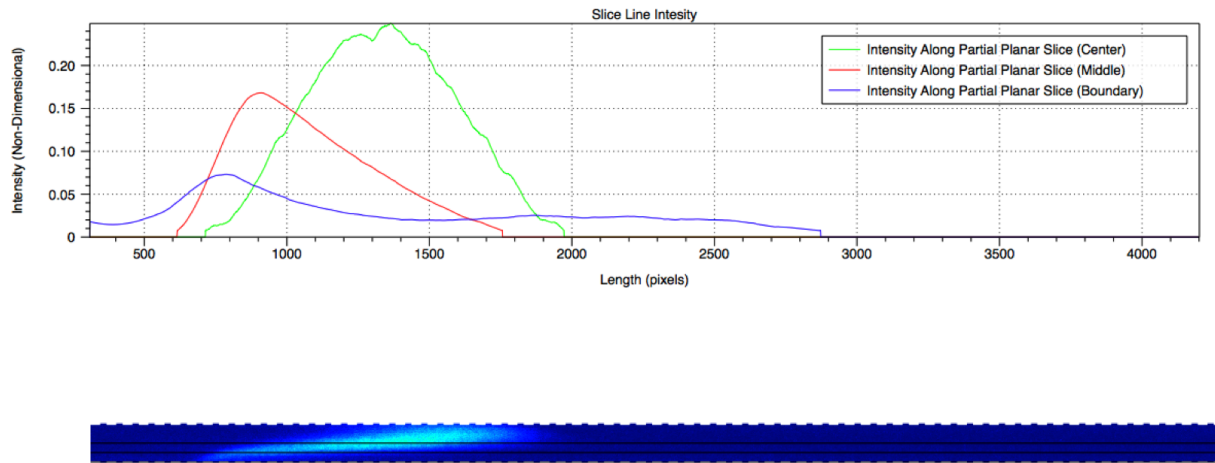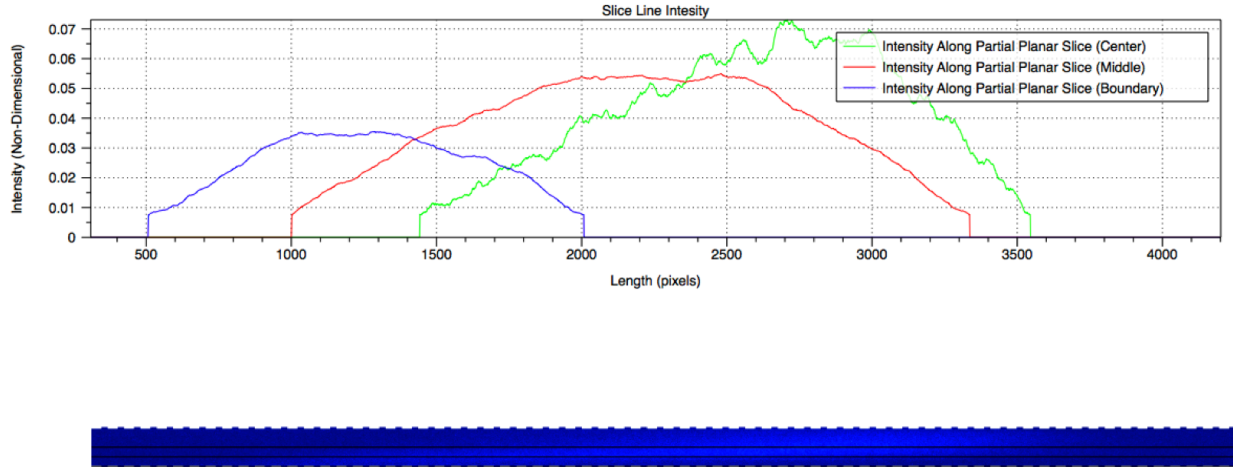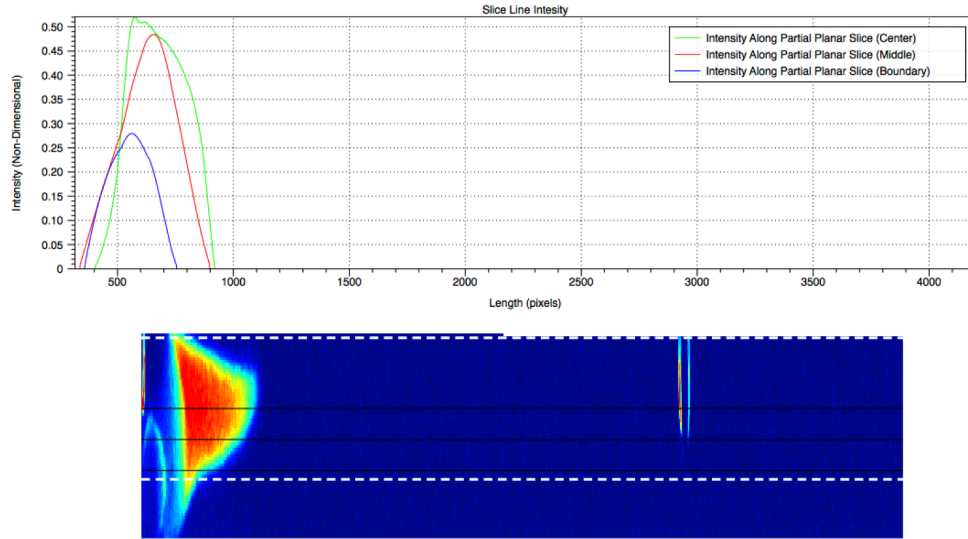
Figure 7.25: The chart above (upper) shows the Intensity (Non-Dimensional) vs. the Position in the Tube (measured in Pixels) of the bitmap image (lower). The intensity plots are shown for the Center, Middle, and Boundary Partial Planar Slices. This data represents Image 50 (5 minutes elapsed time) of the data set taken on 10/29/12.
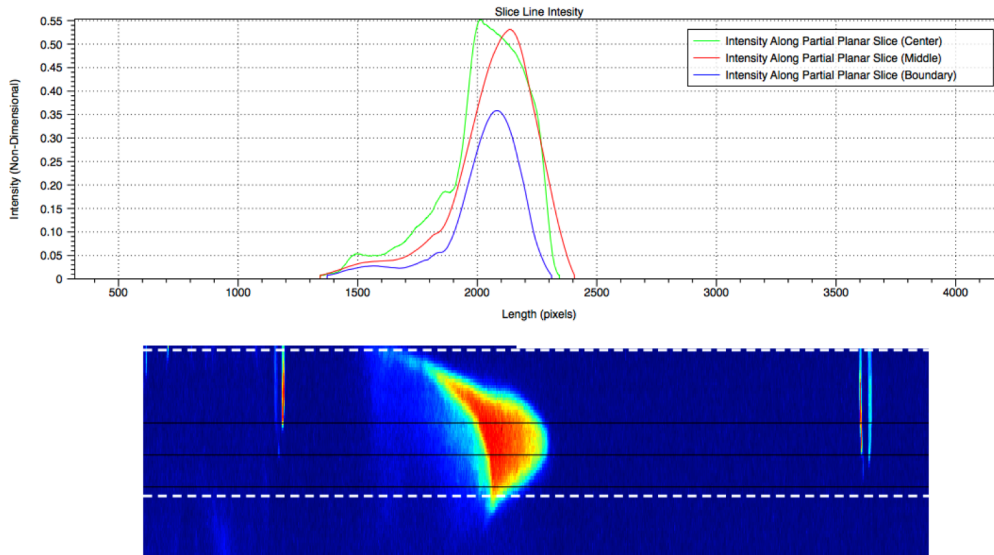
Figure 7.26: The chart above (upper) shows the Intensity (Non-Dimensional) vs. the Position in the Tube (measured in Pixels) of the bitmap image (lower). The intensity plots are shown for the Center, Middle, and Boundary Partial Planar Slices. This data represents Image 205 (20 minutes, 30 seconds elapsed time) of the data set taken on 10/29/12.
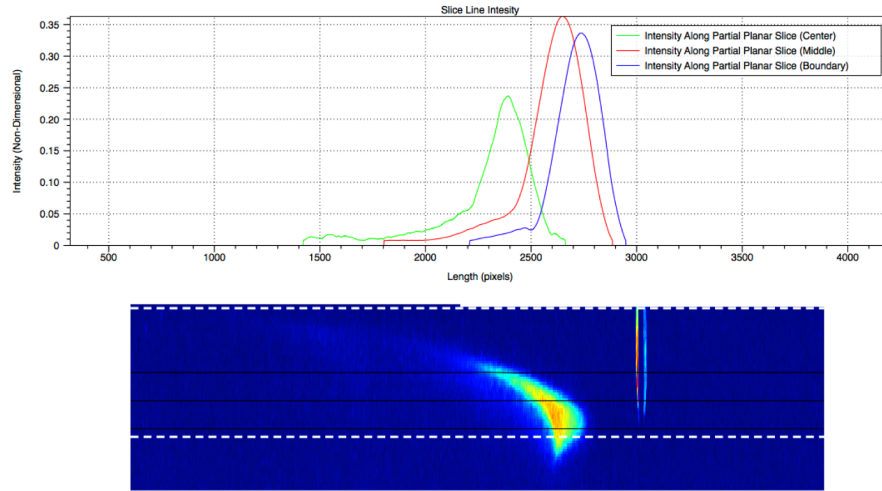
Figure 7.27: The chart above (upper) shows the Intensity (Non-Dimensional) vs. the Position in the Tube (measured in Pixels) of the bitmap image (lower). The intensity plots are shown for the Center, Middle, and Boundary Partial Planar Slices. This data represents Image 535 (53 minutes, 30 seconds elapsed time) of the data set taken on 10/29/12.
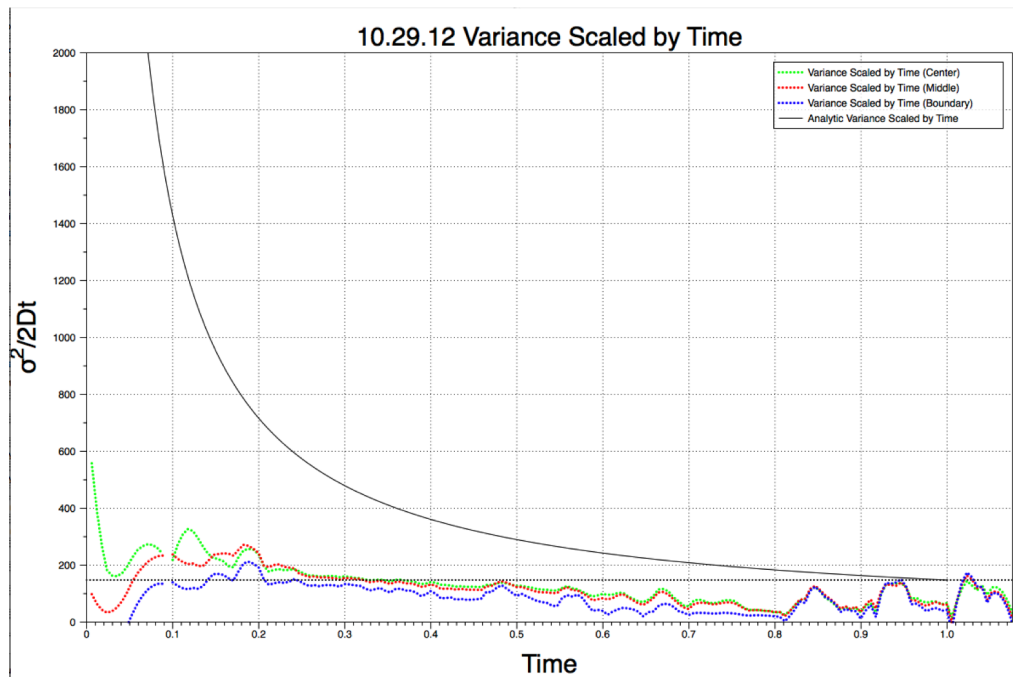
Figure 7.28: The chart above shows the Normalized Variance (Non-Dimensional) vs. Time (Seconds). The Normalized Variance plots are shown for the Center, Middle, and Boundary Partial Planar Slices and the Analytic Solution. This data represents all 999 images (1 hour, 39 minutes, 54 seconds elapsed time) of the data set taken on 10/29/12.

Upon further analysis of the experimental data, it is apparent that the fluorescein/karo mixture was

more dense then the pure karo syrup. That is why Figures 7.25 through 7.27 we see an asymmetrical plug where the passive scalar remains mostly at the bottom of the tube. Due to the asymmetry of the plug, the Y-Average data for the intensity and normalized variance could not be produced. Therefore, the data is only shown for the partial planar slices. Additionally, these figures show several air bubbles in the tube that can be identified by the light reflection on the the right side of each bitmap image. When the passive scalar reaches the bubble the images are significantly distorted and no data after that point is usable for analysis. Due to the significant inaccuracies of the normalized variance shown Figure 7.28 an error study did not produce meaningful data.

8 Conclusion

8.1 Numerical Results

The results of the Monte Carlo simulations agree with the analytical theory presented by Camassa, Lin, and McLaughlin. There are three major conclusions of this Monte Carlo numerical simulation project. First, the 2D and 3D rendering histograms agree with the analytical and experimental theory. Second, the Monte Carlo simulations were consistent with the Variance scaled by time for both the disk initial condition and the plug of finite length initial condition. Lastly, the simulations agree with the Taylor's theory that the advection-diffusion process becomes uniform after one Taylor time scale.

As shown in figures 6.1 and 6.2, the initial plug of dye is subjected to a parabolic flow. The dye then makes a chevron type shape in the 2D histogram showing the initial domination of the advection term. This visual representation agrees with the theories put forward by Taylor and the many subsequent authors on the topic. The 3D rendering of the flow in figure 6.2 provides visualization of how the concentration behaves throughout the entire pipe. This shows that the data is qualitatively accurate as well.

Figures 6.5 to 6.12 show the varaince scaled by time for Peclet numbers of 150, 300, 750, 1000, 1200, 1750, 2000, 2500, and 5000. All of these solutions match quite well with the analytic theory. This is shown most accuratedly by the MC Variance Scaled by Time (y-Average) lines on each chart. Figure 6.2 shows the variance scaled by time using the disk initial condtion. This chart shows the simulation results holding all variables constant except the Peclet number. The Peclet is varied by

the input velocity and ranges from 150-2500. All of the data sets converge to the Asymptote line of $\frac{Pe^2}{192}$ which is consistent with the analytical theory. For example the blue line that represents the Peclet number of 1200 converges to 7500. Finally, figure 6.13 shows the y-Average values from figures 6.4 to 6.12 on one chart. This gives a more complete picture of how varying the Peclet number (and thus speed of mean flow) and effect the variance.

The final numerical result of significance shows that the simulations are consisted with Taylor's diffusive timescale. Recall that Taylor predicted that after a time t_1, diffusiona will cause the plug to regain its transversely uniform profile. He predicted that the plug would become a longer, transversely uniform quantity and move through the pipe at a constant velocity at all points in the pipe. As shown in the results section t_1 for figure 6.14 is 35.33 seconds. The figure below shows a zoomed up version of figure 6.14, isolating the time 35.33 seconds.
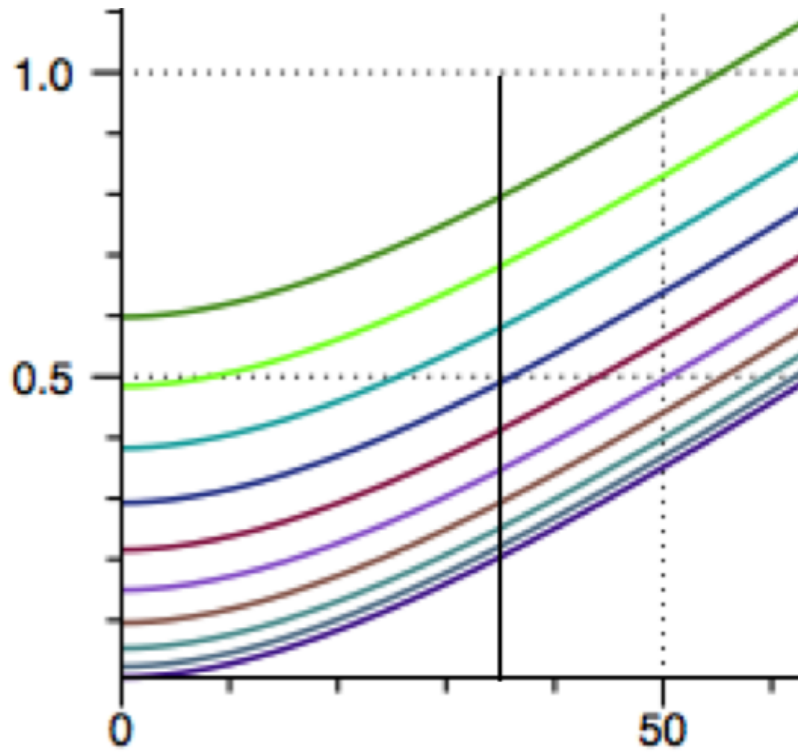

Figure 8.1: The above chart shows a zoomed up version of figure 6.14. The vertical black line in the image is set at 35.33 seconds. This is the first Taylor time scale.

The variance not scaled by time in figure 7.1 shows a distinct shift from a parabolic curve to a

linear curve. This happens precisely at 35.33 seconds or the first Taylor time scale. This shows that the Monte Carlo simulation also agrees with the theory put forth by Taylor.

8.2 Experimental Results

Experimental results of this project are still on going. Over the last 2 years 33 distinct data sets have been taken. 16 data sets were taken with a pipe of inner diameter .10 cm and 17 were taken with a pipe of inner diameter .50 cm. The fluorescein concentration has varied from $0.25 - 0.60$ $\frac{g}{L}$. The liquids tested have been pure deionized water, deionized salt water, Karo syrup, and a water/Karo syrup mixture. Thus far only two experimental data sets have produced a relative error less than 1% for normalized variance.

Through April 2012 a pipe with an inner diameter of .10 cm was used to take the experimental data. However, when analyzing the data there were significant errors in the normalized variance during the intermediate and long time scales. On May 5, 2012, the apparatus for conducting the experiments change from the 1 mm inner diameter pipe to a 5 mm inner diameter pipe. This choice was made because the experimental data achieved with the 1mm inner diameter pipe was not fully matching up with the Numerical and Analytic solutions to the problem. The fact that the inner diameter measurements of the pipe could only be guaranteed by the manufacturer to within a 10% margin of error. This is perhaps the variable that was providing incorrect experimental data. Therefore, the project was changed to a 5mm inner diameter pipe that's measurement can be guaranteed to a 1% margin of error. The goal was that with a more precise inner pipe diameter, better experimental data can be taken.

However, the larger pipe diameter had it draw backs in setting up the initial conditions of the experiment. Producing a uniformly symmetric passive scalar of fluorescein dye was not been achieved. The plugs of dye had significant imbalances in their symmetry. Figure 8.2 shows this lack of symmetry in the passive scalar of fluorescein dye.
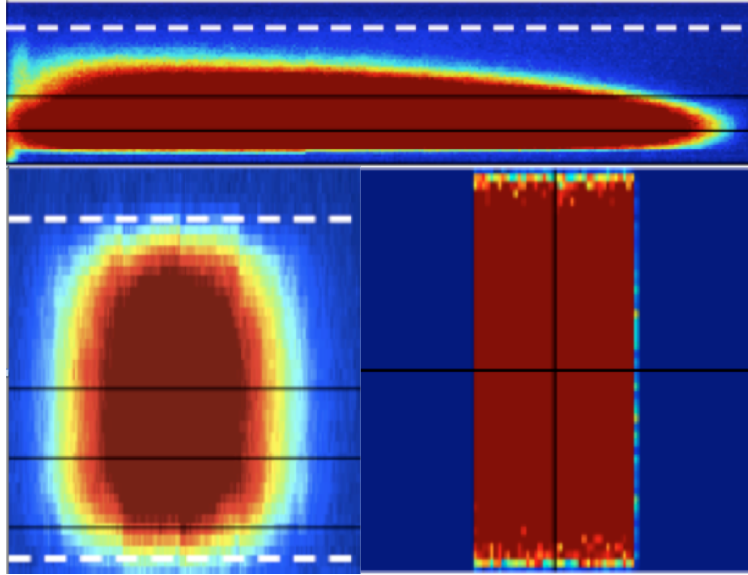
Figure 8.2: The above chart shows three different representations of Initial Condition 4, a plug of finite length. The top picture is plug of fluorescein dye captured in the 5 mm diameter tube. Note the asymmetry and increased length of the plug. The bottom left picture shows a plug of fluorescein dye captured in the 1 mm diameter tube. The bottom right picture shows a plug of dye from the Monte Carlo simulation.

The cause of the up-down asymmetry is currently unknown. It is assumed that the larger tube allows for more effect due to gravity, which is causing this bottom heavy effect. In an effort to delay the effects of gravity, the group attempted using fluids much more viscous than water. Various mixtures of Karo Corn Syrup and watered down Karo corn syrup were attempted with similar problems. Additionally, the group attempted adding trace amounts of NaCl to the water to match the densities of the dye and water to 0.0001 $\frac{g}{cm^3}$. However, the asymmetry has still occurred. It is also unknown as to how the added NaCl would effect the experimental data.

The integration of the XYZ stage occured on July 25, 2012. Currently the stage moves mechanically receiving manual inputs from a computer in the fluids lab. The integration of the XYZ stage has reduced the field of view of the digital camera from 15 cm to approximately 4 cm. This has improved the pixels per cm of the data taken from 115 to 250-350 for each experimental run. These higher resolution pictures should continue to provide more reliable experimental data for post processing.

From June 2012 to January 2013, the pipe flow group was able to collect data from 21 of the laboratory experiments. However, due to the current issues with the asymmetry of the initial plug of fluorescein dye, most of the data does not agree with the analytic and numeric solutions. The two best data sets were taken on 6/11/12 and 9/17/12. The 6/11/12 data in Figure 7.15 shows that the relative error of the Y-Average normalized variance varies between -20.0 % and +20.0 % with the analytic solution. Although the best data analyzed to date, it suggests significant areas for improvement in the experimental process. The 9/17/12 data in Figure 7.20 shows that the relative error of the of the Y-Average normalized variance is between -45.0 % and +15.0 %. It is the second best data analyzed to date, and does not show significant matchings to the numerical and analytical solutions.

In February 2013, after continued problems with the 5 mm inner diameter tube the determination was made to return to the 1 mm inner diameter tubes. The experimental apparatus was set up with the tubes used in early 2012. Four sets of data have been taken as of 3/4/13. However, a company was identified that can make the inner diameter of the tube 1 mm +/- 0.762 %. Set up and experiments with these tube began in late March 2013 after the manufacturing and delivery of the equipment. The new apparatus was set up on 3/25/13 and one preliminary set of data has been taken.

8.3   Areas for Further Study: Numerical Analysis

There are many areas for continued study in this project. Numerically, additional Monte Carlo simulations will be run at varying numbers of particles and time steps. Currently the Monte Carlo simulation code only works in the 3D version. Attempts will continually be made to debug the 2D version of the code. The 2D version of the code should require significantly less computational time. Thus a more refined time grid and a larger number of particles can be used in the 2D version. This should provide more accurate numerical results. Once the code is compiling and producing good data, a more complete convergence study will be conducted. The Monte Carlo simulation can also be adapted to model the asymmetrical initial conditions. Initial conditions should be written based on the asymmetrical plugs taken in the experimental data. Once these have been made the Monte Carlo simulation can run this data and it can be compared directly to the experimental

data. The Monte Carlo method can also be used to investigate skewness in the concentration data. To this point, this project has not yet considered this.

In addition to the Monte Carlo numerical method, efforts can be made to model the concentration and variance using an operator splitting method. This is a more classical approach to numerical modeling and currently has not been considered in this project for pipe flow.

Additionally, a numerical method has been devised to convert the intensity plots into concentration plots using polynomial interpolation. Since the digital camera images measure the intensity of the light, the data must be converted into concentration. To do this intensity readings were taken collected for 0.00 to 1.00 $\frac{g}{L}$ fluorescein water mixtures increments of .05 $\frac{g}{L}$. The tube was then completely filled with the fluorescein-water mixture. A digital image was taken of the picture and then the intensities for each know concentration were mearsured. An example of four intensity images are shown below.

0.10 g/L Fluorescein Concentration, Average Intensity = .2525 (non-dimensional)

0.25 g/L Fluorescein Concentration, Average Intensity = .5050 (non-dimensional)

0.50 g/L Fluorescein Concentration, Average Intensity = .6664 (non-dimensional)

0.75 g/L Fluorescein Concentration, Average Intensity = .7404 (non-dimensional)
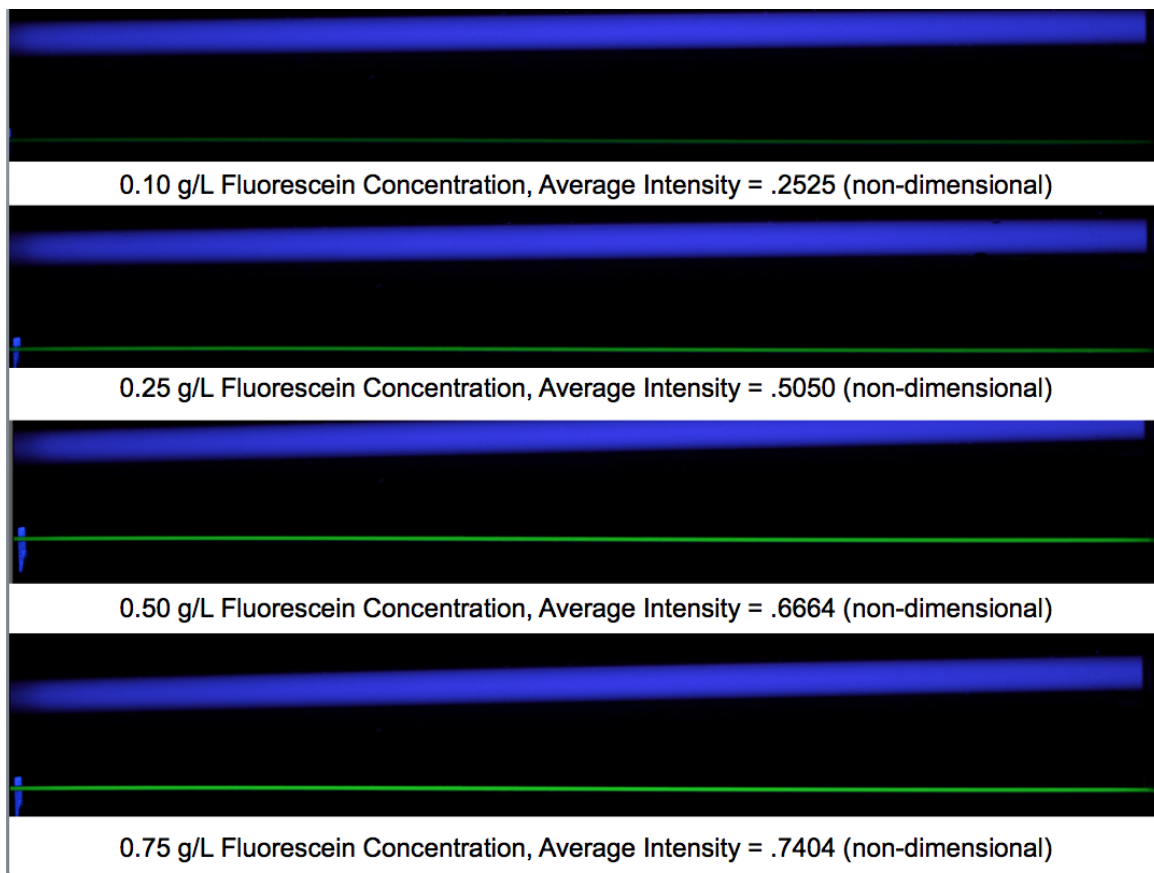
Figure 8.3: The pictures above shows the intensity of the light captured by the digital camera for various concentrations of water and fluorescein.

These intensities were then graphed using the DataTank software. Below, in Figure 8.4 is a graph of all measured intensities corresponding to concentrations of 0.00 $\frac{g}{L}$, 0.05 $\frac{g}{L}$, 0.10 $\frac{g}{L}$, 0.15 $\frac{g}{L}$, 0.20 $\frac{g}{L}$, 0.25 $\frac{g}{L}$, 0.30 $\frac{g}{L}$, 0.35 $\frac{g}{L}$, 0.40 $\frac{g}{L}$, 0.45 $\frac{g}{L}$, 0.50 $\frac{g}{L}$, 0.55 $\frac{g}{L}$, 0.60 $\frac{g}{L}$, 0.65 $\frac{g}{L}$, 0.70 $\frac{g}{L}$, 0.75 $\frac{g}{L}$, 0.80 $\frac{g}{L}$, 0.85 $\frac{g}{L}$, 0.90 $\frac{g}{L}$, 0.95 $\frac{g}{L}$, and 1.00 $\frac{g}{L}$. Figure 8.5 then graphs the Concentration vs. the Intensity. This graph clearly shows that the relationship in non-linear. Here a fourth degree polynomial is used to represent the data.
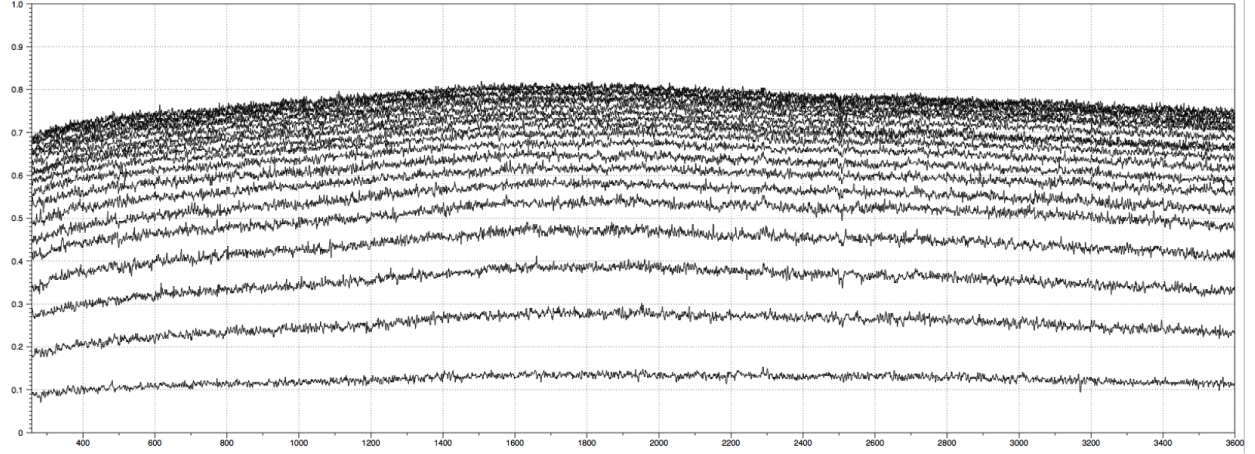
Figure 8.4: The graph above plots the intensity of the digital image (non-dimensional) vs. the distance along the tube (pixels). The different lines from bottom to top represent increasing concentrations of water and fluorescein from 0.05 to 1.00 in increments of .05 $\frac{g}{L}$.
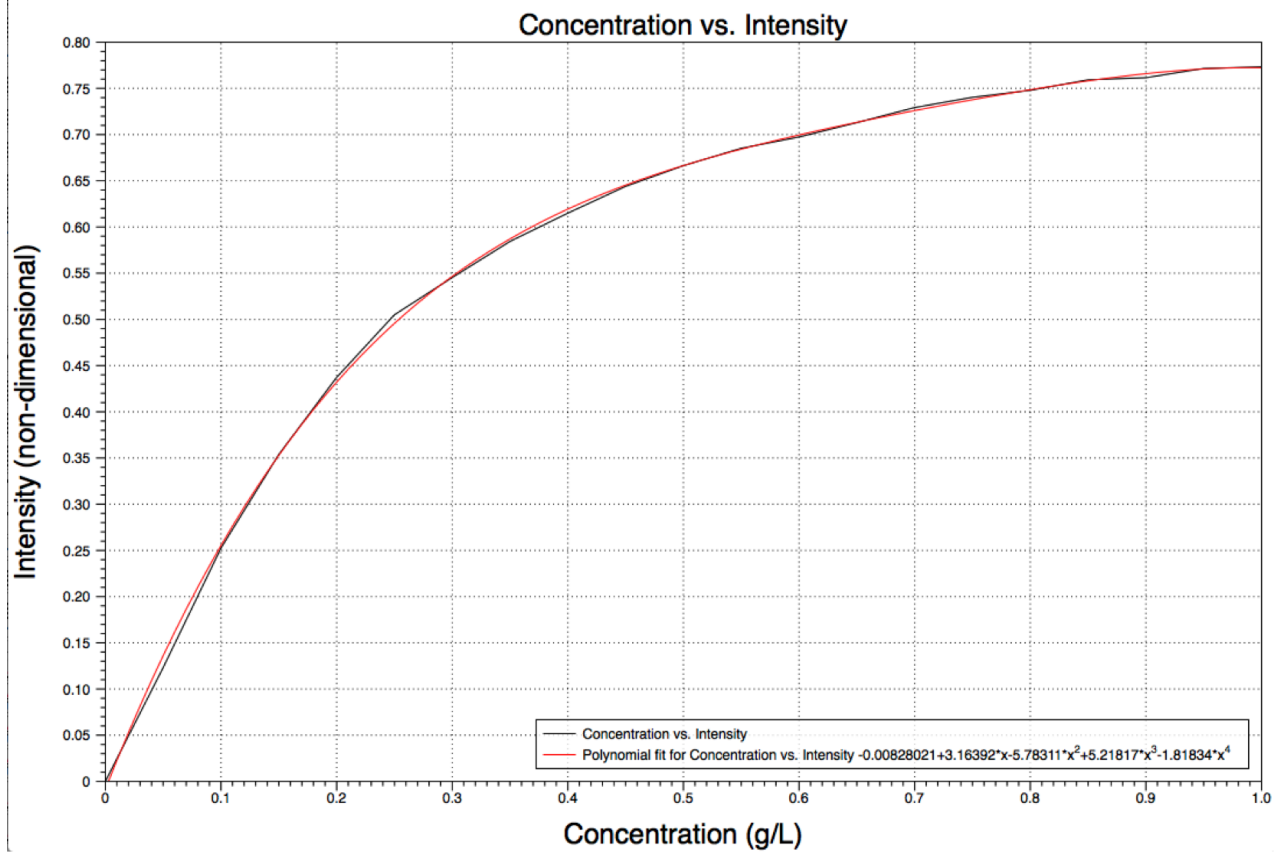
Figure 8.5: The plot above shows the non-linear relationship between concentration and intensity. A fourth degree polyinomial is displayed in red that fits the experimental data.
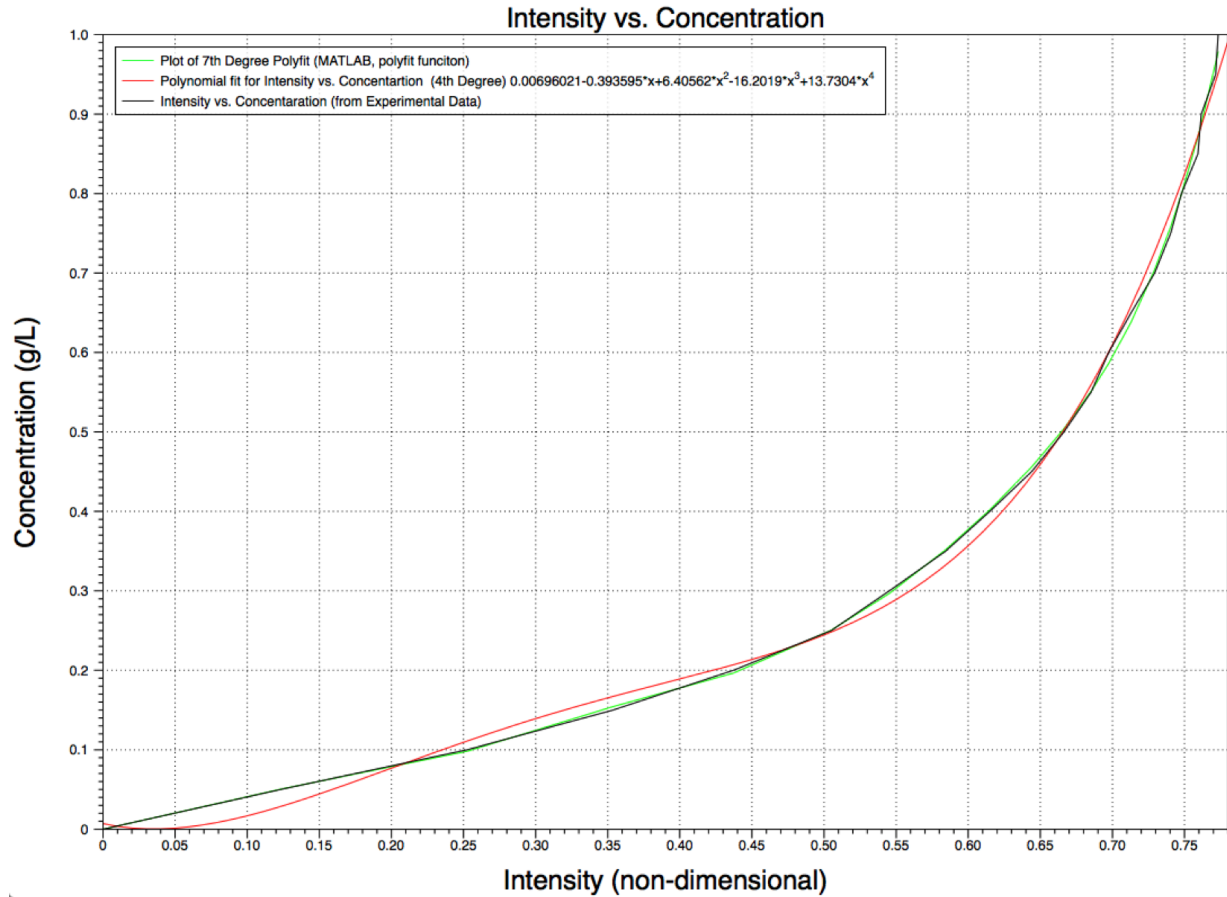
Figure 8.6: The plot above shows the non-linear relationship between intensity and concentration. Fourth and seventh degree polyinomials are displayed in red and green, respectively, that fit the experimental data.

Figure 8.6 graphs the Intensity vs. the Concentration. This is a more accurate way to represent the relationship as the camera measurements are in intensity. Using polynomial interpolation a higher degree polynomial can be used to achieve a more accurate result. The equations for the unique 4th, 7th, and 10th degree polynomials are:

Polyfit for 4th Degree Polynomial (DataTank Polyfit function):

$0.00696021 - 0.393595 * y + 6.40562 * y^2 - 16.2019 * y^3 + 13.7304 * y^4$

Polyfit for 7th Degree Polynomial (MATLAB):

$672.636123317486 * y^7 - 1824.73546647382 * y^6 + 1982.93020714280 * y^5 - 1090.91540678446 * y^4 + 317.100235607670 * y^3 - 45.2987636388086 * y^2 + 2.80972282683326 * y^1 - 4.43531987850241e - 05$

Polyfit for 10th Degree Polynomial (MATLAB):

$308702.431180458 * y^{10} - 1379401.12913651 * y^9 + 2679616.83039466 * y^8 - 2962057.77452650 * y^7 +$

$2046446.26566139 * y^6 - 912581.344915295 * y^5 + 261253.127918266 * y^4 - 45962.3162747279 * y^3 +$

$4462.27030951059 * y^2 - 178.821184878854 * y - 1.76758861252013 \times 10^{-08}$

These polynomials can then be used to map the intensity data to concentration. This correction in the concentration data may help to achieve more accurate results in the normalized variance data.

8.4   Areas for Further Study: Experimental Analysis

Experimentally, the pipe flow group should continue to improve its methods. Continued attempts of density matching the solute and the water will be attempted to regain initial plug symmetry. The two methods currently being considered are the addition of salt to the water and density matching by temperature manipulation. Since the effects of adding trace amounts of NaCl to the system are, it is recommended that temperature manipulation be considered. Since the density of deionized water is known for various temperatures, the density of water and various measurements of fluorescein can be superimposed on the same graph.
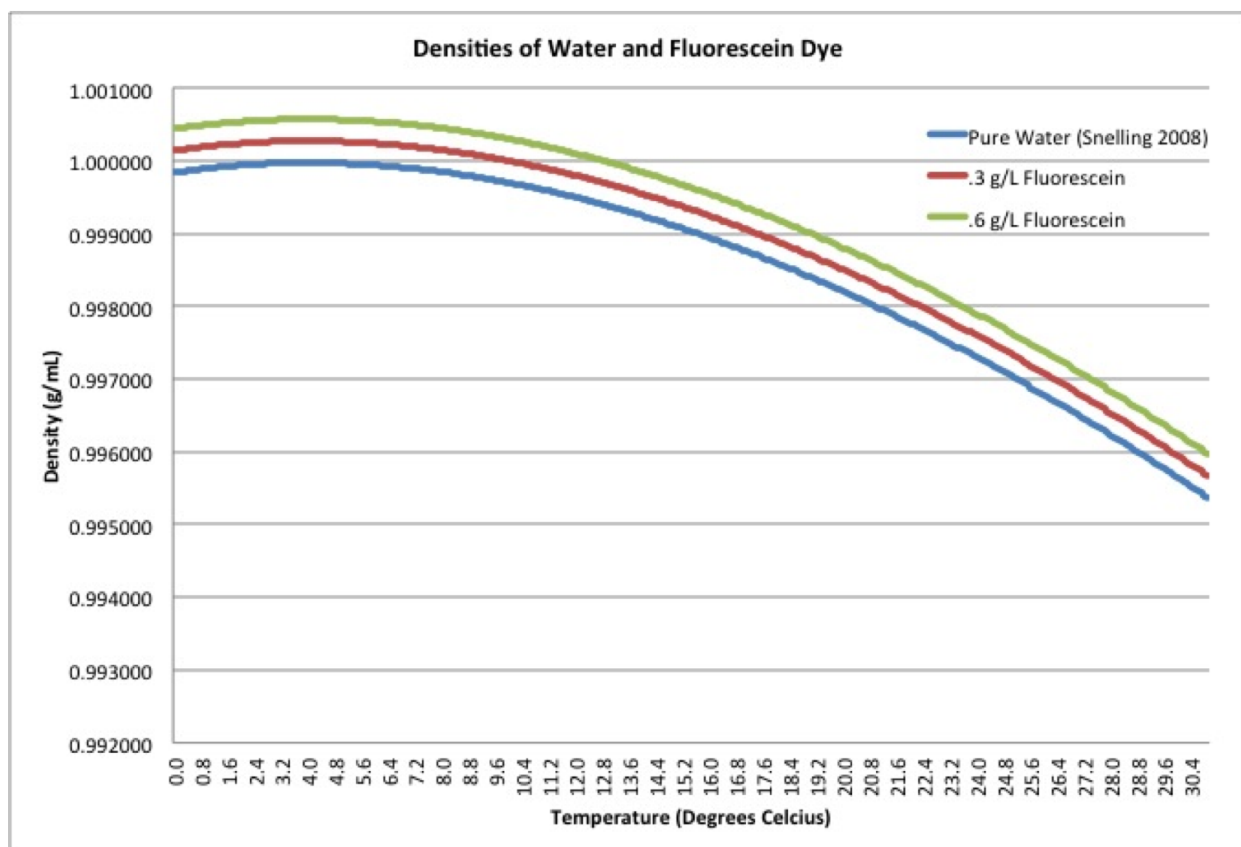
Figure 8.7: The graph above shows the Density of the Liquid ($\frac{g}{mL}$) vs. the Temperature (Degrees Celcius) for Pure Water, .3 $\frac{g}{L}$ Fluorescein, and .6 $\frac{g}{L}$ Fluorescein.

Temp (C)	Density Water (g/mL)	Density Fluorescein (.3 g/L)	Density Fluorescein (.6 g/L)
21.7	0.997837	0.998137	0.998437
21.8	0.997815	0.998115	0.998415
21.9	0.997792	0.998092	0.998392
22.0	0.997770	0.998070	0.998370
22.1	0.997747	0.998047	0.998347
22.2	0.997724	0.998024	0.998324
22.3	0.997701	0.998001	0.998301
22.4	0.997678	0.997978	0.998278
22.5	0.997655	0.997955	0.998255
22.6	0.997632	0.997932	0.998232
22.7	0.997608	0.997908	0.998208
22.8	0.997585	0.997885	0.998185
22.9	0.997561	0.997861	0.998161
23.0	0.997538	0.997838	0.998138
23.1	0.997514	0.997814	0.998114
23.2	0.997490	0.997790	0.998090
23.3	0.997466	0.997766	0.998066
23.4	0.997442	0.997742	0.998042
23.5	0.997418	0.997718	0.998018
23.6	0.997394	0.997694	0.997994
23.7	0.997369	0.997669	0.997969
23.8	0.997345	0.997645	0.997945
23.9	0.997320	0.997620	0.997920
24.0	0.997296	0.997596	0.997896
24.1	0.997271	0.997571	0.997871
24.2	0.997246	0.997546	0.997846
24.3	0.997221	0.997521	0.997821
24.4	0.997196	0.997496	0.997796
24.5	0.997171	0.997471	0.997771
24.6	0.997146	0.997446	0.997746
24.7	0.997120	0.997420	0.997720
24.8	0.997095	0.997395	0.997695
24.9	0.997069	0.997369	0.997669
25.0	0.997044	0.997344	0.997644
25.1	0.997018	0.997318	0.997618
25.2	0.996992	0.997292	0.997592
25.3	0.996967	0.997267	0.997567
25.4	0.996941	0.997241	0.997541
25.5	0.996914	0.997214	0.997514
25.6	0.996888	0.997188	0.997488
25.7	0.996862	0.997162	0.997462
25.8	0.996836	0.997136	0.997436
25.9	0.996809	0.997109	0.997409
26.0	0.996783	0.997083	0.997383
26.1	0.996756	0.997056	0.997356
26.2	0.996729	0.997029	0.997329
26.3	0.996703	0.997003	0.997303

Figure 8.8: The table above shows the densities of water and fluorescein mixtures at various temperatures. Highlighted in yellow, red, green, and blue it illustrates the temperatures for four different densities that can be matched for all the three solutions.

This temperature manipulation scheme has yet to be tested by the pipe flow group. However, if the densities are better matched the initial plug of dye should be much more symmetrical.

Another area for improvement on the experment is to install the new tubes that are due for delivery in March 2013. The installation and use of these tubes should provide much more accurate data then the tubes currently being used.

To improve on the pixels per cm taken in each picture frame efforts can me made to further integrate the XYZ stage into data taking process. The current integration of the XYZ stage has increased the pixels per cm resolution of each experiment from about 115 to a range of 250-350. To further increase this a method has been devised to take three pictures at a closer zoom that could then be stitched together for a higher resolution image.
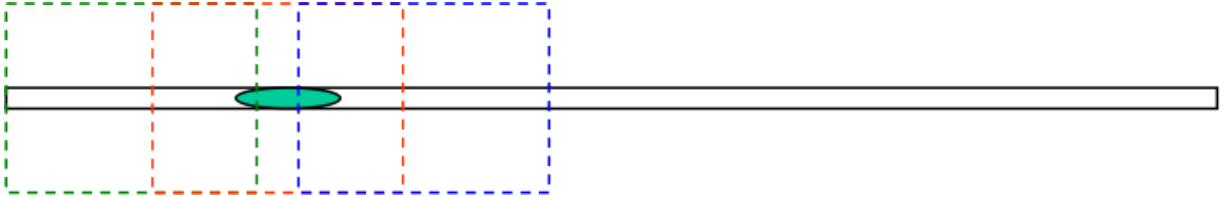

Figure 8.9: The sketch above shows the field of view for 3 separate higher resolution pictures that can be taken with the XYZ stage and later stitched together for a much higher resolution picture.

It is estimated that with this method the resolution can be increased to 1000-1400 pixels per cm. The camera and XYZ stage shopbot system has already been integrated to run together. A circuit diagram of the connection is below.
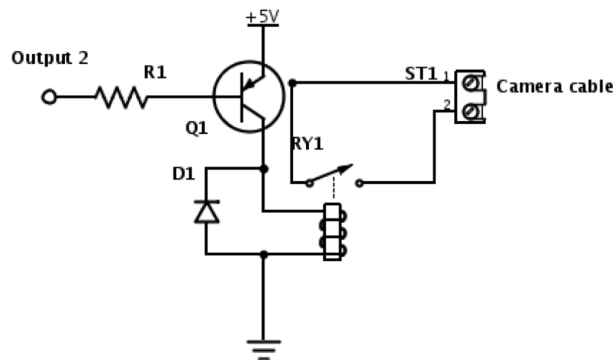

Figure 8.10: The curcuit diagram above shows the integration of the XYZ stage and the camera system. This integration should help to increase the pixels per cm resolution for each data set.

```
SR 'set the motion to relative
INPUT "DISTANCE BETWEEN IMAGES" &DX
INPUT "NUMBER OF TIMESTEPS" &SNUM

&LOOP = 0 'counter for loop, one run through loop is one timestep

STARTOFLOOP: 'label, indicates beginning of loop
PAUSE .1 'pause to ensure camera is stationary
SO 2, 0 'take picture by switching output 2 on and off
SO 2, 1
PAUSE .1 'move camera by &DX
MX &DX

PAUSE .1 'this is copy pasted three times because the alternative was another goto loop.
SO 2, 0
SO 2, 1
PAUSE .1
MX &DX
PAUSE .1
SO 2, 0
SO 2, 1
PAUSE .1 'move the camera back to the starting position
MX -2*&DX

&LOOP = &LOOP+1 'increase the count of the number of times the loop has been executed by
one
IF &LOOP<&SNUM THEN GOTO STARTOFLOOP ' if the loop has not been executed snum
times, go to line 9 and do it again
SA 'set the motion to absolute
```

Figure 8.11: This is the Shopbot code that integrates the XYZ stage and camera system.

This code, when implement, executes the picture taking as shown in Figure 8.9. The distance between number of pictures and the total number of pictures is controlled by inputs selected when the code is initiated. The integration of this system should be attempted to increase the pixels per cm of each experimental data set.

Other types of fluids should continue to be considered for use in the experiment such as corn syrup and silicon oil. Additionally, it has been suggested that the group consider a way to pivot the apparatus vertically to first achieve symmetry in the plug. Then the apparatus can be returned to the horizontal position for the experimental run. Finally, if initial conditions cannot be achieved the group should consider studying a continuous flow (or front) of dye rather than a passive scalar.

References

[1] ALLEN, C.M. 1982, Numerical Simulation of Contaminant Dispersion in Estuary Flows. *Proc. R. Soc. Lond. A*, **381 (1780)** , 179-184.

[2] ARIS, R. 1956, On the dispersion of solute in a fluid flowing through a tube. *Proc. R. Soc. Lond. A*, **235 (1200)** , 67-77.

[3] BAILEY, H.R. AND GOGARTY, W.B. 1962, Numerical and Experimental Results on the Dispersion of a Solute in a Fluid in Laminar Flow Through a Tube. *Proc. R. Soc. Lond. A*, **269 (1338)**, 352-367.

[4] BARTON, N.G. 1983, On the method of moments for solute dispersion *J. Fluid Mech.*, **126** , 205-218.

[5] BRENNER, H. 1980, *Phys. Chem. Hydrodyn.*, **1** , 91.

[6] CAMASSA, R., LIN, Z., AND MCLAUGHLIN, R. 2009, The exact evolution of the scalar variance in pipe and channel flow . *Commun. Math. Sci.*, **8(2)** , 601-626.

[7] CHATWIN, P.C. 1970, The approach to normality of the concentration distibution of a solute in a solvent flowing along a straight pipe. *J. Fluid Mech.*, **43** , 321-352.

[8] CHATWIN, P.C. 1976, The initial dispersion of contaminant in Poiseuille flow and the smoothing of the snout. *J. Fluid Mech.*, **77** , 593-602.

[9] CHATWIN, P.C. 1977, The initial Development of longitudinal dispersion in straight tubes. *J. Fluid Mech.*, **80** , 33-48.

[10] CODD, S.I., MANZ, B., SEYMOUR, J.D., AND CALLAGHAN, P.T. 1999, Taylor dispersion and molecular displacements in Poiseuille flow. *Phys. Rev. E*, **60** 4, R34991-R3494.

[11] DARHUBER, A.A., CHEN, J.Z., DAVIS, J.M., AND TROIAN, S.M. 2004, A Study of Mixing in Thermocapillary Flows on Micropatterned Surfaces *Proc. R. Soc. Lond. A*, **362 (1818)** , 1037-1058.

[12] GOLDSZTEIN, G.H. 2005, Transport of Nutrients in Bones *IMA J. Appl. Math.*, **65(6)** , 2128-2140.

[13] GRIFFITHS, A. 1911, On the Movement of a Coloured Index along a Capillary Tube, and its Application to the Measurement of the Circulation of Water in a Closed Circuit *Proc. Phys. Soc. Lond. A*, **23** , 190.

[14] LATINI, M. AND BERNOFF, A.J. 2001, Transient anomalous diffusion in Poiseuille flow. *J. Fluid Mech.*, **441** , 399-411.

[15] LIGHTHILL, M.J. 1966, Initial Development of diffusion in Poiseuille flow. *IMA J. Appl. Math.*, **2(1)** , 97-108.

[16] MCLAUGHLIN, R.M. AND MAJDA, A.J. 1996, An explicit example with non-Gaussian probability distribution for nontrivial scalar mean and fluctuation. *Phys. Fluids*, **8(2)** , 536-547.

[17] PHILLIPS, C.G. AND KAYE, S.R. 1997, The initial transient of concentration during the development of Taylor dispersion. *Proc. R. Soc. Lond. A*, **453 (1967)** , 2669-2688.

[18] TAYLOR, G.I. 1953, Dispersion of soluable matter in slovent flowing slowly through a tube. *Proc. R. Soc. Lond. A*, **219 (1137)**, 186.

[19] TAYLOR, G.I. 1954, The dispersion of matter in turbulent flow through a pipe. *Proc. R. Soc. Lond. A*, **223** ,446-468.

[20] TAYLOR, G.I. 1954, Conditions under Which Dispersion of a Solute in a Stream of Solvent can be Used to Measure Molecular Diffusion. *Proc. R. Soc. Lond. A*, **225 (1163)**, 473-477.